

Dissertation

submitted to the

Combined Faculty of Natural Sciences and Mathematics of the
Ruperto Carola University Heidelberg, Germany for the degree

of

Doctor of Natural Sciences

Presented by

M. Sc. Biology. Margot Maurer

born in Strasbourg, France

Oral examination: 07 June 2021

*Functional and anatomical interaction
between olfactory and trigeminal signalling*

Referees:

Prof. Dr Stephan Frings

PD. Dr. Richard Carr

Table of content

Summary	1
Zusammenfassung	2
I. Introduction.....	4
A. The olfactory system	4
1. Anatomy	4
a. Nasal cavity	4
b. Olfactory nerve	7
c. Olfactory bulb	7
d. Primary olfactory cortex	10
2. Olfactory signalling	12
a. OSN organization and structure enable an optimal detection of odorant molecules within the nasal cavity ¹²	
b. OSN activation and transduction of an odorant signal	12
c. Generation and transmission of an action potential in OSNs	15
B. Trigeminal system	16
1. Anatomy	16
a. Trigeminal ganglion and its branches	16
b. Trigeminal innervation of the nasal cavity: the anterior ethmoidal nerve	19
c. Trigeminal root projections to the medullary dorsal horn.....	19
2. Trigeminal signalling	21
a. Diversity of trigeminal neurons.....	21
b. Trigeminal signal transduction in primary afferents depends on specialized receptors families.....	23
i. Mechanical transduction.....	23
ii. Temperature transduction	25
iii. Chemical transduction (Chemesthesis).....	26
c. Signalling along trigeminal axons: the role of voltage-gated sodium channels	28
i. Voltage-gated sodium channels TTX-sensitive	29
ii. Voltage-gated sodium channels TTX-resistant	29
iii. Voltage-gated sodium channels and pain	30
d. CGRP, a neuropeptide released by trigeminal neurons	32
C. Interaction between olfactory and trigeminal systems	32
1. Congenital insensitivity to pain: Nav1.7 links olfaction and nociception.....	32
2. Dual detection of volatile compounds in the nose	33
3. Trigeminal signals modulate olfactory perception	34
II. Material & Methods.....	34
A. Animals.....	34
1. Wild type mice.....	35
2. Transgenic mouse lines.....	35
a. Reporter lines.....	35
b. Optogenetic mouse line.....	35
B. Human participants.....	36

1.	Control subjects	36
2.	Patients	36
a.	Congenital insensitivity to pain	36
b.	CIP re-gain	38
c.	Congenital insensitivity to pain with anhidrosis	39
C.	Psychophysical test	39
1.	Experimental design	39
2.	Test substances.....	39
3.	Analysis	40
D.	Forced choice behavioural task in mice	40
1.	Experimental design	40
2.	Test substances.....	41
3.	Analysis and statistics	41
E.	Imaging techniques	43
1.	Tissue preparation	43
a.	Olfactory epithelium	43
a.	Anterior ethmoidal nerve	45
b.	Trigeminal ganglion.....	45
2.	Antibody staining	45
3.	Microscope imaging.....	46
F.	Electrophysiology.....	46
1.	Hemi-skull preparation	46
2.	Electro-olfactogram recording.....	47
a.	Experimental design.....	47
b.	Stimuli	48
i.	Light pulses.....	48
ii.	Chemicals	50
iii.	Voltage-gated sodium channel blocker.....	50
c.	Recordings and analysis	51
3.	Nasal trigeminal afferents recordings.....	51
a.	Experimental design.....	51
b.	Stimuli	54
c.	Recording and analysis.....	54
III. Results	56	
A.	Trigeminal innervation of rodent nasal cavity.	56
1.	The anterior ethmoidal branch of the trigeminal system innervates the respiratory and olfactory epithelia in the nose.....	56
2.	Functional characterization of sensory afferents innervating the nasal epithelium	59
a.	Electrophysiological characterization of nasal trigeminal afferents reveal A-delta and C-type fibres	59
b.	Nasal trigeminal afferents responses to different stimulus modalities	61
i.	Polymodal activation of trigeminal afferents in the nasal epithelium	61
ii.	Nasal trigeminal responses to mechanical stimuli	62
iii.	Nasal trigeminal responses to thermal changes	62
iv.	Nasal trigeminal chemesthesis.....	65
Phenylethyl alcohol (PEA)	65	
Ammonia.....	67	
TRPV1 agonists.....	67	
TRPM8 agonists.....	69	
TRPA1 agonist	70	
3.	The sodium voltage gated channel 1.8 is expressed within an OSN subpopulation.....	71

B.	The odorant PEA mitigates trigeminal-induced nocifensive behaviour in mice	74
1.	Assessment of cross-modal interaction between olfactory and trigeminal systems in mice	74
a.	Water bottle flow and sipping tube diameter influence two bottle preference test measures.....	76
b.	Aversion to volatile trigeminal irritants is mitigated by co-application of the pure odorant PEA in WT mice 77	
i.	Exposure to PEA does not evoke preference nor aversion during the forced choice test.....	77
ii.	The odorant PEA mitigates the aversion evoked by the volatile TRPV1 cyclohexanone in WT mice 79	
iii.	PEA does not reduce the aversion evoked by the undiluted TRPA1 agonist allyl isothiocyanate... 80	
iv.	Nocifensive behaviour caused by milder concentrations of AITC can be mitigated by the addition of PEA.....	80
2.	Assessment of cross-modal interaction between olfactory and trigeminal systems in humans.....	83
a.	Variation of olfactory and pungency perception in humans.....	83
i.	Control participants.....	84
	Distilled water	84
	Phenylethyl alcohol.....	84
	TRPM8 agonists.....	86
	TRPA1 agonist	87
	TRPV1 agonist	87
	Ammonia.....	88
ii.	Patients suffering from insensitivity to pain conditions.....	88
	Congenital insensitivity to pain (CIP)	88
	Congenital insensitivity to pain re-gain of function	89
	Congenital insensitivity to pain with anhidrosis (CIPA).....	89
b.	PEA does not reduce pungency ratings in human subjects	90
i.	Control participants.....	90
ii.	Patients suffering from insensitivity to pain conditions.....	90
C.	Photoactivation of olfactory sensory neurons revealed that the mitigation observed at the behavioural level in mice does not happen within the OE.....	91
IV.	Discussion	93
A.	Characterization of trigeminal afferents within the nasal cavity	93
1.	Trigeminal axons forming the anterior ethmoidal nerve innervate the olfactory epithelium	93
2.	Nasal trigeminal afferents are mostly polymodal A δ - and C-fibre	96
a.	Conduction velocity of nasal trigeminal afferents	96
b.	Nasal trigeminal afferents respond to mechanical, thermal and chemical stimuli.....	97
i.	Mechano-sensitivity	97
ii.	Sensitivity to heating.....	98
iii.	Sensitivity to cooling	99
iv.	Chemesthesis	100
v.	Polymodal C-fibres	101
3.	Nav1.8 in mature OSNs	101
B.	Modulation of nasal trigeminal signalling by olfactory stimuli.....	103
1.	Pure odorants alter volatile irritant perception in mice	103
a.	PEA mitigates irritant-evoked nocifensive behaviour in mice	103
b.	Pungency modulation in normosmic and CIP patients	104
i.	Control subjects	105
ii.	CIP patient.....	105
iii.	CIPA patient.....	106
iv.	Cross-modal interaction between olfactory and trigeminal systems in humans.....	106
2.	Mouse trigeminal signalling is not affected by olfactory co-activation in the nose	107
V.	Conclusion	109

***Supplementary figures* 110**
***References* 114**
***List of figures* 140**
***Abbreviations*..... 141**
***Acknowledgement* 144**

Summary

In humans, the perception of volatile substances is multimodal and requires both olfactory and the trigeminal system activation. While olfactory sensory neurons (OSNs) receptive fields are limited to the nasal cavity, trigeminal axons convey sensory information from the head and the neck. Trigeminal neurons are involved in the initiation to protective reflexes and respond to different stimuli modalities such as mechanical pressure, changes in temperature and chemicals, with intensities extending to the noxious range. In contrast, OSNs are mainly activated by odorant chemicals. In the nose, afferents originating from the ophthalmic and maxillary divisions of the trigeminal ganglion, involved in the detection of pungent substances, reside in parallel with olfactory sensory neurons. The proximity of these two systems and psychophysical evidence have led scientists to investigate the possibility of a cross-modality interaction. Most studies have focused on trigeminal modulation of olfactory signals, unravelling a suppressive effect mediated by calcitonine gene-related peptide (CGRP) released from trigeminal afferents. Recently, scientists began to explore the reverse interaction. However, the effect of olfactory stimuli on pungency perception, the possible site of interaction and the molecular pathways underlying it remain unclear. In this thesis, trigeminal innervation was systematically investigated in mice using imaging and electrophysiological techniques to map and characterize anterior ethmoidal nerve afferents within the nasal epithelium. Unexpectedly, during this study, nasal epithelium sections from transgenic reporter mouse line revealed the presence of a subpopulation olfactory sensory neurons expressing the voltage-gated sodium channel $Na_v 1.8$, characteristic for sensory neurons present within dorsal root and trigeminal ganglia. The possibility of a cross-modal interaction between olfactory and trigeminal was interrogated in mice and human. The pure odorant phenylethyl alcohol mitigated irritant aversion to the TRPV1 agonist cyclohexanone and the TRPA1 agonist allyl isothiocyanate diluted in mice. However, these results could not be reproduced in human psychophysical tests. Therefore, the direct influence of OSN activation on trigeminal signalling was assessed using an optogenetic OMP-hChR2Venus mouse line expressing the light-sensitive channel rhodopsin 2 in mature OSNs. Concomitant OSN photo-activation did not affect action potentials signalling in individual trigeminal afferents within the nasal epithelium, suggesting that the mitigating effect observed at behavioural level in mice is unlikely to happen within the nose.

Zusammenfassung

Beim Menschen ist die Wahrnehmung flüchtiger Substanzen multimodal und erfordert sowohl die Aktivierung des olfaktorischen- als auch des Trigemini-Systems. Während die Empfangsfelder von olfaktorischen sensorischen Neuronen (OSNs) auf die Nasenhöhle beschränkt sind, übertragen Trigemini-Axone sensorische Informationen von Kopf und Nacken. Trigemini-Neuronen sind an der Auslösung von Schutzreflexen beteiligt und reagieren auf verschiedene Reizmodalitäten wie mechanischen Druck, Temperaturänderungen und Chemikalien, wobei sich die Intensität auf den schädlichen Bereich erstreckt. Im Gegensatz dazu werden OSNs hauptsächlich durch Chemikalien, die die olfaktorische Wahrnehmung betreffen aktiviert. In der Nase befinden sich Afferenzen, die aus dem Augen- und Oberkieferast des Trigemini-Ganglions stammen und an der Erkennung stechender Substanzen beteiligt sind, parallel zu olfaktorischen sensorischen Neuronen. Die Nähe dieser beiden Systeme und psychophysische Beweise haben Wissenschaftler veranlasst, die Möglichkeit einer modalitätsübergreifenden Interaktion zu untersuchen. Die meisten Studien haben sich auf die Trigemini-Modulation von Geruchssignalen konzentriert und eine unterdrückende Wirkung entdeckt, die durch das aus Trigemini-Afferenzen freigesetzte, dem Calcitonin-Gene related Peptid (CGRP), vermittelt wird. Vor kurzem begannen Wissenschaftler die umgekehrte Wirkung zu untersuchen. Die Wirkung von Geruchsreizen auf die Schärfeempfindung, den möglichen Ort der Wechselwirkung und die zugrunde liegenden molekularen Pfade bleiben jedoch unklar. In dieser Arbeit wurde die Trigemini-Innervation bei Mäusen mithilfe bildgebender und elektrophysiologischer Techniken systematisch untersucht, um Afferenzen des vorderen Siebbeinns im Nasenepithel abzubilden und zu charakterisieren. Unerwarteterweise zeigten während dieser Studie Nasenepithelschnitte aus der transgenen Reporter-Mauslinie das Vorhandensein einer olfaktorischen sensorischen Subpopulationsneurone, die den spannungsgesteuerten Natriumkanal NaV 1.8 exprimiert, der für sensorische Neuronen charakteristisch ist, die in Rückenwurzel- und Trigemini-Ganglien vorhanden sind. Die Möglichkeit einer Modalübergreifende Wirkung zwischen dem olfaktorischen System und Trigemini wurde bei Mäusen und Menschen untersucht. Der reine Geruchsstoff

Phenylethylalkohol milderte die Reizaversion gegenüber dem in Mäusen verdünnten TRPV1-Agonisten Cyclohexanone und dem TRPA1-Agonisten Allyl isothiocyanate. Diese Ergebnisse konnten jedoch in humanpsychophysikalischen Tests nicht reproduziert werden. Daher wurde der direkte Einfluss der OSN-Aktivierung auf die Trigemini-Signalübertragung unter Verwendung einer optogenetischen OMP-hChR2Venus-Mauslinie bewertet, die den lichtempfindlichen Kanal Rhodopsin 2 in reifen OSNs exprimiert. Die gleichzeitige Aktivierung des OSN-Fotos hatte keinen Einfluss auf die Aktionspotentiale, die bei einzelnen Trigemini-Afferenzen im Nasenepithel signalisierten, was darauf hindeutet, dass der auf Verhaltensebene bei Mäusen beobachtete mildernde Effekt in der Nase wahrscheinlich nicht auftritt.

I. Introduction

A. The olfactory system

The olfactory system detects, and processes odorant substances present in the surrounding aerial environment (Nara *et al.*, 2011). The main roles attributed to this system in mammals concern food localization, protection from noxious environments and social interaction between subjects from different sex or species (Croy *et al.*, 2012). Recent studies also demonstrate the olfactory system to be involved in discrimination of multiple odour sources, which could be a key feature to localize the origin of the smell (Erskine *et al.*, 2019). These roles are supported and processed by different structures present bilaterally along the olfactory pathway.

1. Anatomy

Odorant molecules enter the nasal cavity with the inspired air and activate olfactory sensory neurons. Olfactory signals are then transmitted in the form of action potentials, via axons, in the olfactory nerve and integrated in the olfactory bulb (OB). The signal is finally sent to diverse cortical areas to be processed.

a. Nasal cavity

The nasal cavity is the entrance point of inhaled odorant molecules. It contains 4 distinct olfactory structures: the main olfactory epithelium (MOE), the septal organ (SO), the vomeronasal organ (VNO) and the Grüneberg ganglion (GrG). This project focuses on the main olfactory epithelium, therefore, the SO, VNO and GrG will be briefly described in the second part of this section to provide an overview of the complexity of olfactory structures within the nose.

The mammalian main olfactory epithelium lines the roof of the nasal cavity including the septum and covering 4 endoturbinates (Fig. 1, panel A (1)) (Kara, 2004; Barrios *et al.*, 2014; Barrios, Sanchez Quinteiro and Salazar, 2014; Barrios, Sánchez-Quinteiro and Salazar, 2014; Octura, Maeda and Wakabayashi, 2018).

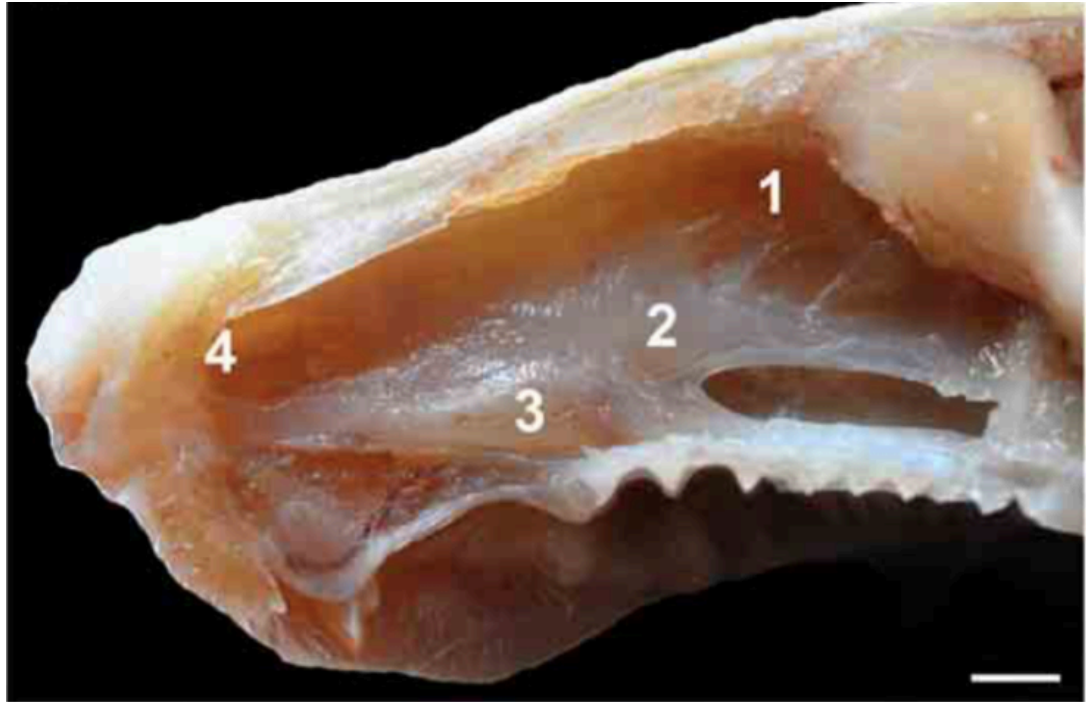
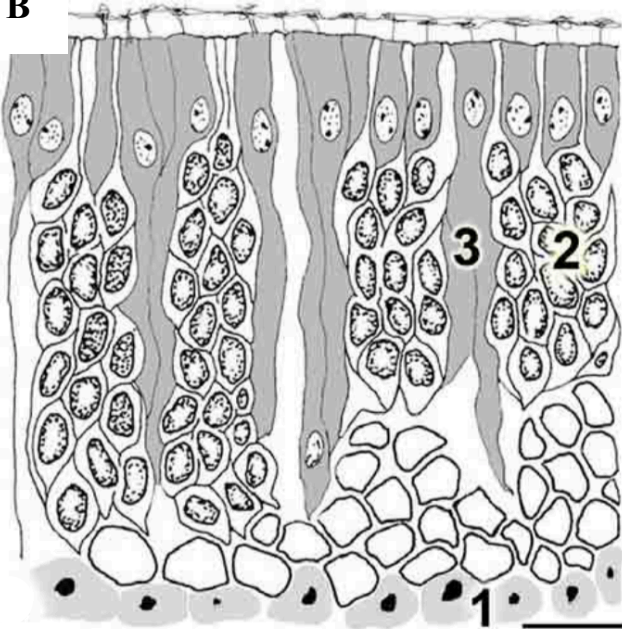
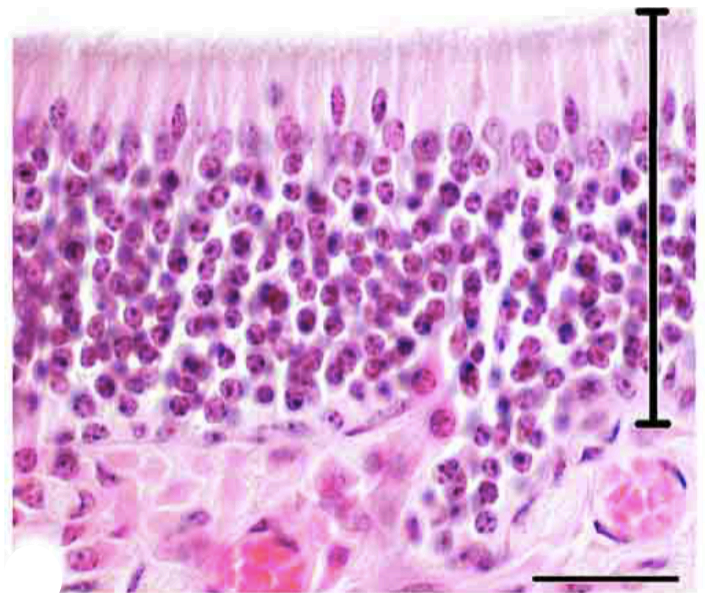
A**B****C**

Figure 1: Main olfactory epithelium located in the nasal cavity of rodents.

A: Open skull of rodent revealing the nasal cavity with the septum separating both nostrils. The main olfactory epithelium (1), the septal organ (2), the vomeronasal organ (3) and Grüneberg's ganglion (4) are identified on the medial side of the nasal cavity. Scale bar = 2 mm. (Barrios *et al.*, 2014)

B, C: Schematic drawing (B) and coronal section (C) of the main olfactory epithelium representing the 3 cell types: basal cells (1), olfactory sensory neurons (2), and supporting cells (3). Scale bar (A) = 10 μ m; scale bar (B) = 25 μ m. (Barrios *et al.*, 2014). The vertical bar in panel C represents the depth of the olfactory epithelium in adult BALB/c mice.

The thickness of this pseudostratified epithelium varies across the rostral-caudal axis and is composed of three different cell types: olfactory sensory neurons (OSN), supporting or microvillar cells (MVC), and basal cells (BC). Olfactory sensory neurons are oriented perpendicular to the surface of the MOE. OSNs present an apical dendrite finishing in a star-shaped ending, and a basal axon (Fig. 1, panels B (2), C). OSNs are further described in section I. A. 2.). Supporting or sustentacular cells are canonically considered as non-neuronal, microvillar cells that surround OSNs (Fig. 1, panels B (3), C) and are believed to provide structural support to the MOE (Miller *et al.*, 1995). However, recent observations identified diverse subpopulations of microvillar cells in the main olfactory epithelium, which may have additional functions (Montani *et al.*, 2006; Lin, Ezekwe, *et al.*, 2008). The third cell type identified in the OE is the basal cell. BCs are located proximal to the lamina propria (Fig. 1, panels B (1) & C) and serve as a cellular reservoir to ensure continuous turnover of OSNs (Brann and Firestein, 2014).

Rostral to the main olfactory epithelium is the septal organ or organ of Masera. The SO is located ventrally, close to the intranasal septum that separates the 2 nasal cavities (Fig. 1, panel A, (2)). The SO is a small chemosensory island presenting a pseudostratified organization similar to the MOE and comprising olfactory neurons, supporting cells and basal cells. Axons from olfactory neurons in the SO project to the main olfactory bulb (Giannetti, Saucier and Astic, 1992; Ma *et al.*, 2003). There is currently no general agreement regarding the role of the septal organ. However, it is believed to be involved in chemical probing and in maintenance of alert behaviour, due to its rostral localization and the increased responses to some odorants when compared to the MOE (Marshall and Maruniak, 1986). Most mammals also detect pheromones, known to be involved in mating and aggressive behaviour. This function is associated with another rostral nasal structure: the vomeronasal organ (Fig. 1, panel A, (3)) (Dulac, 2000; Dulac and Torello, 2003). The fourth neuronal olfactory structure is the Grüneberg ganglion which is located in the rostral nasal cavity, close to the nostrils (Fig. 1, panel A, (4)). Little is known about this olfactory structure besides the fact that it relays on a group of OSNs sending information to the same restricted area in the olfactory bulb (Fuss, Omura and Mombaerts, 2005; Breer, Fleischer and Strotmann, 2006).

b. Olfactory nerve

The olfactory nerve is the first cranial nerve. It comprises OSN axons originating from each neuronal somata located in the MOE and developing through the basal layer of the epithelium (Smith and Bhatnagar, 2019). Upon arrival in the lamina propria, unmyelinated OSN axons reunite in fascicles encapsulated by olfactory ensheathing cells (OECs) (Ashwell, 2012). In the olfactory nerve, OECs are arranged to form a channel, guiding axon fascicles towards the olfactory bulb (Fig. 2, panel A & B) (Garcia-Gonzalez *et al.*, 2013). The outermost part of the olfactory nerve is composed of thin olfactory nerve fibroblasts (ONF) processes surrounding OECs (Fig. 2, panel B) (Field, Li and Raisman, 2003). Both OECs and ONFs play a role in the degradation of degenerating axons and provide a frame for the development of newly formed OSN projections (Li, Field and Raisman, 2005). In humans, 15-20 olfactory nerve fascicles named fila olfactoria, cross the cribriform plate to enter into the cranial vault (López-Elizalde *et al.*, 2018). Upon its exit from the cribriform plate, the olfactory nerve progresses along the ventral side of the olfactory bulb in a meningeal compartment: the arachnoid cistern. Along its trajectory, it is joined by an olfactory artery destined to ramify and vascularize both the olfactory tract and the OB (Favre *et al.*, 1995). Vasa nervorum destined to the olfactory nerve originate directly from the anterior cerebral artery or from its ramification, the medial frontobasal artery. Finally, the olfactory nerve reaches the olfactory bulb ventrally, forming its outermost layer: the olfactory nerve layer.

c. Olfactory bulb

In mice, the olfactory bulb is divided into a caudal accessory bulb (aOB) and a rostral main olfactory bulb (Fig. 2, panel C). Although inexistent in humans, the accessory olfactory bulb receives projections from the vomeronasal organ and integrates pheromone information needed for social behaviours in rodents (Dulac and Torello, 2003; Spehr *et al.*, 2006; Mucignat-Caretta, 2010; Trotier, 2011; D’Aniello *et al.*, 2017). The main olfactory bulb (MOB), located within the anterior cranial fossa beneath the frontal lobes, receives afferent input from OSNs (Dulac and Torello, 2003; D’Aniello *et al.*, 2017; Smith and Bhatnagar, 2019). In this thesis, the denomination “olfactory bulb” (OB) will refer to the main olfactory bulb.

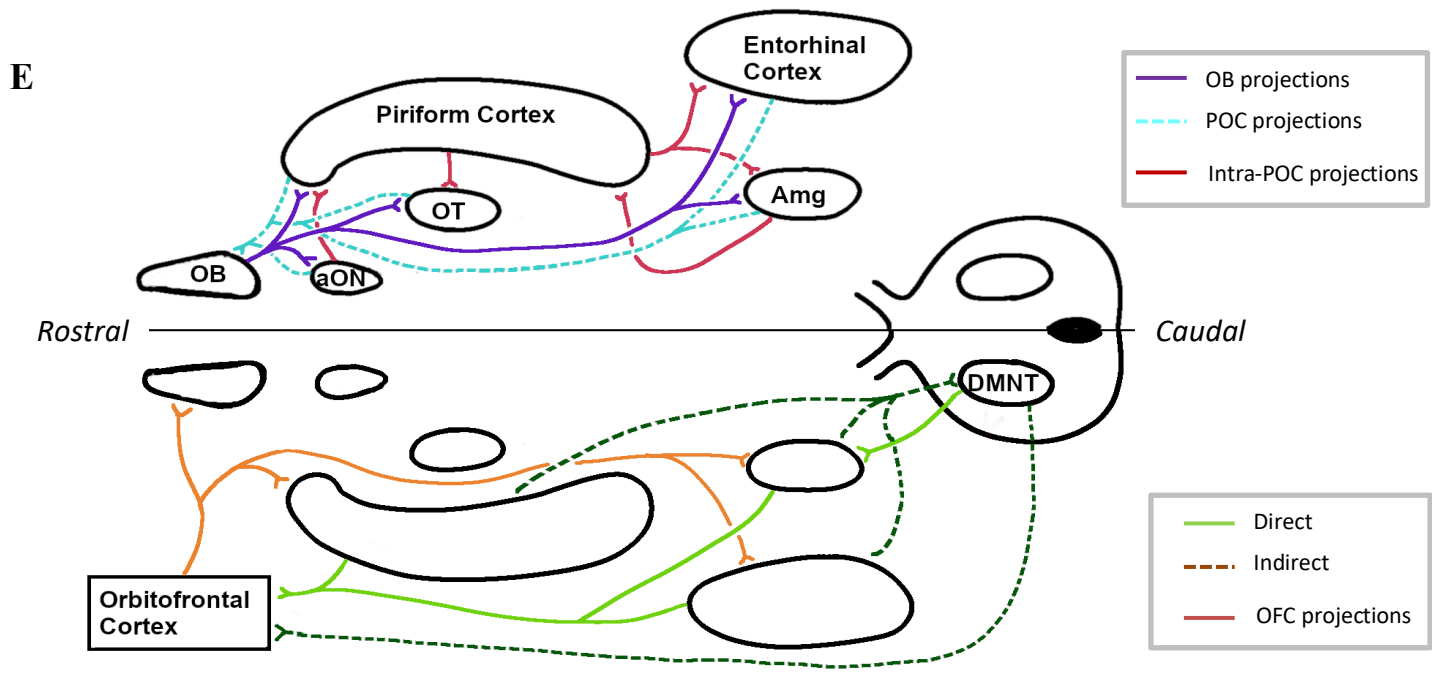
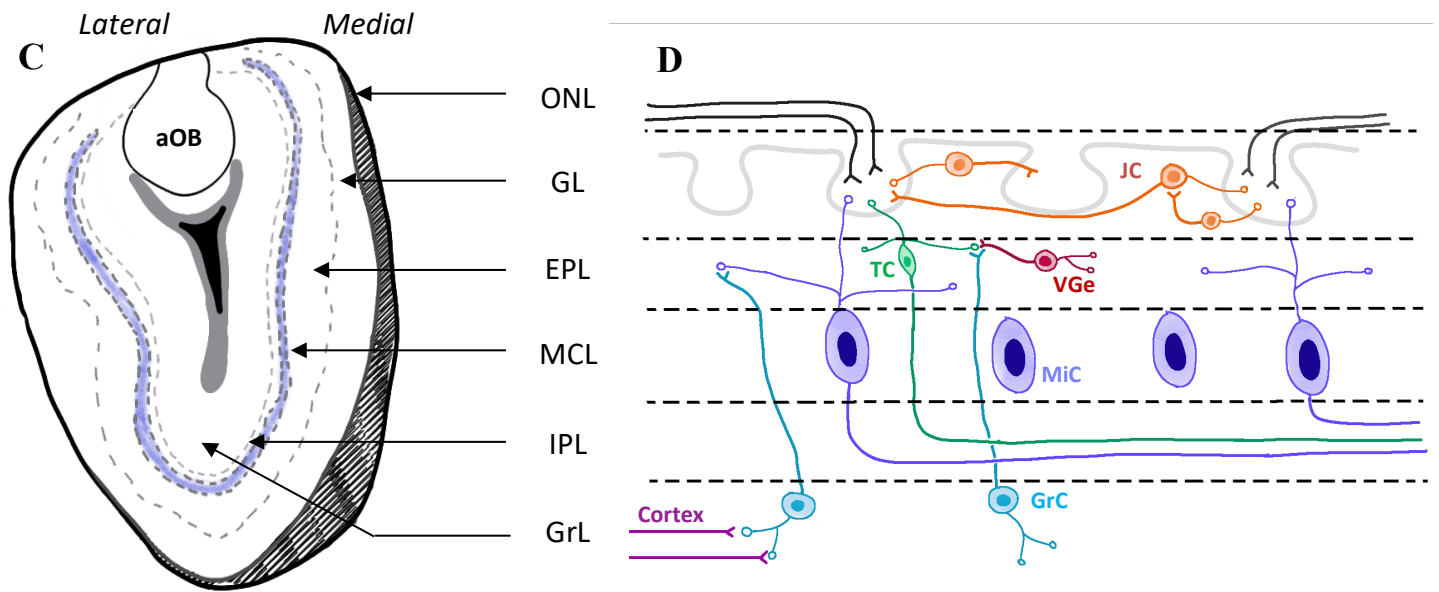
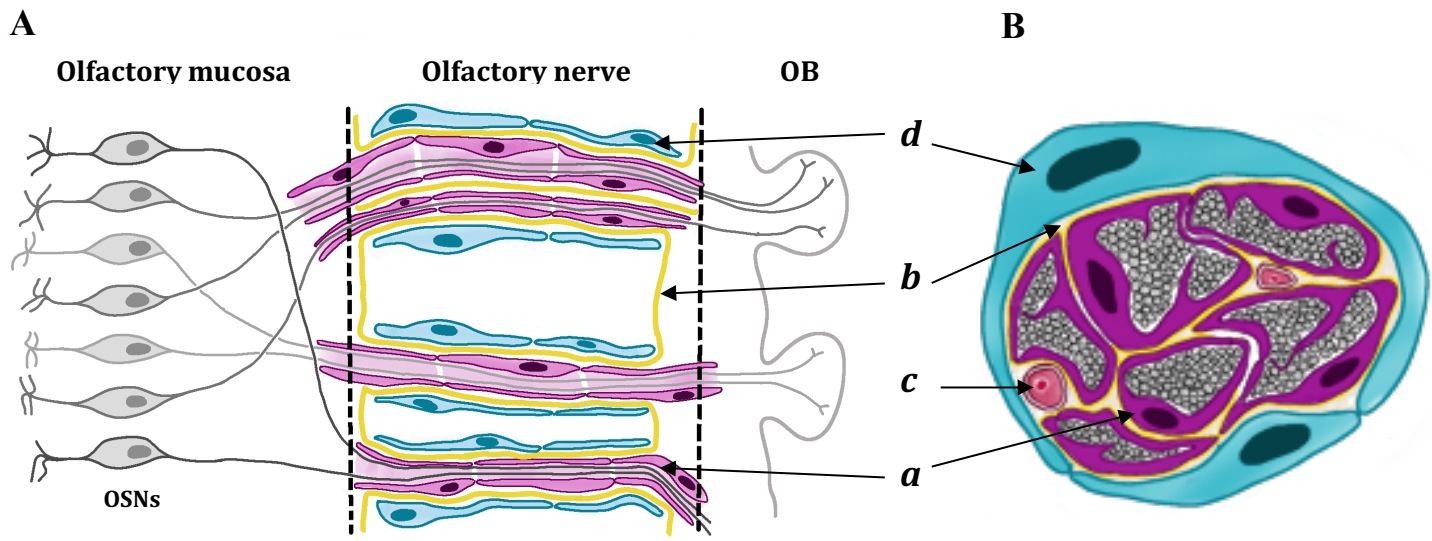


Figure 2: MOE central projections

A, B: Schematic representations of longitudinal (A) or coronal (B) sections of the olfactory nerve fascicles. OSN axons regroup in the olfactory mucosa to form olfactory nerve fascicles directed towards OB glomeruli layer. Along this trajectory, axons are surrounded by olfactory ensheathing cells (*a*) and a basal lamina (*b*). Nerve fascicles are vascularized by blood vessels (*c*) and protected by olfactory nerve fibroblasts (*d*). Adapted from Field, Li and Raisman, 2003 and Li, Field and Raisman, 2005).

C: Olfactory bulb coronal section describing the different concentric cellular layers in rodents (aOB : accessory olfactory bulb ; ONL : olfactory nerve layer ; GL : glomeruli layer ; EPL : external plexiform layer ; ML : mitral cell layer ; IPL : internal plexiform layer ; GrL : granule cell layer). Adapted from Smith and Bhatnagar, 2019.

D: Olfactory bulb cytoarchitecture. OSN axons enter the olfactory bulb through the olfactory nerve layer (ONL) to form a synapse with mitral (MiC) and tufted cells (TC) within a glomerulus. These projection neurons further transfer olfactory signals to cortical areas. Olfactory signals can be modulated at different levels within the OB. Juxtglomerular cells (JC) tune synaptic input while Van Gehuchten cells (VGe) and granule cells (GrC) directly affect projection neurons. Adapted from (Nagayama, Homma and Imamura, 2014).

E: (upper) Mitral and tufted cells comprised in the OB project to the primary olfactory cortex (OB projections) including the anterior olfactory nucleus (aON), the piriform and entorhinal cortices, the olfactory tubercle (OT) and the amygdala (Amg). These projections are reciprocal (POC projections). Adapted from Imai, 2014.

(lower) The primary olfactory cortex projects to the orbitofrontal cortex (OFC) via an indirect and a direct pathway. The OFC send reciprocal connections to the POC (OFC projections). Adapted from Illig, 2005

The cortex of the main olfactory bulb is divided in 6 concentric layers with distinct neuronal populations (Fig. 2, panel D) (Nagayama, Homma and Imamura, 2014). Odorant signals are transmitted along the olfactory nerve to arrive in the glomeruli layer (GL). This layer is composed of more than 1500 spheroid structures called glomeruli (Ennis, Hamilton and Hayar, 2007). Axons originating from OSNs expressing the same olfactory receptor converge within a single or a small group of glomeruli to establish synapses with the apical dendrites of glutamatergic projection neurons (Vassar *et al.*, 1994; Bozza and Kauer, 1998; Mombaerts, 1999; Nagayama, Homma and

Imamura, 2014). In the OB, there are two types of projection neurons: tufted cells (TC) and mitral cells (MiC). TCs cellular bodies are located within the external plexiform layer (EPL), in the direct vicinity of the glomerulus, and transmit odorant information towards the anterior part of the olfactory cortex. In comparison, MiCs display longer dendrites extending deeper in the OB, within the mitral cell layer (MCL) where cellular bodies are organized in a single line. MiCs send axonal projections to the entire olfactory cortex (Golgi, 1875; Orona, Rainer and Scott, 1984; Shepherd *et al.*, 2011; Nagayama, Homma and Imamura, 2014).

The odorant message can be modulated by different subpopulations of interneurons along the trajectory of mitral and tufted cells (Fig. 2, panel D). At the level of TCs and MiCs dendritic arbor, periglomerular (PG) and superficial short axon GABAergic interneurons (SA) inhibit the odorant signal within and between glomeruli respectively (Nagayama, Homma and Imamura, 2014). The glomerular layer also comprises glutamatergic external tufted interneurons (eTI). These cells activate both inhibitory periglomerular and superficial short axon interneurons, therefore playing an important role in the synchronization of excitatory signals received by mitral cells (Hayar *et al.*, 2004). These 3 interneuron subtypes can be reunited under the term of juxtglomerular cells (JC). OB projection neurons can also be contacted more proximal to their somata, within the external plexiform layer or the mitral cell layer. The most common GABAergic interneuron population within the OB are granule cells (GrC). GrCs present a small somata localized deep within the OB in the granule layer and send dendrites radially through the internal plexiform layer to make reciprocal contacts with mitral and tufted cell dendrites (Orona, Scott and Rainer, 1983; Nagayama, Homma and Imamura, 2014). Moreover, a smaller population of inhibitory interneurons, comprising Van Gehuchten cells (VGe) and multipolar cells, are directly located within the EPL and MCL (Kosaka, Heizmann and Kosaka, 1994; Toida *et al.*, 1994; Huang *et al.*, 2013). Altogether, these interneurons tune and synchronize the activity of projection neurons, bringing a contrast to the olfactory signal transmitted towards the primary olfactory cortex (POC).

d. Primary olfactory cortex

The primary olfactory cortex consists of an ensemble of multimodal associative brain regions receiving myelinated axon collaterals from mitral and tufted cells (Imai, 2014). It includes the

olfactory tubercle (OT) involved in odour valence, the anterior olfactory nucleus (aON) playing a role in odour localization, but also areas taking part in odour discrimination like the entorhinal (ECx) and piriform cortices (PCx), or in emotional processing like the amygdala (Fig. 2, Panel E) (Cain and Bindra, 1972; Zald and Pardo, 1997; Kikuta *et al.*, 2010; Chapuis *et al.*, 2013; Imai, 2014; Gadziola *et al.*, 2015). In contrary to other primary sensory cortices, the POC does not present any somatotopy nor chemotopy. Indeed, mitral and tufted cells, receiving input from OSNs activated by similar odorant molecules, in a defined glomerulus, extend axon collaterals over the entire POC area (Fig. 2, panel E, upper section) (Sosulski *et al.*, 2011). However, OB projections are not organized randomly. In fact, tufted cell axons originating in the EPL project preferentially to the olfactory tubercle while mitral cell axons primarily innervate the piriform cortex (Nagayama *et al.*, 2010). This difference suggests two parallel pathways processing olfactory signals arising from the OB. Moreover, similar odorants induce an activation of analogous areas within the anterior piriform cortex, indicating a chemotopy within multimodal associative regions belonging to the primary olfactory cortex (Zou, Li and Buck, 2005). OB activity can be modulated by the POC (Fig. 2, panel E, upper section).

In contrast with other sensory modalities, olfactory signalling reach the primary olfactory cortex via the lateral olfactory tract without any thalamic relay (Wilson and Rennaker, 2010; Garcia-Gonzalez *et al.*, 2013; Courtiol and Wilson, 2015). However, the dorsomedial nucleus of the thalamus (DMNT) is involved in the transmission of olfactory information to the orbitofrontal cortex (OFC), a major secondary olfactory neocortical area (Illig, 2005; Milardi *et al.*, 2017). Indeed, two paths have been described to characterize the output of the primary olfactory cortex to the OFC (Fig. 2, panel E, lower section). In the direct path, different structures comprised within the POC make direct reciprocal connexions with the OFC (Johnson *et al.*, 2000; Illig, 2005). Although this path is predominant, few axons originating in the entorhinal and piriform cortices and the amygdala are addressed to the DMNT which will then relay olfactory information to the OFC, forming the indirect pathway (Öngür and Price, 2000). This second path plays an important role in odour discrimination and hedonic valence (Zald and Pardo, 1997; Tham, Stevenson and Miller, 2011; Courtiol and Wilson, 2015). Both the indirect and direct olfactory pathways converge towards the orbitofrontal cortex which receives input from other sensory modalities, such as

gustatory or visual information and is involved in affective, memory and motivational processes (Wilson and Rennaker, 2010).

2. Olfactory signalling

a. OSN organization and structure enable an optimal detection of odorant molecules within the nasal cavity

The olfactory system can detect a wide range of odours (Bushdid *et al.*, 2014). This is made possible by the broad diversity of olfactory receptors (OR) presented by olfactory sensory neurons cilia (OCil) at the apical surface of the olfactory epithelium (Buck and Axel, 1991; Barrios *et al.*, 2014). Although the airflow circulates unevenly in the nose due to its geometry, and odorants present different solubility within the mucus layer of the MOE, both the structure and spatial distribution of olfactory sensory neurons enable an optimal detection of odorants in the inhaled air (Yang *et al.*, 2007; Scott *et al.*, 2014). Indeed, in rodents, the MOE extends in the dorsal part of the nasal cavity and caudally, on the surface of the endoturbinates (see section I.A.1.a) (Barrios *et al.*, 2014). OSNs expressing the same olfactory receptor are arranged stochastically in one of 4 large zones within the MOE, facilitating the detection of the similar volatile compound in different locations (Ressler, Sullivan and Buck, 1993). Odour probing also relies on OSN structure. Neuronal somata project a single dendrite crossing towards the apical surface of the MOE where it ends in a sensory knob from which cilia arise in a star-shaped conformation (Fig. 3, panel A) (Firestein, 2001; Ennis, Hamilton and Hayar, 2007). Molecules embedded in the mucus layer bind to olfactory receptors present on olfactory cilia, consequently activating OSNs (see section 1.A.2.b). Odorant uptake modelling in the nasal cavity of rodents have shown disparities in airflow rate (Yang *et al.*, 2007). Interestingly, MOE areas with higher airflow rate comprise OSNs with longer olfactory cilia, resulting in a bigger contact surface with odorant and increasing OSN sensitivity (Challis *et al.*, 2015). These results indicate that both the specific structure of OSN dendrites and its distribution across the MOE form an optimal odorant detection system within the nose.

b. OSN activation and transduction of an odorant signal

Human OSNs can detect more than a trillion of different volatile odorants (Bushdid *et al.*, 2014).

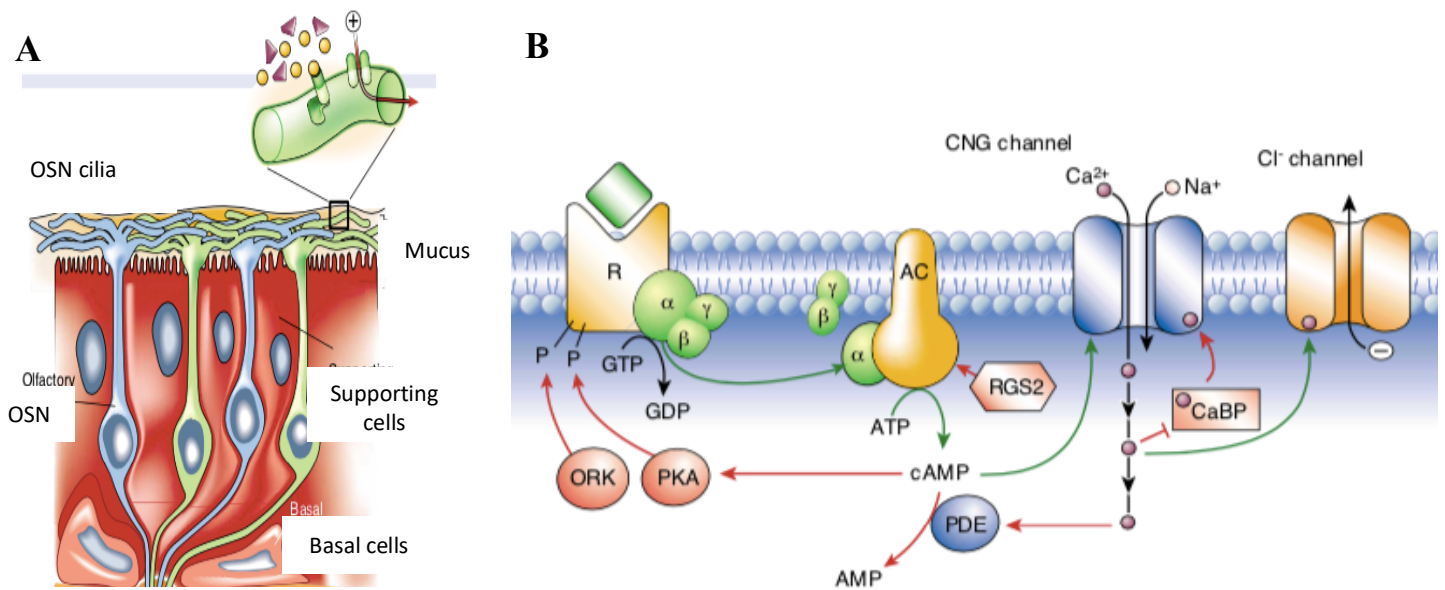


Table 1

Nav isoform	Gene (α- subunit)	TTX response	Expression in MOE	Expression in sensory ganglia	Role in action potential
Nav 1.1	SCN1A	Sensitive		A-fibers (Initial segment, Node of Ranvier)	Subthreshold depolarization
Nav 1.2	SCN2A	Sensitive	Supporting cells		
Nav 1.3	SCN3A	Sensitive	OSN (Axon)		Subthreshold depolarization
Nav 1.4	SCN4A	Sensitive			
Nav 1.5	SCN5A	<i>Resistant</i>	OSN (Sensory knob)		
Nav 1.6	SCN8A	Sensitive	Supporting cells	A-fibers (Node of Ranvier) and C- fibers (axon)	Rising phase
Nav 1.7	SCN9A	Sensitive	OSN (Axon)	A-fibers (Node of Ranvier) and C- fibers (axon)	Subthreshold depolarization, Rising phase
Nav 1.8	SCN10A / SNS	<i>Resistant</i>		A-fibers (Node of Ranvier) and C- fibers (axon, soma)	Rising phase
Nav 1.9	SCN11A	<i>Resistant</i>		A-fibers (Node of Ranvier) and C- fibers (axon, soma, terminal)	Subthreshold depolarization

Figure 3: **Olfactory sensory neuron signalling**

A: Schematic representations of OSN within the main olfactory epithelium. OSN cilia are organized in a star shape within the mucus layer. Adapted from Firestein, 2001.

B: Olfactory signal transduction following odorant binding of OSN receptors. (α, β, γ : protein G subunits ; AC : adenylyl cyclase ; ATP : adenosine triphosphate ; CaBP : calmodulin-binding protein ; cAMP : cyclic adenosine monophosphate ; CNG channel : cyclic nucleotide-gated channel ; ORK : olfactory receptor kinase ; PDE : phosphodiesterase ; PKA : protein kinase A ; R : OSN receptor ; RGS2 : regulator of G proteins). Adapted from Firestein, 2001.

Table 1: Summary of voltage-gated sodium channel expressed in the main olfactory epithelium and sensory ganglia.

This is enabled by the broad repertoire of 7-transmembrane-domain G proteins-coupled receptors expressed at the surface of OSNs dendritic endings (Mombaerts, 1999). Interestingly, each neuron expresses only a single specific olfactory receptor out of the 390 to 1000 subtypes described respectively for humans and mice (Zozulya, Echeverri and Nguyen, 2001; Zhang and Firestein, 2002; Niimura and Nei, 2003). Ligand affinity for olfactory receptors is determined by the length of their carbon chain and their three dimensional structure (Malnic, Hirono and Sato, 1999; Gaillard *et al.*, 2002; Peterlin *et al.*, 2008). Each odorant can bind to multiple ORs whereby odorant discrimination depends on the combinatorial activation of separate OSN subpopulations (Malnic, Hirono and Sato, 1999). ORs are coupled to the olfactory specific G protein Golf (Fig.3, panel B). Upon ligand activation, the α -subunit of Golf separates and activates the enzymatic protein adenylyl cyclase III, resulting in an increase of cyclic adenosine monophosphate (cAMP)(Breer, Boekhoff and Tareilus, 1990). cAMP in turn binds to and opens a cyclic nucleotide-gated ion channel (CNG) leading to an inward flux of sodium (Na^+) and calcium (Ca_2^+) ions that depolarize the dendrites (Liman and Buck, 1994; Dzeja *et al.*, 1999). The increase in intracellular calcium activates the Ca_2^+ -gated chloride channel Anoctamin2 (ANO2). Since OSNs maintain a high intracellular chloride concentration, ANO2 activation results in chloride efflux and thus further depolarization (Fig. 3, panel B) (Reisert *et al.*, 2005). With minimal electrotonic decrement,

dendritic depolarization leads to activation of voltage-gated sodium channels at the axon hillock and the generation of action potentials (Firestein, 2001). In the continued presence of odorant, Ca_2^+ is extruded from OSN dendrites via a Na^+ dependent mechanism reducing the prevailing inward currents in a form of accommodation (Fig. 3, panel B) (Reisert *et al.*, 2005). In addition to odorants, OSNs are sensitive to changes in airflow and can be activated by mechanical pressure however the molecular sensor for this has not been determined yet (Chaput, 2000; Scott, Acevedo and Sherrill, 2006; Grosmaître *et al.*, 2007).

c. Generation and transmission of an action potential in OSNs

OSNs generate action potentials (AP) through the opening of voltage-gated ion channels. Voltage-gated sodium channels (Na_v) are of primary importance for the initial depolarization phase of the AP (see section I.B.2.c) (Hodgkin and Huxley, 1952). The channel is composed of a functional α -subunit associated to one or two modulatory β -subunits (Catterall, 2000). In mammals Na_v s are encoded by 10 genes (SCN), 9 of which lead to the expression of functional voltage-sensitive channels (Catterall, 2000). In mice MOE, 5 Na_v isoforms have been identified so far, two of which, Na_v 1.2 and 1.6, in non-neuronal supporting cells (Figure 3, Table 1) (Ahn *et al.*, 2011; Bolz *et al.*, 2017). Na_v 1.7 is the predominant isoform transcript in rodent and human OSNs (Ahn *et al.*, 2011; Weiss *et al.*, 2011; Zufall *et al.*, 2012). It is expressed along the axon with Na_v 1.3. Voltage-gated sodium channels are characterized and grouped according to their sensitivity to tetrodotoxin (TTX), a poisonous compound found in the viscera, ovaries and skin of Fugu fish (Bane *et al.*, 2014). Both Na_v 1.7 and 1.3 are TTX-sensitive isoforms and contribute to olfactory AP initiation and conduction (Bolz *et al.*, 2017). Interestingly, Na_v 1.7 deletion does not impair action potential generation. However, it plays an essential role at the axon terminal for pre-synaptic release of neurotransmitter to the OB (Weiss *et al.*, 2011; Zufall *et al.*, 2012). Voltage-gated sodium channels are not restricted to the axonal portion of OSNs. Na_v 1.5, a TTX-resistant isoform, can be found in the sensory knob where it delivers a window current to regulate the threshold for excitation (Frenz *et al.*, 2014). Chapter III. A. 3 in this thesis outlines evidence for the functional identification of Na_v 1.8 in OSNs within the olfactory epithelium.

B. Trigeminal system

The trigeminal nerve is the fifth (V) cranial nerve and serves both motor and sensory functions in the head and the neck. This thesis focuses on the sensory portion of the trigeminal system. The trigeminal nerve divides distally to its ganglion into three primary branches, namely ophthalmic, maxillary and mandibular, innervating the different dermatomes in the face and underlying structures. Trigeminal sensory neurons are in most respects commensurate with somatosensory neurons in the dorsal root ganglia and can be activated by one or more sensory stimulus modality including mechanical, thermal and chemical stimuli (Al Ain and Frasnelli, 2017).

1. Anatomy

a. Trigeminal ganglion and its branches

The trigeminal ganglion (TG), also called Gasserian or semi-lunar ganglion, is present bilaterally at the base of the skull. It is enveloped in a thick dura mater layer and lies in a bone recess named Meckel's cave (Fig. 4, panel A) (Leston, 2009). The TG comprises pseudo-unipolar primary afferent neurons varying in shape and size (see section I.B.2.a.). Trigeminal neurons send a unique axon bifurcating in two collaterals towards the periphery and centrally, to the trigeminal nucleus. Projections destined to the periphery divide in 3 main branches addressed to the ophthalmic (V1), maxillary (V2) and mandibular (V3) areas of the face. The ophthalmic branch later ramifies to innervate the forehead, cornea, and dorsal aspect of the nose (Fig. 4, panel B, red) (Leston, 2009). The maxillary branch innervates the skin and underlying tissue defined between the upper lip and the lower eyelid, including the lower part of the nasal cavity (Fig. 4, panel B, blue). The mandibular branch includes a motor component for mastication, and a sensory component innervating the anterior part of the tongue, the lower lip and the chin (Fig. 4, panel B, green). Somata projecting an axon collateral within the same peripheral branch, therefore innervating similar peripheral areas, are clustered in the mediolateral and dorsoventral axis, indicating a somatotopy within the ganglion (Marfurt, 1981; Chai *et al.*, 2014; Messlinger and Russo, 2019). Trigeminal neurons are closely surrounded by a sheath of satellite glial cells (SGC), forming a functional unit embedded in connective tissue (Fig. 4, panel C) (Pannese, 2002; Vit *et al.*, 2006).

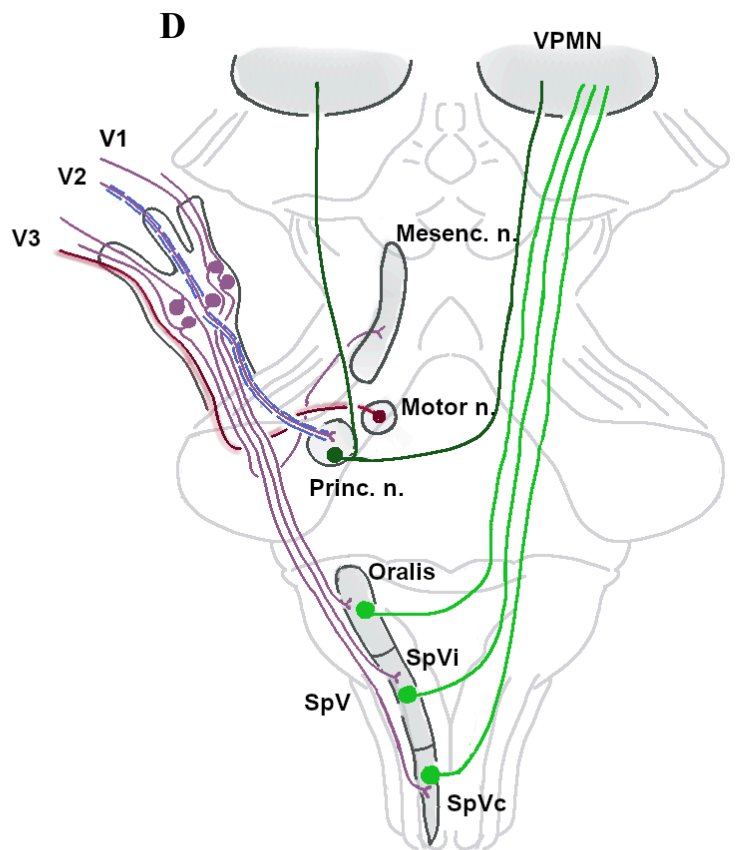
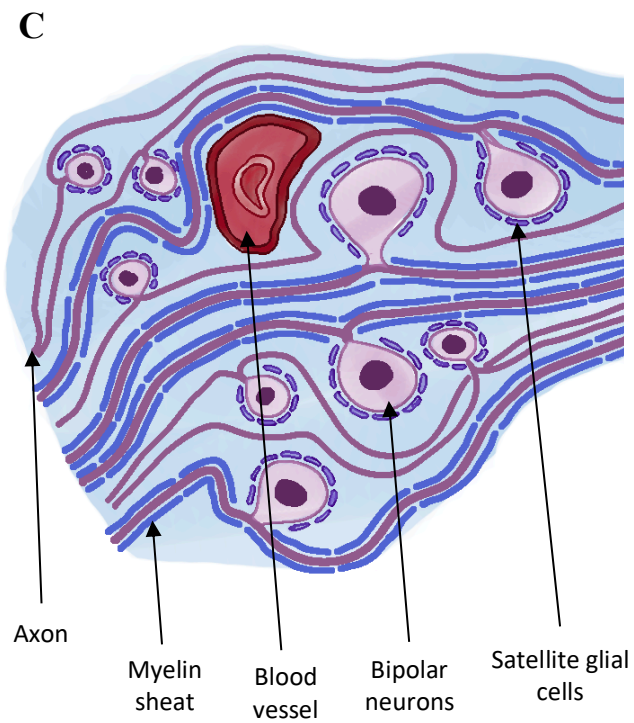
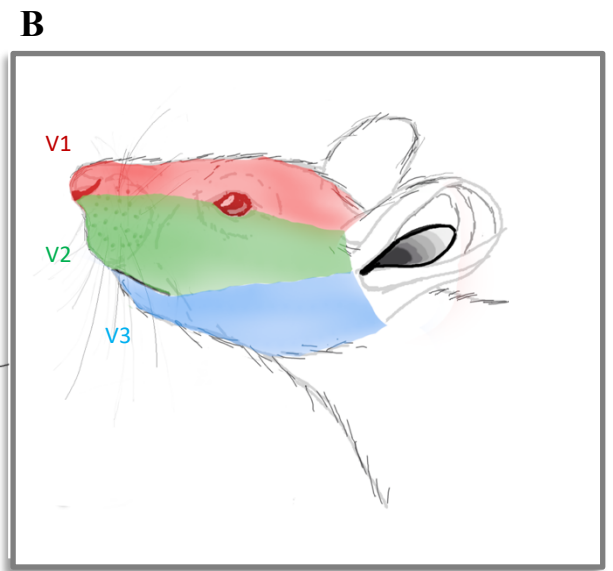
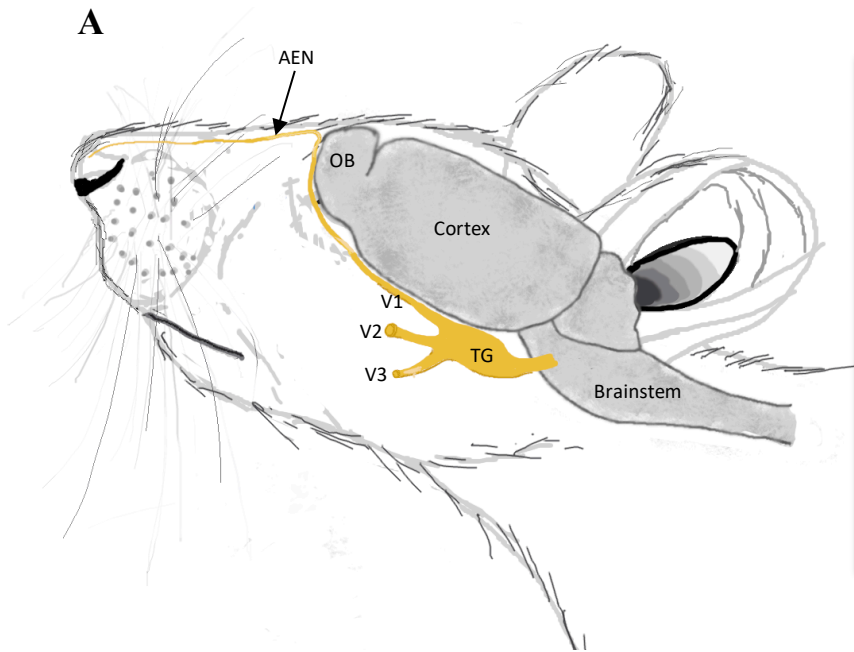


Figure 4: **Trigeminal anatomy**

A: The trigeminal ganglion is located within the Meckel's cave, at the basis of the brain. Three peripheral branches emerge from it while it is connected centrally to the brainstem. The first branch gives the anterior ethmoidal nerve which comes to innervate the nasal cavity. (AEN : anterior ethmoidal nerve ; OB : olfactory bulb ; TG : trigeminal ganglion ; V1 : ophthalmic branch ; V2 : maxillary branch ; V3 : mandibular branch). Adapted from Leston, 2009

B: Representation of a mouse face with different dermatomes innervated by each branch of the trigeminal system.

C: Composition of trigeminal ganglia. Bipolar trigeminal neuron cellular bodies are surrounded by satellite glial cells. Myelinated and unmyelinated axon fascicles can also be observed within the ganglion which is traversed by small blood vessels. Adapted from Vit *et al.*, 2006.

D: Central projections of the trigeminal ganglion are directed towards different nuclei within the brainstem which relay on the ventral postero-medial nucleus of the thalamus. (Mesenc. n. : mesencephalic nucleus ; Motor n. : motor nucleus ; Princ. n. : principal nucleus ; SpV : spinal trigeminal nucleus ; SpVc : pars caudalis of the spinal trigeminal nucleus ; SpVi : pars interpolaris of the spinal trigeminal nucleus ; V1,V2,V3 : peripheral trigeminal branches ; VPMN : ventral postero-medial nucleus of the thalamus). Adapted from Singh, 2019.

SGCs have been estimated to outnumber neurons 10 to 1 in the Gasserian ganglion (Thalakoti *et al.*, 2007). Despite the high number of these cells and their proximity to neuronal somata, SGCs do not form an impermeable barrier (Arvidson, 1979). However, these cells seem to be in constant communication with sensory neurons, notably with gap junctions, and play an important role in controlling the microenvironment within the TG (Hanani, 2005; Vit *et al.*, 2006; Thalakoti *et al.*, 2007). Trigeminal axons are wrapped in myelinating Schwann cells (SC) within and outside of the TG, enabling saltatory AP conduction and metabolic support (Maxwell, 1967; Thalakoti *et al.*, 2007; Salzer, 2015). Trigeminal axons can also be observed embedded in non-myelinating Schwann cells in sensory ganglia connective tissue and in the nerve, forming an ensemble called the Remak fibres. Remak SCs are participating to axonal regeneration following denervation or demyelination (Griffin and Thompson, 2008). The trigeminal ganglion is densely vascularized by a

network of capillaries ramifying within the connective tissue, formed of collagen and fibroblasts. Trigeminal blood supply is maintained by the middle meningeal artery, a branch of the external carotid artery (Qureshi *et al.*, 2018). In humans, several tracing experiments have also shown internal carotid artery collaterals in the close vicinity of the TG to be involved in its vascularization (Ćetković *et al.*, 2020).

b. Trigeminal innervation of the nasal cavity: the anterior ethmoidal nerve

The trigeminal ganglion divides in 3 main peripheral branches addressed to the head. The ophthalmic nerve (V1) further trifurcates into the lachrymal nerve involved in tear production, the frontal nerve directed towards the forehead skin, and the nasociliary nerve. The nasociliary nerve runs under the optic nerve, giving off a ciliary ramification to the ciliary ganglion and cornea while the other branch becomes the ethmoidal nerve. The ethmoidal nerve may divide into an anterior and posterior branch, the latter of which is not always present. The anterior ethmoidal nerve (AEN) enters the cranial vault through the anterior ethmoid foramen whereupon it gives off a collateral to innervate the dura (Panneton, Gan and Juric, 2006; McCulloch *et al.*, 2018). The AEN continues its trajectory to cross the porous cribiform plate via the cribroethmoidal foramen and enter in the nasal cavity (Patron *et al.*, 2015; Escalard *et al.*, 2019). The trajectory of trigeminal divisions leading to the anterior ethmoidal nerve is represented in Fig. 4, panel A. The AEN carries A δ - and C-fiber axons (Sekizawa and Tsubone, 1994). Anatomical reports show that the anterior part of the nasal mucosa belongs to the innervation territory of the AEN, while the nasopalatine nerve, originating from V2, gathers information from the posterior part of the nasal cavity, including the lower turbinates (Doty *et al.*, 1997; Al Ain and Frasnelli, 2017). However, recent anterograde tracing experiments observe AEN projections leaving the nerve before it reaches the cribroethmoid foramen. These branches cross the cribiform plate independently to end in the caudal part of each nasal turbinate (Maurer *et al.*, 2019). Therefore, trigeminal axons in the AEN may also innervate the olfactory epithelium overlying the turbinates.

c. Trigeminal root projections to the medullary dorsal horn

The trigeminal ganglion sends central axonal projections coalescing into the trigeminal nerve, which runs towards the cerebellopontine angle, where it penetrates the brainstem to reach

trigeminal nuclei (Fig.4, panel A). The trigeminal system comprises 4 trigeminal nuclei, two of which are receiving sensory afferents from the TG, namely the principle sensory nucleus and the spinal trigeminal nucleus (SpV). While the ganglion presents a degree of topography with axonal projections forming V1 located anteromedially and those forming V3 in the rostro lateral part of the TG, this somatotopy is not conserved for central projections in ponto-medullary trigeminal nuclei which is segregated by modality (Leston, 2009). In fact, most large caliber myelinated tactile and proprioceptive axons end rostrally in the principle sensory nucleus, while thermal and nociceptive fibers are predominantly directed caudally, to the spinal trigeminal nucleus (Fig.4, panel D) (Doty *et al.*, 1997; Hollandsworth, DiNovo and McCulloch, 2009). SpV second order neurons send contralateral projections to the ventral postero-medial nucleus of the thalamus (VPMN) via the ventral trigeminothalamic tract. A portion of principle sensory nucleus axons follows the ventral trigeminothalamic tract while the second portion is directed towards the ipsilateral VPMN (Singh, 2019).

The SpV is divided into 3 sub-nuclei along its rostro-caudal axis, respectively pars oralis, interpolaris and caudalis. The sub-nucleus caudalis is also referred to as the medullary dorsal horn (MDH) since it forms the rostral extension of the spinal dorsal horn and shares structural similarities with the cervical spinal cord (Hockfield and Gobel, 1982; Schröder, 1993). Trigeminal neurons responsible for chemesthesis, the perception of chemicals (see section I.B.2.b.iii), send ipsilateral projections to pars caudalis (SpVc) and interpolaris (SpVi) (Anton and Peppel, 1991). This observation was confirmed for nasal afferents presenting collaterals directed towards the spinal trigeminal nucleus (Schaefer *et al.*, 2002). Moreover, anterior ethmoidal nerve tracing experiments also showed axonal projections in the superficial laminae of SpVi (Panneton, Gan and Juric, 2006). The afferent pathway via the AEN to SpVc is notably involved in the modulation of breathing frequency after detection of noxious irritants (Rybka and McCulloch, 2006).

Interestingly, the trigeminal nucleus also comprises neuronal somata addressing axons directly towards the periphery. Indeed, the motor portion of the trigeminal nerve derives from motoneurons in the dorsolateral pontine motor nucleus and runs alongside V3 to ultimately fuse with the sensory root and activate facial muscles (Yousry *et al.*, 2004; Sherwood, 2005; Panneton, Pan and Gan, 2017). Proprioceptive pseudo-unipolar neurons are also localized within the

brainstem, in the mesencephalic nucleus, and receive information from extraocular and mandibular muscles via projections running along V1 and V3 (Singh, 2019).

2. Trigeminal signalling

a. Diversity of trigeminal neurons

Trigeminal neurons differentiate from the neural crest and neurogenic placode into pseudo-unipolar cells (Fig. 4, panel C) (Davies and Lumsden, 1990). Classically, this type of neuron presents a single axon leaving the cellular body before bifurcating. Due to the difficulty to image TG neurons with both projections on the same plane, some doubt still remains concerning the exact cellular classification to use (Messlinger and Russo, 2019). Human Gasserian ganglia present about 30,000 neurons and these have been classified according to their size estimated from diameter measurements (Fig. 5, Table 2) (LaGuardia, Cohrs and Gilden, 2000). Large or A-neurons are characterized by a soma diameter greater than 50 μm (Stoyanov Krastev and Apostolov, 2013). These neurons typically signal light touch via myelinated A β axons with conduction velocities ranging from 30 to 70 $\text{m}\cdot\text{s}^{-1}$ (Le Pichon and Chesler, 2014). Medium diameter A-neurons (50-30 μm diameter) also present myelinated axons albeit of small calibre, therefore called A δ -fibres, with conduction speeds ranging between 5 and 20 $\text{m}\cdot\text{s}^{-1}$. Besides large and medium diameter cells, 80% of neurons within the TG are characterized by a diameter inferior to 30 μm and called small C-fibres (Stoyanov Krastev and Apostolov, 2013). C-type neurons project unmyelinated axons with a characteristic conduction velocity below 2 $\text{m}\cdot\text{s}^{-1}$ (Le Pichon and Chesler, 2014). Although C-fibres may respond to individual chemical, thermal and mechanical stimuli, these neurons are generally activated by several stimulus modalities concomitantly applied. Small fibres can encode intensities that extend to the noxious range. For this reason, many C-fibres are referred to as polymodal nociceptors. The heterogeneity of adequate stimuli for individual C-fibres is largely due to the expression of a broad range of receptors for the transduction of sensory stimulus energies.

Table 2

Soma type	Diameter	Axon type	Conduction velocity	Myelination	Sensitivity
Large	> 50 μm	A β	30 – 70 $\text{m}\cdot\text{s}^{-1}$	Myelinated	Mechanical (light touch)
Medium	30 > ... < 50 μm	A δ	5 – 20 $\text{m}\cdot\text{s}^{-1}$	Myelinated	Mechanical Thermal
Small	< 30 μm	C	< 2 $\text{m}\cdot\text{s}^{-1}$	Unmyelinated	Mechanical Thermal Chemesthesis

B

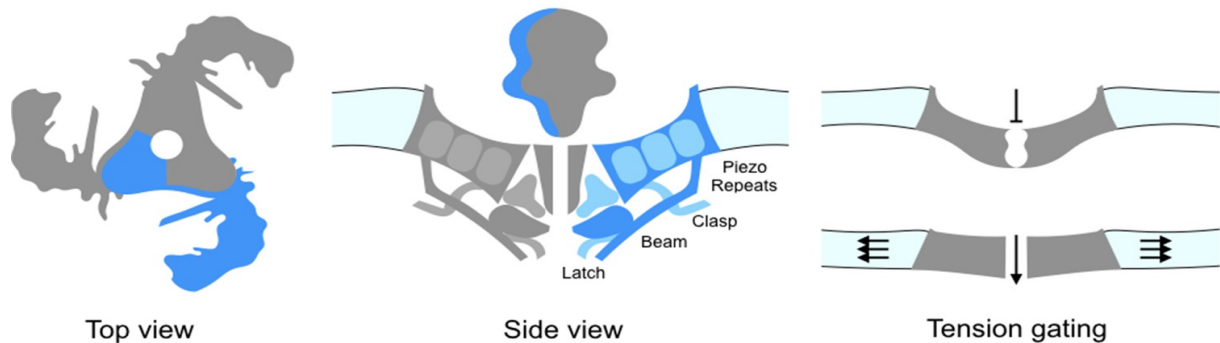


Table 3

	TRPV1	TRPM8	TRPA1
Permeability	Ca ²⁺ , cations	Ca ²⁺ / Na ⁺ , cations	Ca ²⁺ , cations
Expression	Small diameter sensory neurons	Sensory neurons Viscera	Sensory neurons Hair cells Ovaries, testis
Temperature sensitivity	> 42 °C	23 – 28 °C	< 17 °C ?
Chemesthesis (exogenous)	Capsaicin, Piperine, Cannabidiol	Menthol, Eucalyptol, Icilin	Allyl isothiocyanate, Icilin
Chemesthesis (endogenous)	Anandamide, Bradykinin		Pyrophosphate
ROS modulation (H₂O₂, NO)	Sensitive		Sensitive
pH changes	Sensitive		Sensitive

Figure 5: Trigeminal signalling

Table 2: Summary of trigeminal neurons characteristics.

B: Schematic representation of a mechanoreceptor Piezo1 including top and lateral views and the opening mechanisms described in Chesler and Szczot, 2018.

Table 3: Characteristics of 3 TRP channel transducing temperature and chemesthetic signals in trigeminal neurons.

b. Trigeminal signal transduction in primary afferents depends on specialized receptors families

The trigeminal ganglion is homologous to dorsal root ganglia (DRG). While the TG is responsible for sensations within the head, DRG neurons respond to stimuli applied to the rest of the body. Both sensory systems detect different modalities comprising tactile, thermal and chemical changes in the environment, and encode intensities from normal to the noxious range, using a broad variety of specialized receptors. Following the activation of these channels, cationic permeability increases, resulting in a depolarization of sensory neurons. This section aims to present trigeminal receptors involved in tactile, thermal, and chemical perception and their mode of action.

i. Mechanical transduction

Tactile sensation in the face is mediated by trigeminal neurons. Transduction of mechanical energy into an electrical signal requires a specific type of receptor. Recent studies revealed Piezo channels as primary mechanotransducers in sensory neurons (Coste *et al.*, 2010). This mechanosensitive channel family is highly conserved across mammalian species, with pore-forming subunits containing more than 2500 amino acids (aa) and over 14 transmembrane domains (Coste *et al.*, 2010, 2012; Kamajaya *et al.*, 2014). The Piezo channel family is permeable to cations and comprises two members in vertebrates: Piezo1 and Piezo2. Piezo1 transcripts were initially observed in visceral organs and in the skin, and have been more recently identified in small sensory neurons within the DRG and the TG (Coste *et al.*, 2010; Nguyen *et al.*, 2017; Wang, La and Hamill, 2019). The Piezo1 channel is a trimer comprising 3 blade-like subunits organized in

a propeller shape around a central pore (Saotome *et al.*, 2018). This conformation leads to a deflection in the neighbouring membrane creating a “dome-like” structure bended towards the intracellular compartment (Fig. 5, panel B). Applying a local pressure induces a tension in the membrane, causing a deformation of the dome and opening the cationic permeable pore (Guo and Mackinnon, 2017). The tridimensional conformation of Piezo2 has not been revealed yet, however, the high degree of similitude with Piezo1 aa sequence enables to reasonably predict a similar mode of activation. The second member of the Piezo channel family is predominantly found in large neurons within dorsal root ganglia and trigeminal ganglia (Nguyen *et al.*, 2017; Szczot *et al.*, 2017). Interestingly, in the periphery, Piezo2 is expressed in low threshold mechanoreceptor (LTMR) nerve endings and specialized mechanoreceptive cell-types present in the skin, such as Merkel cells (Ranade *et al.*, 2014; Woo *et al.*, 2014). The activation of Piezo2 induces rapidly adapting mechanically-activated currents in sensory neurons (Coste *et al.*, 2010). Its role has been extensively observed in transgenic mice models, revealing the importance of the channel for innocuous tactile perception, mechanical discrimination, and proprioception (Ranade *et al.*, 2014; Schrenk-Siemens *et al.*, 2015; Woo *et al.*, 2015; Chesler and Szczot, 2018). More than 15 alternative splicing of Piezo2 transcript have been found in mice TG, influencing different channel properties, such as permeability or rate of inactivation and therefore explaining the diversity of sensations perceived following the activation of the channel (Szczot *et al.*, 2017). The role of Piezo channels is not restricted to the perception of innocuous mechanical stimuli in sensory neurons. The deletion of Piezo gene in drosophila reduced responses to noxious mechanical stimuli, revealing a possible role of Piezo channels in pain perception (Kim *et al.*, 2012). New studies started to explore the nociceptive role of Piezo channels in mammals. Piezo1 has been found to be involved in nociceptive signalling in meningeal trigeminal afferents, inducing the release of calcitonine gene-related peptide (CGRP), a vasoactive compound notably involved in migraine pain states (Mikhailov *et al.*, 2019). These results, along with the distribution of both Piezo channels members in large and small sensory neurons, suggest that Piezo2 is responsible of innocuous mechanical perception while Piezo1 is involved in nociception. However, further investigations remain to be conducted to unravel the precise function of both mechanotransducers.

ii. Temperature transduction

Trigeminal sensory neurons detect changes in ambient temperature with specialized receptor belonging to the transient receptor potential channels (TRP) family (Dux, Rosta and Messlinger, 2020). TRP channels have initially been identified in *Drosophila*, further leading to the discovery of 6 TRP subfamilies in mammals and more than 50 different members (Cosens and Manning, 1969; Minke, Wu and Pak, 1975; Montell and Rubin, 1989; Clapham, 2003). TRP channels are described as non-selective cationic voltage-gated channels (VGCs) presenting a tetrameric structure. Each TRP subunit contains 6 transmembrane helices (S1 - S6). S1-S4 form the voltage sensor domain while the pore domain is composed of S5 and S6 (Kedei *et al.*, 2001; Beech, Muraki and Flemming, 2004; Gaudet, 2008). Although it is currently accepted that most TRP channels are homotetramers, the possibility to find functional channels formed by different subunits *in vivo* is still discussed (Hofmann *et al.*, 2002; Cheng, Sun and Zheng, 2010). TRP channels are polymodal transducers activated by physical stimuli such as voltage or temperature changes, and chemical stimuli (see section I.B.2.b.) (Voets *et al.*, 2004, 2005; Nilius *et al.*, 2005). TRP channel subfamilies and their principal characteristics are gathered in Figure 5, Table 3. In the TG, several thermosensitive TRP channels have been observed (McKemy, Neuhauser and Julius, 2002; Mishra and Hoon, 2010; Nguyen *et al.*, 2017). TRP vanilloid 1 (TRPV1) is the first member of TRP channels identified in mammals (Caterina *et al.*, 1997). This receptor is preferentially expressed in small-diameter sensory neurons and highly permeable to calcium ions. Alike the 6 other members of the TRPV subfamily, TRPV1 is activated by vanilloid substances, such as capsaicin (described in section I.B.2.b.iii). Moreover, noxious heat corresponding to stimuli over 42°C have been shown to activate TRPV1-positive neurons (Caterina *et al.*, 1997). In contrast, cooling temperatures ranging from 23 to 28°C induce responses in cells containing TRP melastatine 8 (TRPM8). Such cells do not co-express TRPV1 and have been identified in a different subpopulation of sensory neurons and in visceral organs such as the liver and prostate (McKemy, Neuhauser and Julius, 2002; Venkatachalam and Montell, 2007). The TG also comprises sensory neurons expressing the receptor TRP ankyrin 1 (TRPA1), characterized by numerous ankyrin repeat domains present at the cytosolic N-terminal of the protein (Laursen *et al.*, 2015). TRPA1 is the only member of the ankyrin-TRP subfamily found in mammals (Nilius and Owsianik, 2010). In

mice, this thermosensitive channel is found in sensory neurons, hair cells and reproductive organs such as ovaries and testis. It has been shown to respond to temperatures inferior to 17°C, qualified as noxious cold (Story *et al.*, 2003). However, this role does not seem to be conserved across species (Laursen *et al.*, 2015).

In 2004, a possible thermodynamic mechanism explaining the change of opening probability of TRP channels with temperature has been proposed (Voets *et al.*, 2004). As reported by this study, temperature sensitivity is dependent on a significant difference between the activation energies (E_a) associated with channel opening ($E_{a\text{ open}}$) and closing ($E_{a\text{ close}}$). E_a variation is positively correlated with temperature changes. Therefore, high temperatures result in important E_a values. Most voltage-gated channels present equivalent E_a for opening or closing channels. However, heat sensitive channels such as TRPV1 require more energy to be opened than to be closed. The increase in temperature results in a greater the E_a , pushing the channel towards the open state. Accordingly, TRPV1 channels are more likely to open with warm temperatures. In contrary, TRPM8 channels require more energy to be closed. Thus, the opening probability of the channel decreases with warming, suggesting that TRPM8 is activated at lower temperatures (Voets *et al.*, 2004). TRP channels are VGCs, indicating that the opening state of the channel is also dependent on the membrane potential. Temperature changes in the cellular environment might thus shift the voltage threshold towards more physiological membrane potential, facilitating their activation by smaller voltage changes (Voets *et al.*, 2005).

iii. Chemical transduction (Chemesthesis)

Chemical detection is termed chemesthesis and is notably involved in sensory processes such as olfaction and gustation. The trigeminal system is notably involved in the encoding of a specific property of odorants and tastants called pungency. Pungency ranges from mild sensation of tingling to painful biting and sharp irritation (Viana, 2011; Nilius and Appendino, 2013). In contrast with olfactory sensory neurons, using metabotropic channels to detect chemical stimuli (see section I.A.2.b), trigeminal chemesthesis is dependent on TRP channels. In fact, many members of the TRP channel family, including the 3 thermosensors described previously, respond to exogenous or endogenous chemical substances (Voets *et al.*, 2004; Venkatachalam and Montell, 2007). TRPV1 is a canonical example used to explain TRP channel-related chemesthesis. Capsaicin,

a vanilloid substance extracted from hot chili peppers, was found to selectively activate TRPV1, resulting in a burning painful sensation, and therefore explaining the thermal “hot” component perceived in spicy food (Caterina *et al.*, 1997). The TRPV1 agonist has been reported to modulate the opening probability of the channel with the same thermodynamic mechanism described temperature detection (see I.B.2.b.ii) (Voets *et al.*, 2004). The comparison of TRPV1 protein sequences in different species presenting distinct sensitivities to hot chili peppers revealed the importance of the linker between transmembrane helices S2 and S3 in capsaicin binding (Jordt and Julius, 2002). Further in vitro experiments showed that the vanilloid compound is buried within the receptor, in a pocket formed by S3, S4 and the linker between S4-S5 (Gavva *et al.*, 2004). Capsaicin interacts with the S4-S5 linker, pulling the attached S6 transmembrane helix away from the pore, resulting in the opening of the activation gate (Yang *et al.*, 2015). The capsaicin binding domain is similar to the ligand-binding domain in TRPM8, suggesting that the mechanism explained above might be conserved between several members of the TRP channel family (Chuang, Neuhausser and Julius, 2004).

Chemesthetic TRP channels are bound by a multitude of chemicals eliciting different sensations which are listed in Fig. 5, Table 3. Besides vanilloid compounds, TRPV1 is activated by pungent substances like piperine, extracted from black pepper, but also by cannabidiol, which probably leads to a desensitization of the receptor (Bisogno *et al.*, 2001; McNamara, Randall and Gunthorpe, 2005). TRPM8 responds to several plant-derived substances like menthol or eucalyptol, which are found in a range of cosmetics and oral hygiene products, mimicking the sensation of cooling and freshness (Laska, 2001). However, the synthetic component icilin has proven to be 200-fold more potent to activate the cold receptor (Wei and Seid, 1983). Alike TRPM8, TRPA1 is involved in cold perception (Story *et al.*, 2003). Therefore, it is not surprising to observe that icilin is also able to activate the ankyrin receptor. Although, TRPA1 is also responsible for sensations elicited by compounds such as allyl isothiocyanate, also known as mustard oil, which confers wasabi its pungency and ability to evoke sensations of heat (Jordt *et al.*, 2004). Aside from their role probing the environment for thermal or chemical stimuli, TRP channels can be modulated by endogenous substances, notably during inflammatory processes. Endogenous products of inflammation sensitize TRPV1, resulting in heat allodynia, a phenomenon

characterized by painful sensation elicited by innocuous stimuli, and hyperalgesia, described as an exaggerated response to noxious stimuli (Davis *et al.*, 2000). Alike the endocannabinoid lipid anandamide, bradykinin, a pro-inflammatory mediator, generates a cascade of reaction leading to the activation of the protein kinase C (PKC). PKC further phosphorylates TRPV1, lowering its temperature threshold required to open the channel and therefore sensitizing the channel (Premkumar and Ahern, 2000; Mizumura *et al.*, 2009). Different inflammation processes are affected by oxidative stress (Lugrin *et al.*, 2014). Several studies have been focusing on the product of oxidative stress, called reactive oxygen species (ROS). Two ROS of particular interest are oxygen peroxide (H_2O_2) and nitric oxide (NO), which have been shown to oxidize cysteine residues at the amine-terminal region of TRPV1 and TRPA1, facilitating their activation (Yoshida *et al.*, 2006; Andersson *et al.*, 2008; Miyamoto *et al.*, 2009). The chemesthetic transduction mechanisms of TRP channel can be elicited by exogenous and endogenous substances. However, another population of ionic voltage-gated channels are responsible of the transmission of action potentials along trigeminal sensory neurons.

c. Signalling along trigeminal axons: the role of voltage-gated sodium channels

Alike OSNs, trigeminal neurons require voltage-gated sodium channels (Na_v) for the propagation of action potentials along their axons (Hodgkin and Huxley, 1952; Puil and Spigelman, 1988; Cardoso and Lewis, 2018). The importance of these channels in action potential generation and their involvement in pain processes is has been extensively studied (Bennett *et al.*, 2019). Na_v isoforms are highly expressed in sensory neurons comprised in trigeminal and dorsal root ganglia. Several studies have investigated transcriptomic differences between these two systems and confirmed previous functional and immunohistochemical data indicating a significant expression of Na_v 1.1 and Na_v 1.6 - 1.9 in sensory neurons (Manteniatis *et al.*, 2013; Lopes, Denk and McMahon, 2017). Interestingly, RNA sequencing data revealed an increased number of transcripts for Na_v 1.6 in trigeminal neurons. Voltage-gated channel isoforms are divided in two groups depending on their sensitivity to tetrodotoxin (see section I.A.2.c). Na_v 1.1-1.4 and 1.6-1.7 are TTX-sensitive (TTX-S) while Na_v 1.5, 1.8 and 1.9 are resistant to the toxin (TTX-R). A summary of voltage-gated sodium channel properties can be found in Fig. 3, Table 1.

i. Voltage-gated sodium channels TTX-sensitive

TTX-S Na_v s present fast activation and inactivation kinetics and relatively low thresholds compared to TTX-R Na_v s (Roy and Narahashi, 1992; Gold, 2005). Na_v 1.1 is preferentially found in myelinated A-fibres at the axon initial segment or in node of Ranvier where it plays a role in the amplification of subthreshold stimuli taking part in the generation of an action potential (Leterrier *et al.*, 2010; Osteen *et al.*, 2016; Meents *et al.*, 2019). Two other sensory voltage-gated sodium channels, Na_v 1.6 and Na_v 1.7 have also been described at the node of Ranvier in A-fibres, however they can also be found along C unmyelinated axons and at the peripheral nerve terminal, notably found in the skin (Black *et al.*, 1996; Caldwell *et al.*, 2000; Black and Waxman, 2002). Na_v 1.6 activation contributes to the rising phase of the action potential (Bennett *et al.*, 2019). This channel is characterized by a faster recovery, enabling neurons to fire at high frequency (Herzog *et al.*, 2003). In contrast, due a slower inactivation, Na_v 1.7 is particularly adapted to create a ramp current. Alike Na_v 1.1, the seventh isoform has been suggested to amplify subthreshold depolarizations, increasing the probability to create an action potential (Herzog *et al.*, 2003). Recently, this role has been contrasted by electrophysiological data showing an increased neuronal response with unchanged subthreshold depolarization following the mutation of Na_v 1.7 in cells derived from inherited erythromelalgia patient sample (Meents *et al.*, 2019). These results imply that Na_v 1.7 also takes part in the rising phase of the AP.

ii. Voltage-gated sodium channels TTX-resistant

TTX-resistant Na_v s have been found in trigeminal endings within the cornea and the dura (Brock, McLachlan and Belmonte, 1998; Strassman and Raymond, 1999). Na_v 1.8, previously called sensory neuron specific (SNS), is present in most small nociceptive neurons, unmyelinated axons, and about half of the myelinated A-fibres originating in the DRG and TG (Bongenhielm *et al.*, 2000; Black and Waxman, 2002; Shields *et al.*, 2012). SNS current are considered to be the main contribution to the rising phase of the action potential (Bennett *et al.*, 2019). Na_v 1.8 is characterized by slow kinetics of activation and inactivation and a short repriming phase, enabling axons to adapt to high frequency firing rates (Blair and Bean, 2003). Alike Na_v 1.8, the ninth isoform is expressed in small diameter neurons, preferentially in non-peptidergic nociceptors (Dib-Hajj *et al.*, 2002; Fang *et al.*, 2002). This isoform can be found in the soma, at nodes of Ranvier

in A β and A δ fibres, along unmyelinated axons and in terminals of ophthalmic, maxillary and mandibular branches of the trigeminal system (Fjell *et al.*, 2000; Padilla *et al.*, 2007). SCN11A is the human gene encoding Nav 1.9 α -subunits. SCN11A^{-/-} cells generate action potentials with similar properties than wild type cells, however, more current was required to reach the AP threshold (Priest *et al.*, 2005). These results suggest that Nav 1.9 plays a role in increasing of the subthreshold depolarization leading to an AP.

iii. Voltage-gated sodium channels and pain

Navs are one of the main components generating action potentials in sensory and nociceptive neurons. Chemical substances have been used to activate these channels and study their effect on pain behaviours. A selective tarantula toxin for Nav 1.1 notably helped to reveal the implication of this channel in mechanical hypersensitivity (Osteen *et al.*, 2016). Similarly, the role of Nav 1.6 in chemotherapy-induced cold allodynia in A-fibres was observed using the anti-cancer drug oxaliplatin (Sittl *et al.*, 2012). In pathological states, pain can result from structural, functional and expression level changes in different Nav isoforms. For example, Nav 1.3 is transiently expressed in sensory neurons during embryonic stages before disappearing in adults (Waxman, Kocsis and Black, 1994; Rush *et al.*, 2006). Following nerve injury, the expression of transcripts from the Scn3A gene, encoding the α -subunit of Nav 1.3, is upregulated in rat trigeminal primary afferents, coinciding with the apparition of mechanical pain (Liu *et al.*, 2019). In contrast, knocking down the Scn3A gene in DRGs results in a decrease in mechanical allodynia after spared nerve injury, confirming the role of Nav 1.3 in pain behaviours (Samad *et al.*, 2013). Similarly, nerve injuries lead to an increase in the expression of the TTX-resistant channel Nav 1.8 in surrounding healthy axons (Zhang *et al.*, 2004). This increase has also been described in unmyelinated and myelinated fibres after inflammation and confirmed by the application of inflammatory mediators such as prostaglandin E2, tumour necrosis factor α or interleukin-1 β which induced the activation of Nav 1.8 (Gold *et al.*, 2002; Coggeshall, Tate and Carlton, 2004; Jin and Gereau IV, 2006; Binshtok *et al.*, 2008). Transgenic mice models have revealed an implication of SNS channels in mechanical and thermal hyperalgesia (Akopian *et al.*, 1999). Interestingly, Nav 1.8 seems to ensure pain perception in a cold environment since it is still active in nociceptors at low temperatures (Zimmermann *et al.*, 2007). In consideration of the expression of SNS in peripheral nociceptors

and its association with mechanical and thermal hypersensitivity, Nav 1.8 appears to be a reliable target to modulate pain (Djouhri *et al.*, 2003; Bennett *et al.*, 2019). Important efforts have been made to find a specific inhibitor for this channel. Although poorly soluble in water, A-803467 selectively binds to Nav 1.8, mimicking local analgesic effects in neuropathic and inflammation pain models (Jarvis *et al.*, 2007; Scanio *et al.*, 2010). Several studies have been conducted on A-803467 with the aim to modify its chemical structure and increase its solubility in aqueous solutions without losing the analgesic properties of the initial compound, therefore making it a good candidate to treat painful pathologies (Scanio *et al.*, 2010). The second member of TTX-resistant voltage-gated sodium channels, Nav 1.9, is involved in thermal and spontaneous pain behaviour after injury (Priest *et al.*, 2005). Sodium currents elicited by this channel have been shown to increase in presence of an inflammatory soup comprising bradykinin, histamine, prostaglandin E2 and norepinephrine, partially explaining the hypersensitivity observed during inflammation (Amaya *et al.*, 2006; Maingret *et al.*, 2008). Moreover, some peripheral neuropathies can be linked to mutations in the Nav 1.9 gene SCN11A (Han *et al.*, 2015). Notably, three mutations have been described on S4-S6 transmembrane domains, leading to a hyperpolarization of the activation threshold, a slowed deactivation and an increase of firing frequency in cultures neurons (Huang *et al.*, 2014).

Loss of function mutations have also been described for Nav 1.7, encoded by the gene SCN9A. Indeed, this channel has largely been studied to explain phenotypes such as congenital insensitivity to pain (Cox *et al.*, 2006; Goldberg *et al.*, 2007; McDermott *et al.*, 2019). Conditional knock out of SCN9A in sensory Nav 1.8-positive neurons resulted in reduced responses to complete Freund adjuvant (CFA)-induced inflammation, including thermal and mechanical allodynia (Nassar *et al.*, 2004). This effect was confirmed in global knock out mouse line (Gingras *et al.*, 2014). In sciatic nerve chronic constriction injury models, Nav 1.7 expressed in different neuronal populations was also responsible of the development of cold and mechanical allodynia (Minett *et al.*, 2014). These studies validate Nav 1.7 as an undeniable target for the treatment of pain.

d. CGRP, a neuropeptide released by trigeminal neurons

The role of C-fibre neurons extends beyond simple detection and signalling of impending and overt damage and includes the mediation of an immediate efferent response to noxious insult. This manifests in the synthesis and release of sensory neuropeptides from C-fibre nerve terminals in response to strong stimuli. Calcitonin gene-related peptide (CGRP) is a 37 amino acid sensory neuropeptide expressed (Lopes, Denk and McMahon, 2017) and released by A δ - and C-trigeminal fibres (Maggi, 1995). CGRP is a potent vasodilator (Meng *et al.*, 2009) and mitogen that flushes and initiates an immune response in an injured area (Holzmann, 2013). CGRP-positive neurons and fibres have been identified in the nasal epithelium, trigeminal ganglion and SpV (Finger *et al.*, 1990; Kageneck *et al.*, 2014). In the TG, 70% of neurons co-express TRPV1 and CGRP (Silver, Farley and Finger, 1991; Price and Flores, 2007). CGRP has recently been identified as pivotal mediator of some forms of intense migraine and the development of anti-CGRP strategies has found substantial clinical success in the treatment of migraine (Goadsby, Edvinsson and Ekman, 1990; Durham and Masterson, 2013).

C. Interaction between olfactory and trigeminal systems

Trigeminal afferents and olfactory sensory neurons reside in parallel in the nasal cavity. This raises the possibility of interactions between these two chemical detection systems under both normal physiological and pathological conditions.

1. Congenital insensitivity to pain: Nav1.7 links olfaction and nociception

Congenital insensitivity to pain (CIP) is a pathological condition first described in 1932 by Van Ness Dearborn (Van Ness Dearborn, 1932). CIP is characterized by a dramatic phenotype with an apparent lack of pain perception and absence of protective reflexes resulting from nociceptive stimuli. Recently, genome sequencing of CIP patients led to the identification of nonsense mutations in the SCN9A gene encoding Nav 1.7 (Cox *et al.*, 2006). Three mutations in SCN9A, leading to truncation of the Nav 1.7 α -subunit were reported by Cox *et al.* and have since been extended in other patients (Ahmad *et al.*, 2007; Goldberg *et al.*, 2007). Interestingly, patients with nonsense Nav 1.7 mutations also suffer from anosmia (Weiss *et al.*, 2011). Indeed, when asked to

perform a 40-item UPSIT odour detection task, CIP patients were unable to recognize volatile compounds. Experiments in mice lacking Na_v 1.7 specifically in OSNs showed the olfactory neurons can generate action potentials but cannot release glutamate from their pre-synaptic terminals in the olfactory bulb (Zufall *et al.*, 2012). In the nose, both OSNs and C-fibre trigeminal nociceptors require functional Na_v 1.7 to relay olfactory and nociceptive signals (McDermott *et al.*, 2019). This double pain and olfactory phenotype indicates a common feature between nociceptive and olfactory systems at the molecular level (Zufall *et al.*, 2012) and could underlie possible interactions between these two systems.

2. Dual detection of volatile compounds in the nose

Trigeminal neurons innervate the respiratory and olfactory epithelia in the nasal cavity (Finger *et al.*, 1990; Patron *et al.*, 2015). Psychophysical experiments in humans indicate that the detection and identification of volatile compounds relies on both systems being functional within the nose (Doty, 1975). In an article from 1978, Doty *et al.* ranked the trigeminal and olfactory potency of range of chemical compounds. Compounds that were described as “pungent” were taken to indicate trigeminal activation while lack of pungency was taken to indicate olfactory potency (Doty *et al.*, 1978). Confirmation of this ranking was provided by anosmic patients who were only able to detect substances with non-zero pungency. More recently, imaging techniques involving functional magnetic resonance have been used to localize brain structures activated during chemical stimulation in the nasal cavity. Normosmic people have shown a difference in cortical areas activated following intranasal stimulation by phenylethyl alcohol and CO_2 , a mix of substances activating both olfactory and trigeminal systems, when compared to their individual components (Boyle *et al.*, 2007). In a study published later, the odorant vanillin and the trigeminal irritant CO_2 were tested on normosmic people, both inducing an increase in blood flow in the operculo-insular cortex (Lötsch *et al.*, 2012). Similar studies have been repeated with piperine and pepper essential oil, respectively the pungent and odorant components of black pepper. The insula was identified as a brain area activated by both compounds in normosmic participants, corroborating previous experiments (Han *et al.*, 2018). In addition, cortex activity was observed

within the secondary somatosensory cortex and the thalamus. These results suggest an interaction between trigeminal and olfactory systems at the level of perception, within the brain.

3. Trigeminal signals modulate olfactory perception

The possibility of cross-modal interaction between somatosensory and olfactory systems has been discussed for several decades, focusing on the modulation of olfactory signals by trigeminal afferents. Initial observations shown a reduced OSN activity after antidromic stimulation of the ophthalmic branch of the trigeminal in the frog (Bouvet *et al.*, 1987). In contrast, trigeminal inhibition by a local anaesthetic enhanced odorant-evoked responses in the mediodorsal thalamus of rats (Inokuchi, Kimmelman and Snow, 1993). A similar effect has been reported in human subjects, displaying impaired olfactory abilities and an increase of the detection threshold for the pure odorant phenylethyl alcohol, exhaling a rose-like fragrance, when presented in combination with increasing concentrations of the trigeminal agonist CO₂ (Daiber *et al.*, 2013). The modulation of olfactory signals by trigeminal afferents might involve the release of CGRP in the nasal cavity. Indeed, the application of the peptide on the MOE reduced significantly electro-olfactogram responses recorded from OSNs during odorant stimulations (Daiber *et al.*, 2013; Genovese *et al.*, 2017). While it seems likely that nociceptive trigeminal activation affects olfactory signalling, whether a reciprocal cross-talk might occur has not been explored yet. In this thesis aims to characterize and document sites and mechanisms of structural and functional influences of olfactory sensory neurons activation on trigeminal nociceptive signalling.

II. Material & Methods

A. Animals

Animal housing and management were taken care of by the animal facility of the Centre for biomedicine and technology of Mannheim (CBTM, Mannheim, Germany). Mice had access to food and water ad libitum and cages were placed in a room with a 12h light/dark cycle. Behavioural tests were performed in the Interdisciplinary Neurobehavioral Core (INBC, Medizinische Fakultät,

Heidelberg, Germany) in collaboration with Dr. Claudia Pitzer. All procedures were realized in accordance with the Animal welfare guidelines as stipulated by the Federal Republic of Germany (approval number: 35-9185.81/G-104/16).

1. Wild type mice

Ten weeks old male C57BL/6 N mice were ordered from Charles River (Paris, France) and acclimatized in the animal facility for a week. Wild type mice with body weights between 25 and 32 g were used for behavioural tasks, immunohistochemical labelling of the transient receptor potential channel ankyrin1 (TRPA1), and electrophysiological recordings of trigeminal afferences within the nose.

2. Transgenic mouse lines

a. Reporter lines

Trigeminal anatomical structures were identified using two transgenic mouse lines. TRPM8-eGFP mice were provided by Dr. David D. McKemy (University of Southern California, San Diego, USA). Heterozygous TRPM8-eGFP mice express the enhanced green fluorescent protein (eGFP) from the locus for the transient receptor potential melastatine 8 (TRPM8) on one allele (Dhaka *et al.*, 2008). In addition, B6.Cg-Gt(ROSA)26Sortm9(CAG-tdTomato)Hze/J Tg(Scn10a-cre)1Rkun transgenic mice, abbreviated *Scn10a-Cre:tdTomato* mice were kindly provided by Dr. Rohini Kuner (University of Heidelberg, Heidelberg, Germany). Animals from this line express a Cre-recombinase under the *Scn10a* promoter encoding sodium channel isoform Na_v 1.8 (Agarwal, Offermanns and Kuner, 2004). To establish this mouse line, *Scn10a-Cre* mice were crossed with *Rosa26-tdTomato* mice expressing the tdTomato reporter preceded by a STOP cassette and flanked by loxP sites, under the ubiquitous promoter Rosa 26. In cells expressing the sodium channel Na_v 1.8, such as sensory neurons, Cre-mediated recombination removes the STOP cassette, enabling the expression of Td-Tomato reporter.

b. Optogenetic mouse line

Recordings after optogenetic stimulation were realized on OMP-hChR2Venus mice (Genovese *et al.*, 2016) kindly provided by Dr. Thomas Bozza (Northwestern University, Evanston, IL, USA).

Animals from this transgenic mouse line are heterozygous and express the light-sensitive channel Rhodopsin2 (ChR2) under the promoter for the olfactory marker protein (OMP). OMP is observed in mature olfactory sensory neurons (OSNs). This neuronal subpopulation is therefore photoactivable in OMP-hChR2Venus mice. In addition, the reporter Venus yellow fluorescent protein was fused to ChR2, enabling the identification of photosensitive OSNs within the olfactory epithelium (Li *et al.*, 2014).

B. Human participants

1. Control subjects

Four control subjects were participating to psychophysical olfactory tests. Two participants named F1 and M1, were evaluated in China in collaboration with Dr. Roman Rukwied and under the supervision of Prof. Xianwei Zhang (Department of anaesthesiology, Tongji Hospital, Tongji Medical College, Huazhong University of Science and Technology, Wuhan, China). F1 and M1 were the parents of 2 patients suffering from congenital insensitivity to pain disorders (described in section II. B. 2.a - c.). Another part of the experiment took place in Germany where a 32 year-old man and a 27 year old woman were evaluated in the Centre for biomedicine and medical Technology of Mannheim (CBTM, University of Heidelberg, Mannheim, Germany).

2. Patients

Three patients displaying different degrees of insensitivity to pain were also part of the psychophysical study. All of them had been previously identified by Prof. Xianwei Zhang (Department of anaesthesiology, Tongji Hospital, Tongji Medical College, Huazhong University of Science and Technology, Wuhan, China) in collaboration with Prof. Dr. Angelika Lampert (Physiology Institute, Uniklinik RWTH Aachen university, Aachen, Germany).

a. Congenital insensitivity to pain

Patients suffering from congenital insensitivity to pain display an inability to perceive normal painful stimuli (Van Ness Dearborn, 1932).

A

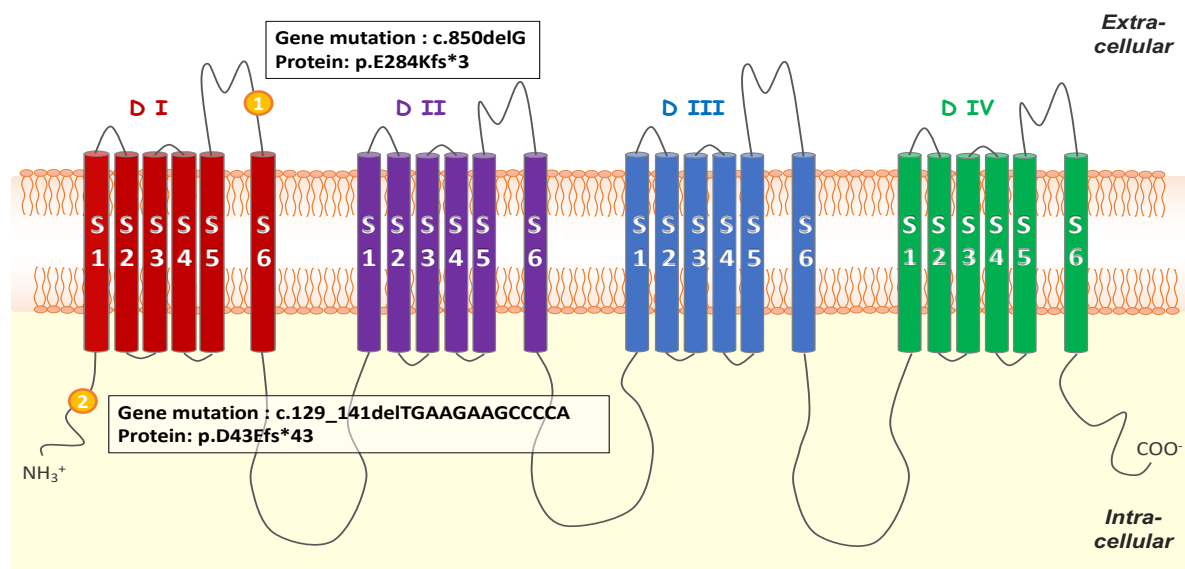


Table 4

Falcon tube number	Substance	Concentration	Company	Product n°	Characteristics	Vapor pressure at 25 ± 1°C (mm Hg) (Source)
1	Ammonium Bicarbonate	1M	Carl Roth (Karlsruhe, Germany)	T871.2	Volatile irritant	58.9 (HSDB)
2	Phenylethyl alcohol	pure	Sigma-Aldrich (Darmstadt, Germany)	77861	Volatile odorant (rose smell)	8.68 x 10 ⁻² (HSDB)
3	Cyclohexanone	pure	Sigma-Aldrich (Darmstadt, Germany)	398241	Volatile irritant (TRPV1 agonist)	5.2 (HSDB)
4	Cyclohexanone + Phenylethyl alcohol	Ratio 1:1				
5	<i>trans</i> -cinnamaldehyde	pure	Sigma-Aldrich (St Louis, MO, USA)	C80687	Volatile irritant (TRPA1 agonist)	2.89 x 10 ⁻² (HSDB)
6	(1S,2R,5S)-(+)-Menthol	1mM	Sigma-Aldrich (Darmstadt, Germany)	224464	TRPM8 agonist	7.67 x 10 ⁻³ (HSDB)
7	Icilin	10 µM	Sigma-Aldrich (Darmstadt, Germany)	19532	TRPM8 agonist	unknown
8	Distilled water	pure	Purified with a Milli-Q system from Millipore, (Darmstadt, Germany)		Control no odor, no pungency	23.8 (Oxford university)

Figure 6: **Psychophysical experiment in patients**

A: Bi-dimensional schematic representation of the transmembrane sodium channel Na_v 1.7 illustrating transmembrane domains (D I - D IV) and corresponding subunits (S1 – S6). Mutations observed on a patient suffering from a congenital insensitivity to pain are depicted by orange circles (1 and 2).

Table 4: Volatile compounds used for psychophysical olfactory and pungency ratings psychophysical experiments in humans.

This condition has been linked with mutations on the SCN9A gene, encoding the voltage-gated sodium channel 1.7 isoform (Na_v 1.7) present in nociceptors (Cox *et al.*, 2006). Na_v 1.7 is also present in olfactory sensory neurons. Therefore, in addition to pain insensitivity, patients presenting a mutation on the SCN9A gene leading to non-functional voltage gated sodium channel expression, display an inability to perceive odorant substances called anosmia (Weiss *et al.*, 2011). The patient described by Prof Zhang (Department of anaesthesiology, Tongji Hospital, Tongji Medical College, Huazhong University of Science and Technology, Wuhan, China) was a 6-year-old girl harbouring two mutations in SCN9A. Primarily, a deletion of a guanine in position 850 (c.850delG) resulting in a substitution of glutamic acid in lysin (p.E284Kfs*3), and the introduction of a stop codon truncating the protein after the domain I of the channel (Fig. 6, panel A, “1”). The second mutation, a 13 base pair deletion c.129_141delTGAAGAAGCCCCA, lead to a change from aspartic acid to glutamic acid in position 43 of the protein sequence (p.Asp43Glufs*43) and the apparition of a stop codon resulting in a truncated Na_v 1.7 protein close to the N-terminus (Fig. 6, panel A, “2”).

b. CIP re-gain

In this study, a second patient was recruited. The 14-year-old boy had been previously identified as suffering from congenital insensitivity to pain by Prof. Zhang (Department of anaesthesiology, Tongji Hospital, Tongji Medical College, Huazhong University of Science and Technology, Wuhan, China) and had recovered painful stimuli perception for 6 years at the time of the experiment.

c. Congenital insensitivity to pain with anhidrosis

The brother of the CIP patient (described in section II. B. 2. a.), suffering from conditional insensitivity to pain with anhidrosis (CIPA), was also included in the study. CIPA is a condition with a phenotype similar to CIP in regard to pain perception. In addition, CIPA patients exhibit an inability to sweat since the pathology affects both sensory and autonomic systems (Swanson, 1963). CIPA disorders have been linked to a mutation in the NTRK1 gene, encoding the high affinity nerve growth factor receptor tropomyosin receptor kinase A (TrkA) (Indo *et al.*, 1996). Unlike CIP patients, individuals suffering from CIPA do not display anosmic phenotypes.

C. Psychophysical test

To assess volatile odorant and irritant perception in human subjects, a psychophysical test was realized. Participants were asked to rate olfactory and pungency potencies for 7 substances.

1. Experimental design

Test substances were kept at room temperature (24 ± 1 °C). Volatile olfactory stimuli were presented to each subject for 10 seconds, in a random order. During a 30 seconds time interval between two consecutive stimuli, participants, were asked if they could perceive any stimulus. If a perception was reported, subjects were asked to rate both olfactory intensity and pungency on a scale from “0”, corresponding to “no odour” on the olfactory scale or “no discomfort” on the pungency scale, to “10”, corresponding to “strong odour” or “most painful” sensations. The protocol was translated into Chinese and shown to each subject to provide a better understanding of abstract notions like “pungency” (Supp. Fig. S1 & S2).

2. Test substances

Each test substance was prepared in a 50 mL Falcon tube comprising 15 mL of solution. To ensure a sufficient concentration of volatile substances in the gaseous phase, tubes were kept sealed for an hour prior experiment. Evaporation was reduced with parafilm (Parafilm M, Bemis North America, Neenah, USA) covering the screw cap. In addition, Falcons were wrapped in aluminium foil to protect test substances from light. Falcon tubes were labelled numerically from 1 to 8 (Fig.

6, Table 4). Distilled water (dH₂O) served as a negative control. Olfactory perception was assessed using pure phenylethyl alcohol (PEA) which was previously described as a “pure” odorant (Doty, 1975). In addition, pungency perception was tested using ammonia vapor (NH₃), obtained from a solution of ammonium bicarbonate (NH₄HCO₃) warmed at 40 °C for 10 minutes and known to activate C-fibres (Lindberg, Dolata and Mercke, 1987). Olfactory and pungency ratings were also assessed for 4 transient receptor potential (TRP) channel agonists, including menthol (MEN, 1 mM) and icilin (IC, 10 μM), 2 cold mimicking TRPM8 activating chemicals (Chuang, Neuhauser and Julius, 2004; Bautista *et al.*, 2007). Furthermore, the TRPA1 agonist cinnamaldehyde, the principal compound of cinnamon oil (CIN) (Bandell *et al.*, 2004) and the TRPV1 agonist cyclohexanone (CYC) (Silver *et al.*, 2006), present in cigarette smoke were presented undiluted to participants. The possibility of a cross-modal interaction between pungent and olfactory systems was addressed presenting a test sample composed of a mixture of cyclohexanone and phenylethyl alcohol with a ratio 1:1 (CYC + PEA).

3. Analysis

Interindividual variations due to cultural, gender and age differences were assessed while comparing the results obtained for control subjects. Olfactory and pungency ratings were subsequently averaged for these participants, constituting the control group which would be further compared with results from patients suffering from different degrees of insensitivity to pain. Finally, ratings obtained for cyclohexanone and phenylethyl alcohol presented individually were compared to responses to the mixture CYC + PEA to interrogate the possibility of a cross-talk between olfactory and pungent modalities evoked by volatile stimuli in humans.

D. Forced choice behavioural task in mice

1. Experimental design

A water consumption preference test was developed to assess volatile stimuli perception in mice. Animals were housed individually in isolated-ventilated cages (GM500882, Tecniplast, Hohenpeissenberg, Germany) maintained at 22 ± 1°C with a 12h light/dark cycle and access to

food and water ad libitum. Water was provided with two bottles (ACBT0152, Tecniplast, Hohenpeissenberg, Germany) placed next to one another at the same end of the cage (Fig. 7, panel A). The two bottles were identical and spaced at a minimum of 5 cm from one another to avoid confusion between water sources, in accordance with forced choice water consumption settings explained by Blednov et al. (Blednov *et al.*, 2001). Water consumption was determined by weight and was assessed daily over a 7-day habituation period (Fig. 7, panel A) before adding the rings containing volatile substances to the sipping tubes (Fig. 7, panel B). Volatile substances were presented for 24h, housed in custom-made annular aluminium rings (Fig. 7, panels C, D) designed with Fusion 360 (Autodesk, San Francisco, USA) software. The annular housing comprised two parts that screwed together (Fig. 7, panel C). The housing was 8.5 mm in diameter with a central opening (Fig. 7, panel D, D = 8,5mm) enabling its positioning around sipping tubes of water bottle. One surface had 9 ventilation holes (Fig. 7, panel D, d = 4mm) through which volatile substances could evaporate. The internal space was filled with a piece of felt previously loaded with 10 μ L of the test substance.

2. Test substances

The pure odorant phenylethyl alcohol (PEA) and two irritants, namely cyclohexanone (CYC) and allyl isothiocyanate (AITC) were tested undiluted. Mice were presented consecutively with a choice between “water and water”, “water and PEA”, “water and irritant”, “PEA and PEA combined with an irritant”. These conditions were applied in a random order. Bottles were rinsed daily and refilled with fresh water; sipping tubes were cleaned with 70% ethanol and rinsed with water.

3. Analysis and statistics

Water consumption was used as an indicator of preference or aversion to a volatile substance. Mice had free access to both bottles. Water consumption was measured between 9 am and 11 am each day by weighting each bottle with a precision balance (PCB6000-1, Kern & Sohn GmbH, Balingen-Frommern, Germany).

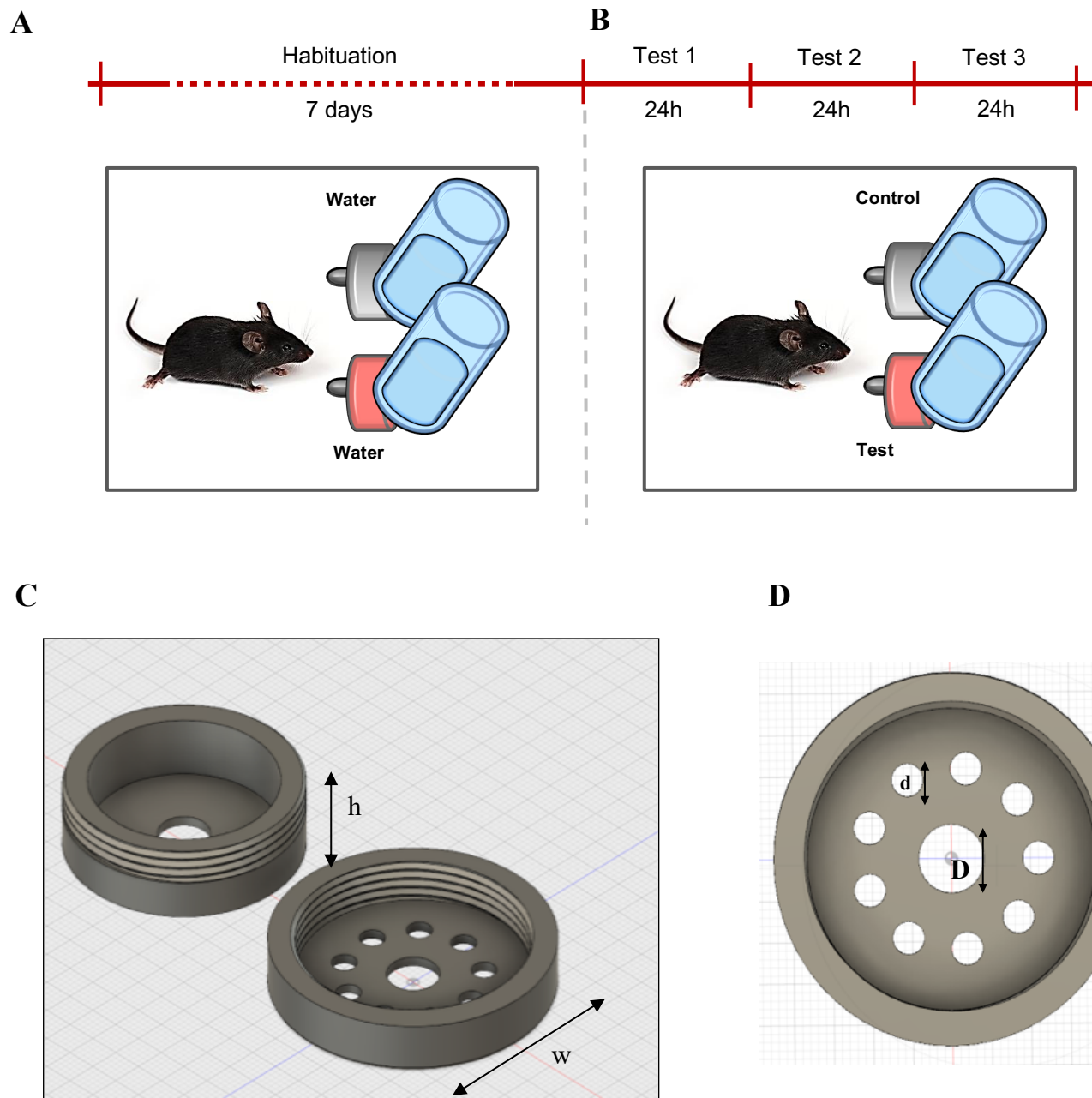


Figure 7: Forced choice behavioral task in mice

A, B: Water consumption preference test. Wild type C57Bl6 male mice received water from two similar bottles during a habituation period of 7 days (A). Subsequently, volatile substances were coupled to each bottle. Odorants, irritants and a mix of both volatile compounds were randomized and tested consecutively for 24 hours (B).

C, D: Dimensions of the two parts to be assembled to form the annular housing ($h = 11$ mm , $w = 30$ mm) (C). Dimensions of the upper part of the annular housing. Holes were drilled to enable the fixation of the device around bottle drinking tubes ($D = 8.5$ mm) and the diffusion of volatile substances ($d = 4$ mm) (D).

Raw water consumption was determined by the following subtraction for each bottle: “weight_{24h} – weight_{0h}” and the total water consumed was the sum of raw water consumption from two bottles for each animal. Statistical analyses were carried out with Statistica (StatSoft, Hamburg, Germany). Data groups comprised 8 to 10 mice and Student’s t-test were used to assess differences in water consumption between the two conditions “no exposure to volatile chemicals” or “application of the odorant PEA”. In order to assess the influence of combinations of odorant and irritant a 2-way ANOVA followed by Tuckey’s post hoc test was used. A p-value of 0.05 or less was considered as significant.

E. Imaging techniques

1. Tissue preparation

Adult mice from both sexes were anaesthetized with Sevoflurane (Abbot, Wiesbaden, Germany) in a sealed glass chamber (2 litres volume) and subsequently killed by cervical dislocation. The head was removed and cleaned of overlying skin and muscles before removing the lower jaw.

a. Olfactory epithelium

The cleaned skull was fixed in 4% paraformaldehyde (P6148, Sigma-Aldrich, St Louis, MO, USA) for 2 hours. The dorsal side of the skull was cut out, revealing the brain and olfactory bulbs which were subsequently detached with a dissecting spoon and the olfactory epithelium was isolated using the deboning protocol described by Dunston et al. (Dunston *et al.*, 2013) (Fig. 8, panel A). Briefly, the palate was removed, opening the nasal cavity and revealing the vomer bone which would subsequently be broken from its caudal to its rostral part using a rongeur (14090-G, World Precision Instruments, Sarasota, FL, US). After cleaning the skull from remaining pieces of broken bones, the right and left maxillae were loosened and removed, freeing the nasal epithelium laterally. The nasal bone was separated from both the zygomatic arch and the remaining frontal bone, and gently lifted from the caudal to the rostral part of the nasal cavity using forceps. Finally, the molars and palatine bones were broken using the rongeur and gently removed alongside the ethmoid bone to free the nasal turbinates. The nasal epithelium was cleaned of remaining bone fragments and placed in sucrose (10% w/v, S-2395, Sigma-Aldrich, St Louis, MO, USA).

A

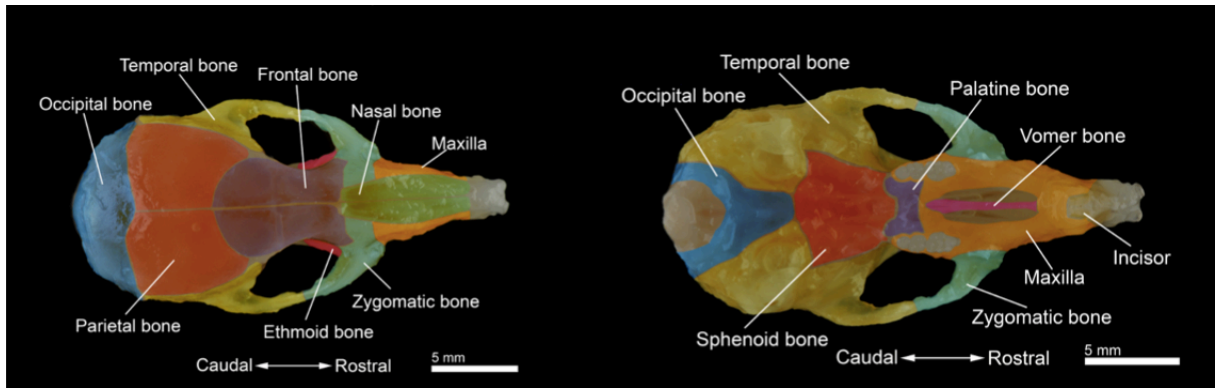


Table 5

<i>Antibody</i>	<i>Host</i>	<i>Supplier</i>	<i>Catalogue number</i>	<i>dilution</i>	<i>Immunogen</i>
Anti-GFP	Rabbit (polyclonal)	Abcam (Cambridge, UK)	Ab6556	1:400	Recombinant full length GFP protein
Anti-RFP	Rabbit (polyclonal)	Rockland (Limerick, USA)	600-401-379	1:200	Full length RFP protein
Anti-TRPA1	Rabbit (polyclonal)	Abcam (Cambridge, UK)	ab58844	1:400	Amino acids 1060-1075 of rat TRPA1

Table 6

<i>Antibody</i>	<i>Host</i>	<i>Supplier</i>	<i>Catalogue number</i>	<i>Dilution</i>	<i>Maximum Wavelength (Absorption/Emission)</i>
Anti-rabbit Alexa Fluor 488	Goat (polyclonal)	Invitrogen (Cambridge, UK)	A-11008	1:1000	499 nm / 520 nm
Anti-Rabbit Alexa Fluor 568	Goat (polyclonal)	Invitrogen (Cambridge, UK)	600-401-379	1:1000	580 nm / 603 nm

Figure 8: Imaging techniques

A: Dunston et al. 2013 deboning protocol to isolate the nasal epithelium of adult mice. Scale bar = 5 mm

Table 5: List of primary antibodies used for immunohistochemistry.

Table 6: List of secondary antibodies used for immunohistochemistry.

a. Anterior ethmoidal nerve

The clean skull was separated in two halves on the mid-sagittal axis. The cortex and olfactory bulb were removed from each skull half and the anterior ethmoid nerve was identified along its course on the internal side of the skull proximal to the anterior cranial fossa. The nerve was cut proximal to its entrance in the nasal cavity through the cribriform plate, and distal to its entrance into the cranial vault. This was repeated for the contralateral nerve. The dura surrounding the ethmoid nerve was removed and the sample fixed in 4% paraformaldehyde for 2 hours.

b. Trigeminal ganglion

The skull was placed in a petri dish and the occipital, parietal and frontal bones were removed with a rongeur. Using a small dissecting spoon, olfactory bulbs were gently lifted from their bony cavity, revealing the optic chiasma. After severing both optic nerves, the brain was lifted out, exposing trigeminal ganglia and their afferents. The first trigeminal branch (V1) was held with forceps and lifted. This step was repeated for the two other trigeminal branches (V2 and V3). Once freed from adhesion tissue with scissors, the three branches were sectioned distal to the trigeminal ganglion. This step was repeated for the contralateral ganglion and both samples were fixed in a 4% paraformaldehyde solution for 2 hours.

2. Antibody staining

Samples were dehydrated in a sucrose solution comprising 10% *w/v* sucrose (S-2395, Sigma-Aldrich, St Louis, MO, USA) and 0.05% *w/v* sodium azide (SigmaUltra, NaN₃, S8032, Sigma-Aldrich, St Louis, MO, USA) in phosphate buffer saline (pH=7.4) for 2 hours and cryoprotected in 30% sucrose solution (30% *w/v* sucrose, 0.05% *w/v* NaN₃ in PBS, pH=7.4) overnight. Tissue was then embedded in optimal cutting temperature medium (OCT, Sakura Finetek, CA, USA) and stored at -20°C before sectioning.

Tissue was sectioned serially at 25 µm on a cryotome (Thermo Scientific Microm HM 550, Darmstadt, Germany, object temperature = -20°C, chamber temperature = -24°C). Sections were mounted onto glass slides (Superfrost Plus™, Thermo Fisher Scientific, Darmstadt, Germany), dried for 30 minutes at room temperature and stored overnight at -20°C. The following day,

sections were dried at room temperature for 30 minutes and washed three times in 0.1 M phosphate buffer saline (PBS) for 5 minutes before blocking for an hour in a 5%_{v/v} Chemiblocker solution (Millipore, Darmstadt, Germany) containing 0.5%_{w/v} Triton X100 (T8532, Sigma-Aldrich, St Louis, MO, USA) and 0.05%_{w/v} NaN₃ in PBS (pH=7.4). Primary antibodies (Fig. 8, Table. 5) were added overnight in the same Chemiblocker solution. On the next day, sections were washed three times in PBS for 10 minutes. Secondary antibodies (Fig. 8, Table. 6) were diluted in a solution of 5%_{v/v} Chemiblocker (2xChemiblocker, 2170-S, Chemicon, Merck, Darmstadt, Germany) in PBS and 100µL per section was applied subsequently for 90 minutes at room temperature in the dark. Sections were washed three times in PBS for 5 minutes after which 1 µg/ml DAPI (DAPI, dilactate 98%, Sigma-Aldrich, Germany) was added for 1 minute. After washing three times for 7 minutes in PBS, slides were dried, mounted with fluorescence mounting medium (Dako, Agilent, Italy) and covered (BB02200500AC13MNT0, ThermoFisher, Darmstadt, Germany) before being stored in the dark at room temperature.

3. Microscope imaging

Slides were imaged using a Nikon Eclipse 90i/C1 confocal microscope (Nikon, Japan) D-Eclipse C1 laser scanning system (Nikon, Japan) and NIS-Element Advanced Research software (version 4.0, Nikon Instrument Inc., Melville, USA). Excitation wavelengths used were 408 nm, 488 nm and 543 nm respectively for DAPI, Alexa 488 and Alexa 568. Images were stacked and cropped with ImageJ (ImageJ 1.52e, Bethesda, MA, USA) before adding a scale bar.

F. Electrophysiology

1. Hemi-skull preparation

The hemi-skull preparation was identical to tissue preparation for anterior ethmoidal nerve imaging (see section II. E. 1. b.). The skull was cleaned from remaining muscles and connective tissue, cut along the mid-sagittal plane and the septum was detached to expose olfactory turbinates. Ex vivo half-skull preparations were embedded in 8 % w/v agar in a Perspex recording chamber (Agar agar, Kobe I, 5210.3, Carl Roth GmbH, Karlsruhe, Germany ; Fig. 10, panel A). The

nasal cavity and the bony cavity of the olfactory bulb formed a contiguous tissue bath which was perfused continuously at 4 ml/min and tempered at 32.0 ± 0.5 °C with a physiological solution comprising (in mM): hydroxyethyl piperazine ethane sulfonic acid solution (HEPES), 6 ; NaCl, 118 ; KCl , 3.2 ; NaGluconate, 20 ; D-Glucose 5.6 ; CaCl₂, 1.5 ; MgCl₂, 1. The pH was adjusted to 7.4 with NaOH. The temperature of the perfusing solution was controlled with an in-line resistive heating element regulated by feedback from a thermocouple positioned in the bath. Recording glass electrodes were pulled (P77 Brown-Flaming micropipette puller, Sutter instruments, San Francisco, SF, USA, temperature: 90°C, strength: 549) from borosilicate glass capillaries (GC150TF-10, 30-0066, Harvard apparatus, Edenbridge, UK) and placed in a micro-manipulator (NMN-25, Narishige, Japan) over an Ag/AgCl electrode (EP2, World precision instrument, Sarasota, FL, USA). The tip aperture was adjusted with a sapphire blade (double edge lancet, 504072, World precision instrument, Sarasota, FL, USA) to ca. 30 µm diameter and the glass electrode was filled with physiological solution from the recording bath.

2. Electro-olfactogram recording

a. Experimental design

An electro-olfactogram (EOG) is a signal recorded extracellularly and represents the activation of olfactory sensory neurons (OSNs) (Ottoson, 1954). Volatile chemical substances induce EOG responses with a specific shape (Gesteland, 1964). Moreover, the area under the curve of EOG responses increase proportionately with odorant concentration (Lapid *et al.*, 2009). Lapid *et al.* (Lapid *et al.*, 2011) also reported a correlation between perception and EOG response magnitude in humans. Furthermore, according to the same study, non-contiguous receptive fields activated by a volatile substance qualified as “pleasant” are more likely to be responsive to similarly pleasant odorants.

In the olfactory epithelium, EOG responses represent the summation of local surface field potentials elicited by the activation of certain populations of OSNs (Ottoson, 1958; Lowe and Gold, 1991). The EOG signal arises primarily from inward currents associated with transduction and depolarization in the olfactory cilia (Ottoson, 1954; Getchell, 1974; Simmons and Getchell, 1981). Indeed, EOG responses recorded at the rostral extremity of the second endoturbinat

(Fig., 9, panel A, B) display a monophasic negative deflection corresponding to cilia activation. Depending upon the location of the recording electrode, it is also possible to record extracellular signals from the nasal epithelium that represent conducted action potentials (Genovese *et al.*, 2016). In accordance with this observation, EOG signals recorded from the middle of the second endoturbinat on OMP- hChR2Venus mice (examples are shown in Fig. 9 panel C), display biphasic EOG signals indicating axonal contribution to the response. To avoid any variation due to the zonal distribution of olfactory receptors amongst the OSN population (Ressler, Sullivan and Buck, 1993) and the contribution of axonal action potentials, EOG responses were always recorded from the middle of the second endoturbinat in mice.

b. Stimuli

i. Light pulses

Photostimulation was used to activate olfactory sensory neurons in isolation and synchronously in preparations from OMP-hChR2Venus mice (Genovese *et al.*, 2016). To establish the efficacy of this stimulation, electro-olfactogram signals from the surface of the olfactory epithelium were recorded during stimulation with sinusoidal light pulses at 473 nm (LEDMOD V2, Omicron-Laserage, Rodgau-Dudenhofen, Germany). At short (≤ 20 ms) durations of photostimulation, a largely biphasic EOG response was recorded in the middle of the second endoturbinat. A maximal negative amplitude for EOG responses appeared around 35 ms latency for all stimulation durations tested (Fig. 9, panel C). The maximal EOG response amplitude and presumably most synchronous OSN photoactivation, was observed for 10-20 ms duration light pulses (Fig. 9, panel D). Responses to stimuli of longer duration comprised a sustained tonic component subsequent to the initial bi-phasic response. By virtue of the maximum peak-to-peak EOG amplitude observed in response to a 10 ms light pulse width, the effect of odorants and toxins on photo-evoked EOG responses were performed using 10 ms sinusoidal light stimuli. The longest sinusoidal stimulus duration tested was 100 ms and this corresponds to the approximate length of a sniffing cycle in the mouse (Wesson, Verhagen and Wachowiak, 2009).

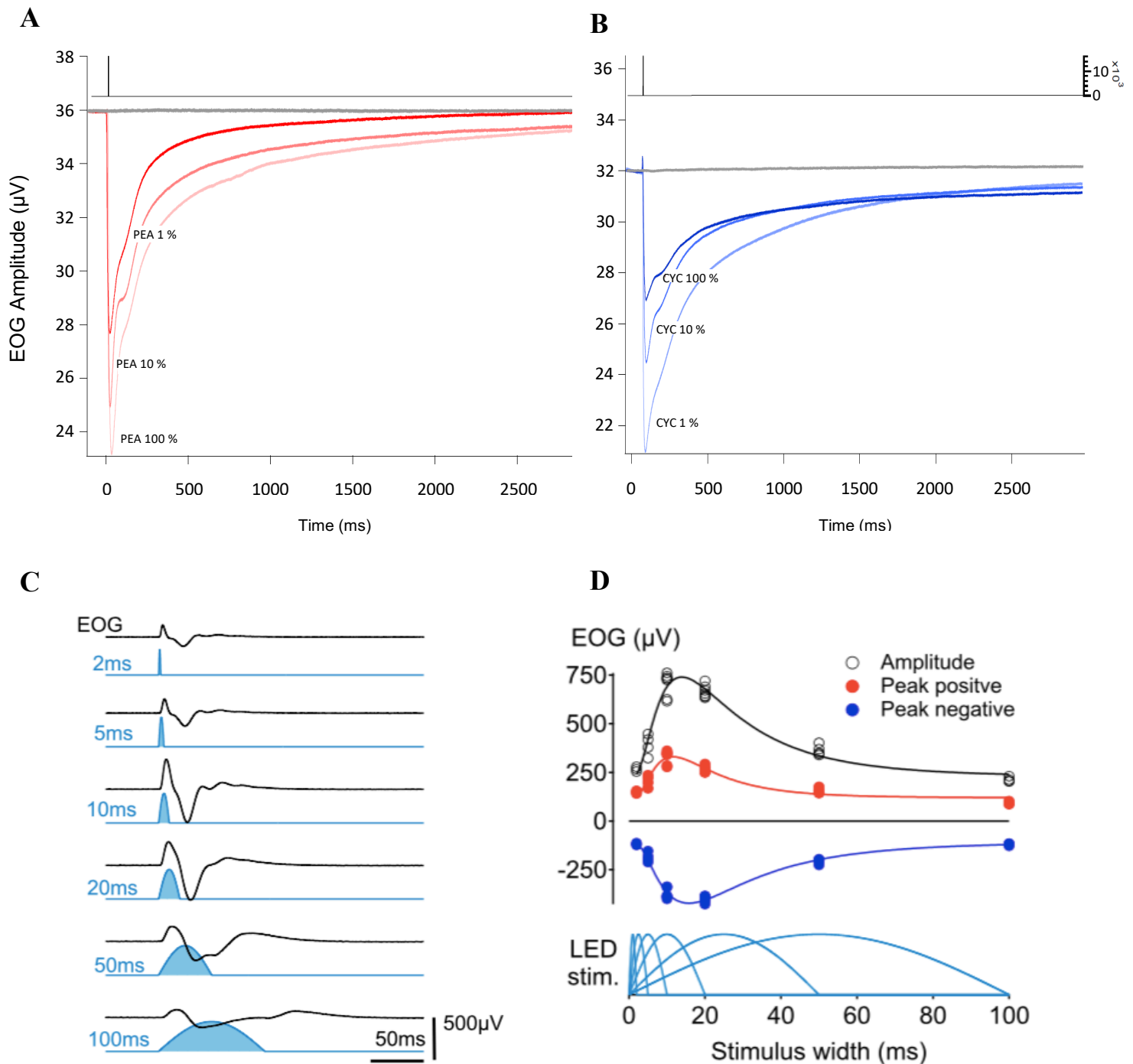


Figure 9: Electro-olfactogram recordings

A, B: EOG recordings from the most rostral part of the second endoturbinate in response to pressurized air stimuli mixed with PEA(A) or cyclohexanone (B) diluted at 1 %, 10 % and undiluted. C: EOG responses (black traces) evoked by light pulses stimuli with different durations (light blue traces).

D: Summary of EOG signals amplitudes (black) with positive (red) and negative (blue) compounds, in response to different optogenetic stimuli durations.

ii. Chemicals

Chemicals were also used to activate OSNs within the nasal cavity. Phenylethyl alcohol was dissolved in mineral oil (Mineral oil light, 101880364, Sigma-Aldrich, Munich, Germany) to produce a 1 mM stock solution. Irritants and toxins were diluted in dimethyl sulfoxide (DMSO) or PBS to make stock solutions and stored at -20 °C. Each substance was diluted to the desired concentration in physiological solution on the day of the experiment. In contrast to previous experimental paradigms that applied substances in the liquid phase to mice nasal epithelia (Neureither *et al.*, 2017), few experiments were performed using a fully submerged half skull preparation. Instead, odorants were applied in the gaseous phase by rapidly dispensing the air volume above ca. 200 μ l of liquid odorant within a 1ml syringe, using a 20 ms air pulse controlled by a pneumatic pico pump (PV830; World precision instrument, Sarasota, FL, USA). The region of nasal epithelium to which the stimulus was applied was exposed to air at the time of stimulus application. This was achieved by lowering the bath volume over the 10-20 s period preceding and succeeding odorant application.

iii. Voltage-gated sodium channel blocker

To functionally assess the presence of voltage-gated sodium channels in the nasal epithelium, EOG responses to light stimuli were recorded in the presence of toxins and small molecules added to the solution perfusing the recording bath. Previous reports using immunohistochemical methods and electrophysiological recordings indicated that Nav 1.3, 1.5 and 1.7 are present within the olfactory epithelium (Ahn *et al.*, 2011; Frenz *et al.*, 2014; Bolz *et al.*, 2017). The compound A-803467 is known to block Nav 1.8 TTX-resistant channels at low doses (E_{c50} = 8 nM) and other voltage-gated sodium channel isoform such as Nav 1.2, 1.3, 1.5 and 1.7 with concentrations higher than 2 μ M (Jarvis *et al.*, 2007; Tan *et al.*, 2014). Light-evoked EOG signals were recorded during application of A-803467 (1 μ M, Tocris, Wiesbaden-Nordenstadt, Germany) in the recording bath to interrogate the presence of Nav 1.8 in OSNs. The Nav 1.8 blocker was subsequently washed out of the bath with a physiological HEPES solution (composition described in section II. F.1.) for 10 minutes before exposing the hemi-skull to a solution of 1 μ M tetrodotoxin (TTX, tetrodotoxin citrate, T-550, Alomone labs, Jerusalem, Israel), expected to inhibit all TTX-sensitive voltage-gated sodium channel isoforms, namely Nav 1.1 – 4 and Nav 1.6 and 1.7. The

TTX-resistant Na_v 1.5, isoform has been localized in the sensory knob of OSNs (Frenz *et al.*, 2014) and remains unaffected by low concentrations of the compound A-803467 (Jarvis *et al.*, 2007). However, Na_v 1.5, also expressed in cardiac cells, can be blocked by lidocaine (Fan *et al.*, 2010). Therefore, after a second 10-minute perfusion of HEPES, lidocaine (100 μM , Sigma, Darmstadt, Germany), was applied to the bath in an attempt to block all Na_v present in olfactory sensory neurons.

c. Recordings and analysis

Local surface potentials were recorded using the software Spike 2 (CED, Cambridge, UK) over the sealing resistance relative to an Ag/AgCl pellet placed in the bath, using a differential amplifier (NL104A, Digitimer, Wewlyn Garden City, UK), filtered (lowpass 5 kHz, 80 dB Bessel), digitized (20 kHz, micro 1401, Cambridge Electronic Design, Cambridge, UK) and stored to disk for subsequent analysis. EOG were analysed offline initially with Spike 2 (CED, Cambridge, UK) to ascertain maximum, minimum and area under the curve values. Significant differences between EOG measures in absence or presence of Na_v blockers was determined with a paired t-test using Igor Pro 7 (WaveMetrics, Lake Oswego, OR, USA).

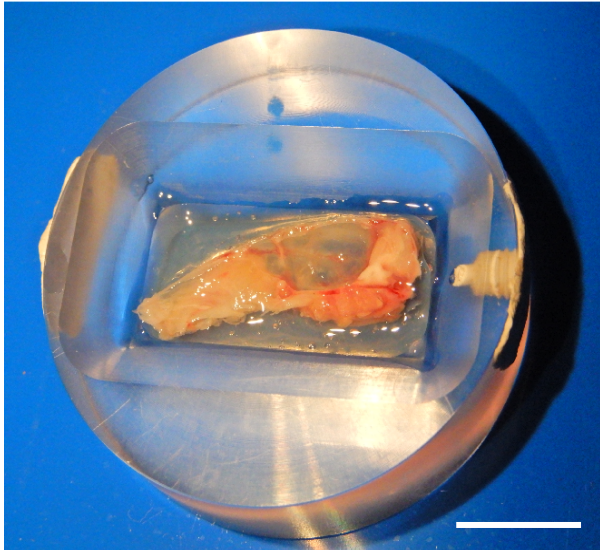
3. Nasal trigeminal afferents recordings

a. Experimental design

Adult male and female C57BL/6 N wildtype mice between 8 and 20 weeks of age were used to characterize trigeminal afferents within the nasal cavity. OMP-hChr2Venus mice (Genovese *et al.*, 2016) in the same age range were used to test whether the photoactivation of OSNs affected the conduction velocity of trigeminal afferents. Extracellular techniques were used to record from functionally single peripheral C-fibre trigeminal afferents innervating the nasal cavity. Single axons endings are difficult to localize and record from within the olfactory epithelium. Therefore, extracellular recordings are typically performed by teasing the cut end of a nerve manually into progressively smaller filaments. However, the olfactory epithelium is innervated by the anterior ethmoid nerve (AEN). The AEN is comprised in the nasociliary nerve which passes through the anterior ethmoid foramen into the anterior cranial fossa and subsequently divides to innervate

the nasal cavity through the criboethmoidal foramen (Patron *et al.*, 2015). Tracing experiments realized in collaboration with Dr. Schüler (Physiology and Pathophysiology, in Erlangen, Germany) confirmed this description (Fig. 10, panel B). The short length of nerve within the anterior cranial fossa limits access and precludes the use of split fibre techniques for the anterior ethmoid nerve at this site in the mouse. To circumvent these problems, a loose extracellular patch technique was adopted to record from the entire anterior ethmoidal nerve in the mouse. Briefly, the ethmoid nerve was cut immediately distal to its passage through the anterior ethmoid foramen and freed of the surrounding dura mater over a length of approximately 4 mm. The tip of a glass recording electrode filled with physiological solution was fashioned with a sapphire blade to an opening size matching that of the nerve and attached via suction to the cut end of the ethmoid nerve. In this configuration, individual axons were identified by time-locked action potential responses to electrical or mechanical stimulation at their sites of termination within the nasal cavity (see example in Fig. 12, panel C). To determine whether other types of stimuli were able to activate trigeminal axons, the response latency of individual axons to electrical stimulation at constant frequency (typically 0.5 Hz) was monitored. According to previous studies, the conduction latency of a single axon is dependent upon the level of action potential traffic, whereby at constant action frequency, in this case delivered by electrical stimulation, the response latency is constant. Any additional action potential activity will produce a slowing of the subsequent response to electrical stimulation. A slowed response to electrical stimulation thus indicates activity and this is referred to as “marking” (Thalhammer *et al.*, 1994) (see example in Fig 13, panel B and Fig. 13, panel B). To assess the influence of temperature and chemical substances on trigeminal afferents, the response latency of individual electrically-evoked action potentials were monitored during application of chemical to the perfusing solution or during changes in temperature of the perfusing solution. Marking observed during this period was taken to indicate activation of the axon by the stimulus.

A



B

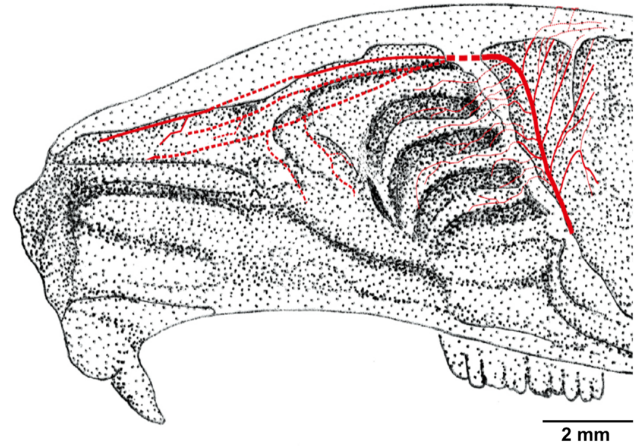


Table 7

Substance	Concentration	Product number	Supplier (location)
Cyclohexanone	1% v/v	398241	Sigma-Aldrich (Darmstadt, Germany)
PEA	1 mM	77861	Sigma-Aldrich (Darmstadt, Germany)
(1S,2R,5S)-(+)-Menthol	10 μ M	224464	Sigma-Aldrich (Darmstadt, Germany)
Icilin	10 μ M	19532	Sigma-Aldrich (Darmstadt, Germany)
Allyl isothiocyanate	20 μ M	W203408	Sigma-Aldrich (Darmstadt, Germany)
Capsaicin	250 nM	M2028	Sigma-Aldrich (Darmstadt, Germany)

Figure 10: **Electrophysiological recordings of single trigeminal afferents**

A: Half skull embedded in agar in a Perspex recording chamber. Scale bar = 1 cm.

B: Representative drawing of the right nasal cavity after anterograde tracing of the anterior ethmoidal nerve (Dr. Markus Schüler, Physiology and pathophysiology department, Erlangen, Germany). Scale bar = 2 mm.

Table 7: Substances used to assess chemesthesis in single nasal trigeminal afferents.

b. Stimuli

Receptive field locations for individual trigeminal axons were sought using either mechanical or electrical search stimuli. Mechanosensitive receptive fields were initially searched coarsely with von Frey hair of 1.47 mN buckling load (120 μm -diameter, 130 kPa pressure). Regions identified as mechano-sensitive were subsequently explored using a servo-driven mechanical stimulator, previously described in De Col et al. (De Col, Messlinger and Carr, 2012), to deliver dynamic stimuli with a sinusoidal profile (10 ms duration). Several nasal trigeminal receptive fields were also identified directly using an electrical stimulus. Constant current electrical pulses of 1 ms duration, ranging in amplitude from 40 to 100 μA , were delivered by a rayon insulated platinum iridium wire (ISA OHM, Isabellenhütte, Dillenburg, Germany). This wire was cut to a plane flat ending at a length to ensure a buckling load of ca. 0.4 mN. The iridium wire was placed on the tissue and served as the cathode while an Ag/AgCl pellet (WPI, Sarasota, Florida, USA) placed in the recording bath served as the anode. Positioned at a given site, if a time-locked and reproducible evoked response was observed, this site was considered to be within the receptive field of that single trigeminal afferent. Trigeminal axons thermo-sensitivity was assessed by changing the temperature of the solution perfusing the recording bath. A heating-element was used to warm up physiological solution to 40 ± 1 °C with a time constant of ca. 14 s while cooling to 21 ± 1 °C was obtained with a recirculating Chiller (Accel 500 LT, Thermo Fisher, Darmstadt, Germany). Chemical stimuli used to assess chemosensitivity are listed in Fig. 10, Table 7 and these were delivered directly by adding them to the solution perfusing the bath. Photostimulation comprised light pulses (470nm, 10 ms duration, LEDMOD V2, Omicron-Laserage, Rodgau-Dudenhofen, Germany) applied via a fibre optic conduit positioned above the second endoturbinat.

c. Recording and analysis

The experimental recording time for each half skull lasted between 2 and 6 hours. Alike electro-olfactogram responses, extracellular signals were recorded with Spike 2 (CED, Cambridge, UK) using an amplifier (NL104A, Digitimer, Wewlyn garden city, UK), filtered with a lowpass filter (5 kHz, 80 dB Bessel), and digitized (20 kHz, micro 1401, Cambridge Electronic Design, Cambridge, UK) before being stored to disk for subsequent analysis.

Individual trigeminal axons were identified by the response latency to either or both electrical and mechanical stimuli and further characterized by their axonal conduction velocity. The site at which the electrode or mechanical probe was placed for each recording was transposed onto an image of the rat nasal cavity adapted from Barrios *et al.*, (Barrios *et al.*, 2014) (Fig. 12, panel A). Axonal conduction velocity was calculated using the latency of electrically- or mechanically-evoked action potential response and the distance between the stimulation site and the recording electrode which was estimated visually by reference to a graticule placed in the light path of the microscope ocular objective. Using the marking technique e (described in section II. F.3.a.), tracked axons were considered sensitive to temperature and/or chemical stimuli if the latency of their response to electrical stimulation increased or if the axon became transiently refractory to electrical stimulation, leading to an absence of visible response. The threshold for thermal activation was taken as the temperature at which the tracked response disappeared. Electrically and mechanically evoked response latencies were determined using Spike 2 software (CED, Cambridge, UK). Similarly, chemical activation was determined by a transient loss of time-locked responses to electrical stimuli. For each individual axon, latencies were normalized to the average latency value obtained over 3 minutes stimulation in absence of any chemical in the recording bath. To best describe chemesthesis in nasal trigeminal afferents, we reported for each recording a baseline value and a treatment value. The baseline value was defined as the averaged latencies or the 3 last stimulation prior treatment. In contrast, the treatment value was defined as the averaged latencies corresponding to the last three stimuli before the disappearance of tracked responses. Pooled baseline and treatment values from different experiments were represented on bar charts.

III. Results

A. Trigeminal innervation of rodent nasal cavity.

1. The anterior ethmoidal branch of the trigeminal system innervates the respiratory and olfactory epithelia in the nose

Both trigeminal and olfactory chemosensory systems reside in parallel in the nasal cavity, contributing to the detection and identification of volatile compounds probed from the surrounding environment (Doty *et al.*, 1978). The main trigeminal ramification innervating the nasal epithelium is called the anterior ethmoidal nerve (AEN). The AEN is known to run laterally under the olfactory bulb in the skull before traversing the cribiform plate to enter the nose, however, its innervation pattern within the nasal cavity remains unclear. Initially, the macroscopic AEN innervation of nasal cavity was observed in rat hemisected skulls. Anterograde tracing experiments performed together with Dr. Schüler (Physiology and Pathophysiology, in Erlangen, Germany) were used to identify anterior ethmoidal nerve projections (Fig. 10, panel B). Briefly, a crystal containing the anterograde tracer carbocyanine dye Di-I3 (1,1'-Dioctadecyl-3,3',3'-Tetramethylindocarbocyanine Perchlorate, D282, Molecular Probes, Eugene, OR, USA) was applied on the distally cut end of the anterior ethmoidal nerve, previously cleaned of surrounding dura on about 2 mm beyond its traverse to the anterior cranial fossa. The crystal was covered by a piece of gelatine sponge (Abgel, Sri Gopal Labs, Mumbai, India) and the dye was transported for 3 months. Interestingly, while the main ramification of the AEN entered the nasal cavity medio-dorsally to run along the dorsal roof of the nasal cavity and reach the respiratory epithelium close to the nostrils, thin collaterals were observed crossing the cribiform plate at different levels to innervate the olfactory epithelium (Fig. 10, panel B). The nasal trigeminal innervation was then further characterized using transgenic mice lines. Scn10a-Cre:tdTomato mice express the red transcriptional reporter TdTomato under the promoter of the voltage-gated sodium channel Nav 1.8 gene which is specifically expressed in sensory neurons. Using antibodies directed against red fluorescent proteins (RFP), tdTomato signal could be amplified and RFP-positive trigeminal cell bodies were identified within 25 μ m thick sections of the Gasserian ganglion (Fig. 11, panel A,

Maurer et al., 2019, data acquired and kindly offered by Nunzia Papotto, Center for Organismal Studies, Heidelberg, Germany). Expectedly, tdTomato-positive fibre bundles were observed in 25 μm thick coronal sections of the anterior ethmoidal nerve, cut before its entrance within the nasal cavity (Fig 11, panel B-D, Maurer et al., 2019, panel B acquired and kindly offered by Nunzia Papotto, Center for Organismal Studies, Heidelberg, Germany). Pictures of nasal sections revealed the presence of sensory fibres in both the septal and the vomeronasal organs, which are specific areas located at the entrance of the nose and mainly responsible for alert behaviour and pheromone detection (see section I.A.1.a, Fig. 11, panel C). Interestingly, symmetric fibre bundles were also identified dorsally in the septum and at the basis of the first endoturbinete, supporting the olfactory epithelium (Fig. 11, panel C). The potential colocalization of sensory axons with olfactory axons was explored using *Scn10a-Cre:tdTomato-OMP-hChR2Venus* mice bred in collaboration with Nunzia Papotto (Centre for Organismal Studies, Heidelberg, Germany). This mouse line presents two reporter genes, namely tdTomato expressed in sensory neurons under the *Scn10a* promoter, and the yellow fluorescent protein Venus expressed in mature OSNs. Venus is a mutated protein derived from the green fluorescent protein (GFP) initially identified in the jellyfish *Aequorea Victoria*. In immunohistochemistry experiments, Venus signal was enhanced using antibodies directed against GFP. Within the *Scn10a-Cre:tdTomato-OMP-hChR2Venus* mouse nasal septum, very few colocalization was observed between Venus-labelled olfactory and tdTomato-positive sensory fibres. OMP labelling was observed at the surface of the septum with some fascicles localized ventrally while sensory tdTomato fascicles remained more dorsal (Fig. 11, panel D). A similar organization was observed in the first endoturbinete, at the level of the olfactory epithelium suggesting that axons conveying sensory or olfactory information remain separated within the nose (Fig. 11, panel E). Surprisingly, after an extensive research, not any sensory axon nor bundle was observed within the nasal epithelium of *Scn10a-Cre:tdTomato* mice. However, the use of specific markers for 2 members of the TRP channel family revealed the presence of sensory projections at the level of the nasal epithelium. TRP channels are activated by different chemicals. Chemical responses of nasal trigeminal afferents are detailed in the section III. A. 2.c.

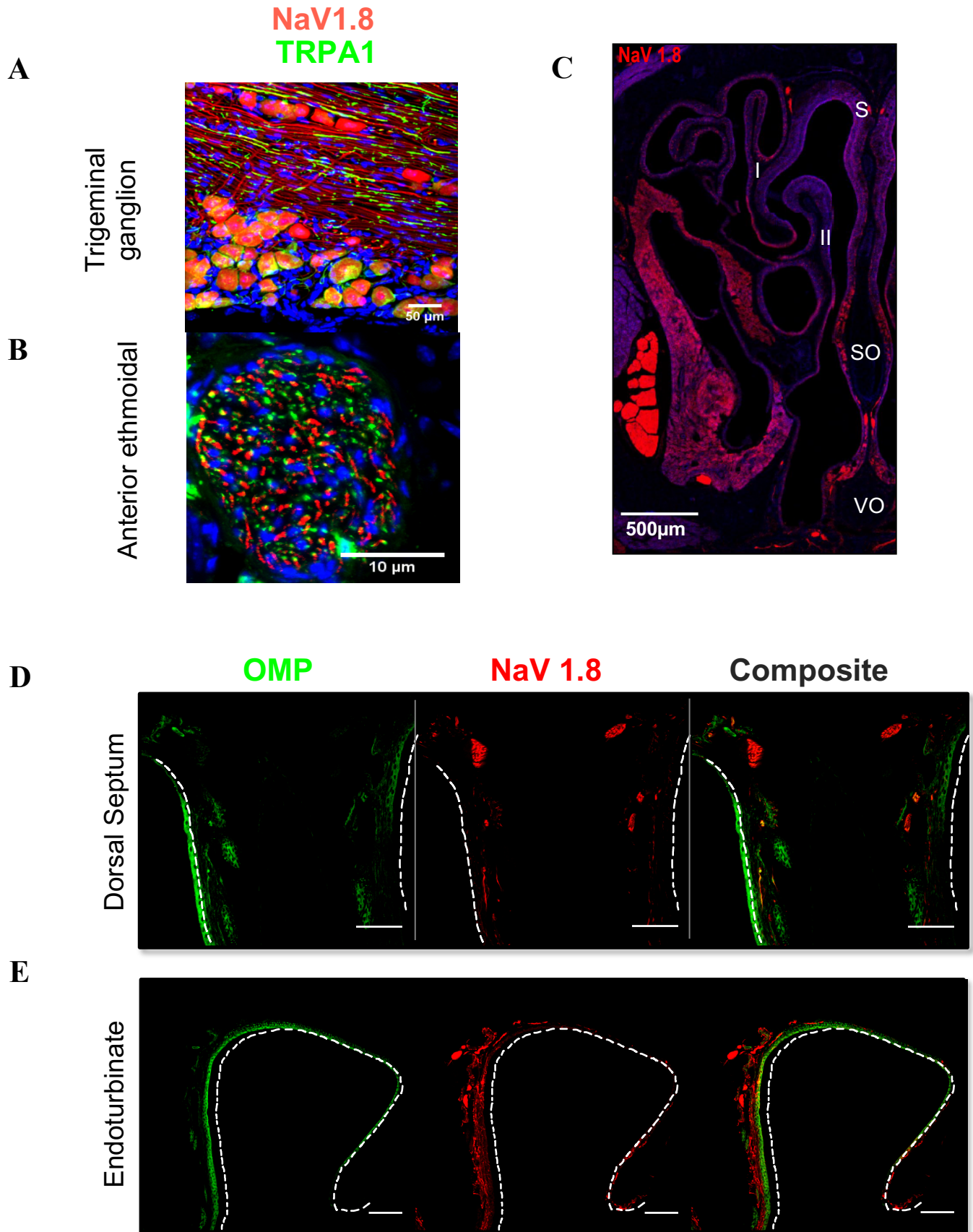


Figure 11: TRPM8, TRPA1 and Nav1.8 expression in trigeminal cellular bodies and projections.

A: Cellular bodies TRPA1(green) and Nav1.8 (red, right) positive in trigeminal ganglia sections. Cell nuclei are labelled with DAPI. Scale bar = 50 μm . (Maurer et al., 2019, data acquired and kindly offered by Nunzia Papotto, Center for Organismal Studies, Heidelberg, Germany)

B: Axon bundles TRPA1 (green) and Nav1.8 (red, right) positive in coronal sections of the anterior ethmoidal nerve. Cell nuclei are labelled with DAPI. Scale bar = 10 μm . (Maurer et al., 2019, data acquired and kindly offered by Nunzia Papotto, Center for Organismal Studies, Heidelberg, Germany)

C: Left half of a coronal section of the caudal nasal cavity. Bundles of sensory fibers expressing Td-tomato under the Scn10A promoter are observed in the septum (S), at the level of septal (SO) and vomeronasal organs (VO) and at the base of the first endoturbinates (I). Sensory innervation, in red, is also distributed in the nasal epithelium covering the first (I) and second endoturbinates (II). Scale bar = 500 μm . Nuclei are stained with DAPI.

D: The dorsal septum (delimited by white dashed lines), covered by OSNs (left panel, green), contains bundles of sensory fibers (middle panel, red) at the caudal level of the nasal cavity. Some bundles include both olfactory and sensory fibers (right panel, white arrow). Scale bar = 50 μm

E: At a more rostral level, the dorsal septum and first endoturbinates (delimited by white dashed lines), also present a thin layer of OSNs (left panel, green), and contains bundles of sensory fibers (middle panel, red). However, co-labelling did not reveal shared olfactory and sensory bundles (right panel). Scale bar = 100 μm .

2. Functional characterization of sensory afferents innervating the nasal epithelium

a. Electrophysiological characterization of nasal trigeminal afferents reveal A-delta and C-type fibres

In order to assess the properties of trigeminal neurons innervating the nose via the anterior ethmoidal nerve, single AEN sensory afferents were identified using extracellular recording to monitor action potentials evoked by either electrical or mechanical stimulations applied directly to the nasal epithelium. A total of 82 individual trigeminal afferents were observed within the respiratory and olfactory epithelia (Fig. 12, panel A). Sensory neurons can be categorized in different subpopulations given their conduction velocity in rodents (Hursh, 1939; Harper and Lawson, 1985).

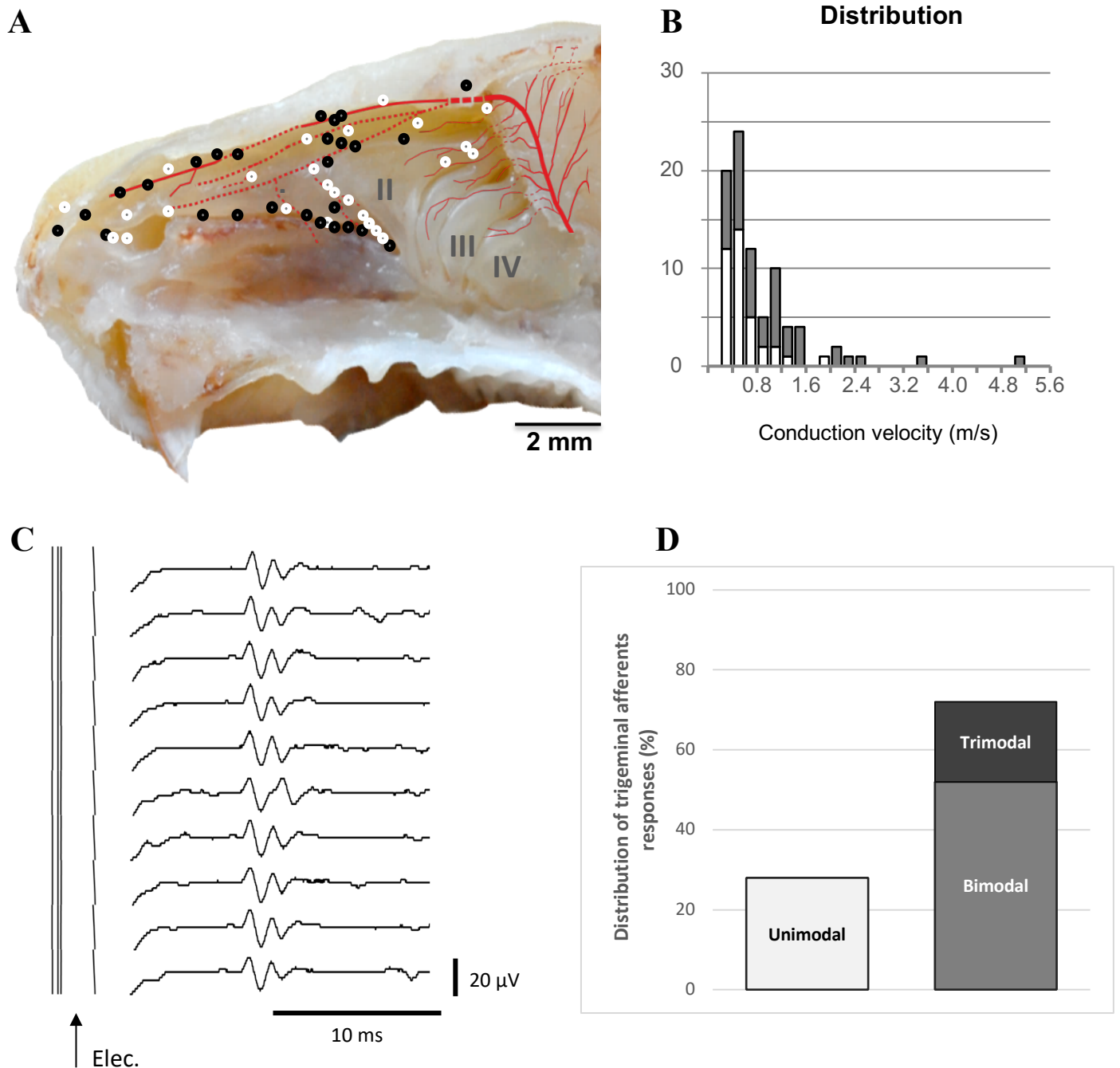


Figure 12: Trigeminal receptive fields in the nasal epithelium.

A: Mapping of every individual sensory trigeminal axon recorded from in the nasal cavity, after electrical (white markers) or mechanical (black markers) stimuli. Anterior ethmoidal nerve projections are represented in red. Scale bar = 2 mm. Background adapted from barrios et al. 2014.

B: Distribution of conduction velocities of mechanically (black markers) and electrically activated (white markers) afferents of the anterior ethmoidal nerve.

C: Example of consecutive AP with a stable latency evoked by 0.25 Hz electrical stimuli (stimulus artefact is indicated by an arrow). Horizontal scale bar = 10 ms ; vertical scale bar = 20 μ V.

D: diagram representing the distribution of individual trigeminal afferents responding to one or more stimulus modalities within the rodent nasal epithelium.

Individual axons were identified by the ability to generate a time-locked action potential response to regular stimuli at 0.25 Hz. Axonal conduction velocity was calculated for each identified fibre with the response latency and the distance between the stimulation site and the tip of the recording electrode which was measured by visual inspection. The lowest axonal conduction velocity recorded was 0.2 m.s⁻¹. Seventy-one axons innervating the nasal cavity had conduction velocities ranging between 0.2 and 1.5 m.s⁻¹ (mean = 0.63 m.s⁻¹ ; median = 0.54 m.s⁻¹), corresponding to C-type fibres while 11 receptive fields, mainly identified by mechanical stimuli, generated responses with a conduction velocity equal to or over 1.5 m.s⁻¹ (mean = 2.35 m.s⁻¹ ; median = 2.08 m.s⁻¹) rendering them A-delta axons (Fig. 12, panel B). The maximal conduction velocity recorded was 5.2 m.s⁻¹.

b. Nasal trigeminal afferents responses to different stimulus modalities

Trigeminal afferents were further characterized according to their responses to different stimuli modalities. Pressure sensitivity was tested directly using a mechanical servo-driven stimulator while the “latency marking” technique previously described in Thalhammer et al., (Thalhammer *et al.*, 1994) was used to determine the sensitivity of individual sensory afferents to thermal changes or chemicals. This technique is based on a physiological axonal property particularly prominent in C-fibres nociceptors, whereby a decrease in axonal conduction velocity is observed in the period subsequent to each action potential. Accordingly, marking was used to detect action potential activity in response to sensory stimuli. Specifically, with a fixed stimulation frequency of 0.25 Hz, electrically-evoked action potentials entrain to a stable latency (Fig 12, panel C). If an extra sensory stimulus-evoked action potential is conducted in addition to the regular electrical stimuli, the latency of the subsequent electrically-evoked action potential will be delayed (examples can be seen in Fig. 13, panel B and Fig. 14, panel B). This delay in action potential response is therefore representative of sensitivity to the sensory stimulus applied.

i. Polymodal activation of trigeminal afferents in the nasal epithelium

Trigeminal sensory neurons are known to respond to different stimuli modalities such as mechanical pressure, thermal changes and chemicals either in isolation or in a polymodal fashion

(Viana, 2011). Eighteen out of 25 trigeminal receptive fields were activated by more than one stimulus modality, representing 72 % of all fibres tested (Fig. 12, panel D). Amongst these fibres, 13 responded in a bimodal fashion to either mechanical pressure and thermal changes in the recording bath, or thermal and chemical stimuli (Suppl. Fig. S4). None of the bimodal units recorded were found to be activated by both mechanical and chemical stimuli. Five tracked trigeminal afferents were activated by all 3 stimuli modalities including chemicals such as transient receptor potential channel agonists (detailed in section III. A. 2. b. iv). Out of 25 units recorded, only 7 were sensitive to one modality (Fig.12, panel D).

ii. Nasal trigeminal responses to mechanical stimuli

Forty-one receptive fields were identified using an electrical search stimulus (Fig. 12, panel A, white markers, n= 41) and another 41 units using a mechanical servo-driven stimulator delivering 0.4 mN pressure stimuli (Fig. 12, panel A, black markers, n= 41). Mechanical receptive fields comprised areas of approximately 0.1–0.8 mm² identified primarily within the respiratory epithelium (Fig. 12, panel A) and had conduction velocities ranging between 0.2 and 5.2 m.s⁻¹ (mean = 1.06 m.s⁻¹; median = 0.84 m.s⁻¹; Fig. 12, panel B), while units within the olfactory epithelium were typically identified with an electrical stimulus (Fig. 12, panel A) and had conduction velocities that did not exceed 2 m.s⁻¹ (mean = 0.57 m.s⁻¹; median = 0.48 m.s⁻¹; Fig. 12, panel B).

iii. Nasal trigeminal responses to thermal changes

Nasal trigeminal afferents thermal sensitivity was assessed by changing the temperature of the physiological solution perfusing the recording bath. Ion channels involved in the propagation of action potentials along axons are highly dependent on temperature (Voets *et al.*, 2004). Over 20 °C, the relationship between conduction latency and temperature is one of negative proportionality in sensory neurons (Paintal, 1965; Carr *et al.*, 2003; De Col, Messlinger and Carr, 2008). Making allowance for this relationship, heating the solution in the recording bath led to a decrease in electrically-evoked response latency and therefore an increase in conduction velocity.

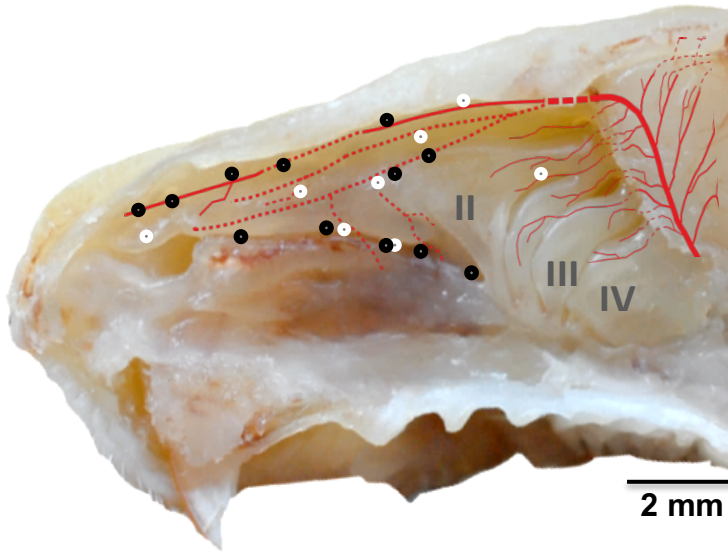
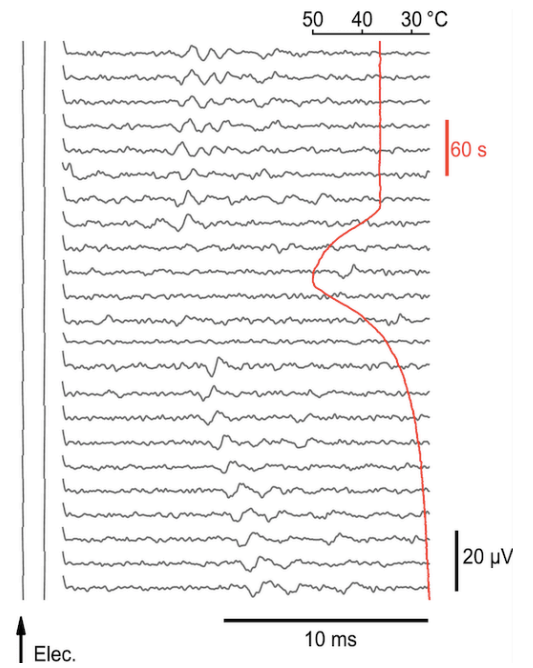
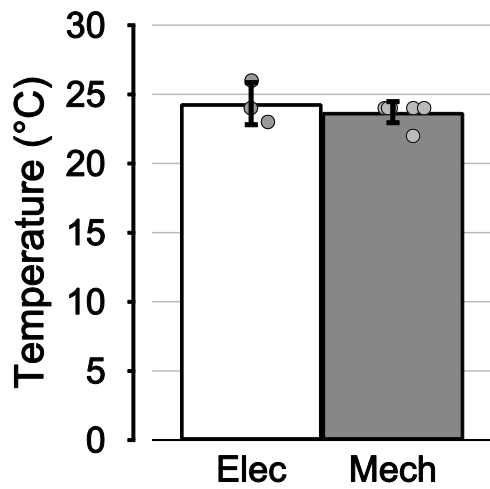
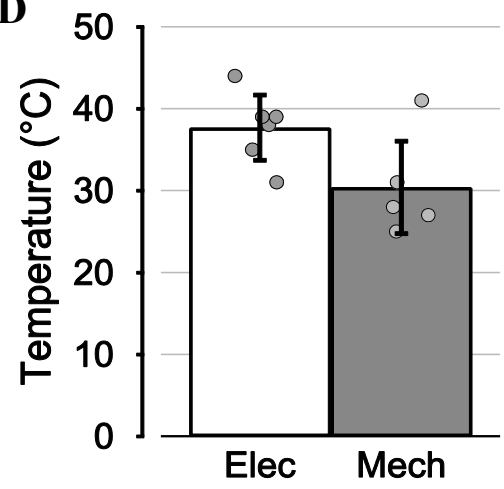
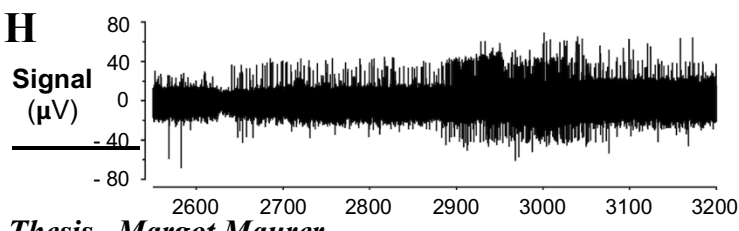
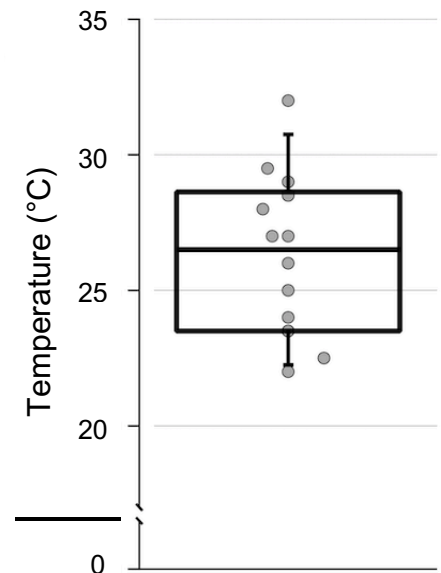
A**B****C****D****E****F****G****H****I**

Figure 13: Thermosensitivity of trigeminal afferents within the nasal cavity.

A: Mapping of thermo-sensitive individual sensory trigeminal axon recorded from in the nasal cavity, after electrical (white markers) or mechanical (black markers) stimuli. Anterior ethmoidal nerve projections are represented in red. Scale bar = 2 mm. Background adapted from Barrios et al. 2014.

B: Example of an electrically-evoked response disappearing during warming co-activation of the trigeminal axon. Each line corresponds to an electrical stimulation. The red curve represents the measure of the temperature in the recording bath.

C: Threshold of activation for cold temperature in trigeminal fibers initially identified with electrical (white bar) or mechanical (grey bar) stimuli.

D: Threshold of activation for warm temperature in trigeminal fibers initially identified with electrical (white bar) or mechanical (grey bar) stimuli.

E: Example of increase in activity of a background unit during cooling with a representation of its specific spike shape (insert ; vertical scale bar = 50 μ V ; horizontal bar = 2 ms).

F: Second background unit displaying an increase in activity during cooling with a representation of its specific spike shape (insert ; vertical scale bar = 50 μ V ; horizontal bar = 2 ms).

G: Bath temperature measures.

H: Trigeminal background recording during cooling in the recording bath.

I: Temperature threshold inducing an increase in activity represented in a box and whisker plot.

Reciprocally, cooling the solution perfusing the bath naturally resulted in an increased latency and a lower conduction velocity.

A receptive field was considered sensitive to heat when marking produced an increase in latency in the opposite direction to that expected from the effect of temperature alone or when the responses transiently disappeared (Fig. 13, panel B). During cooling, deviations from the linear decline in action potential latency were considered to be evidence of marking. A total of 20 identified trigeminal afferents displayed sensitivity to temperature changes within the nasal cavity, most of them located within the respiratory epithelium (Fig. 13, panel A). Twelve mechano-sensitive units were also activated by temperature in the recording bath (Fig. 13, panel A, black markers). Seven units responded to cooling at an average threshold of 23.7 ± 0.7 °C (Fig. 13, panel C, grey bar) and 5 units displayed an average heat threshold at 30.4 ± 5.6 °C (Fig. 13, panel D, grey

bar). Seven individual trigeminal axons responded to heating alone with thresholds at 37.9 ± 3.7 °C (Fig. 13, panel D, white bar) and 3 units responded during cooling at an average threshold temperature of 24.3 ± 1.2 °C (Fig. 13, panel C, white bar).

During cooling, the induction of activity was often observed in the recording from the whole anterior ethmoidal nerve (Fig. 13, panel G, H). This indicates that trigeminal afferents from the nasal cavity, not specifically identified as having an electrical or mechanical receptive field within the search area, also responded to a decrease in temperature. Using action potential shape to identify these discharges, 11 individual units could be identified that increased firing during cooling (two examples are shown in Fig. 13, panel E, F). Background firing was evoked at a median temperature of 26.5 °C. The lowest cooling threshold observed was 22 °C, while the highest threshold for firing during cooling was 32°C (Fig. 13, panel I).

iv. Nasal trigeminal chemesthesis

Following electrical, thermal and mechanical identification, the chemosensitivity of tracked trigeminal afferents was assessed in the nasal cavity. Psychophysical tests have shown that both the olfactory and trigeminal systems take part in odour detection and discrimination in humans (Doty, 1975). Chemicals can be sorted according to their pungency with “pure odorants” ranked with the lowest trigeminal potency. To characterize trigeminal chemesthesis in the mouse nasal cavity, the pure odorant phenylethyl alcohol (PEA) and specific TRP channel agonists further described below were used. Sixteen mechanically and electrically-activated axons were responsive to chemical stimuli with receptive fields located primarily within the respiratory epithelium (Fig. 14, panel A, black & white markers). Responses to chemical stimuli were identified using the “latency marking” technique previously described (an example is shown in Fig 14, panel B).

Phenylethyl alcohol (PEA)

As a substance which does not contribute to pungency in people (Doty, 1975), PEA was used to examine the sensitivity of trigeminal axons to a pure odorant.

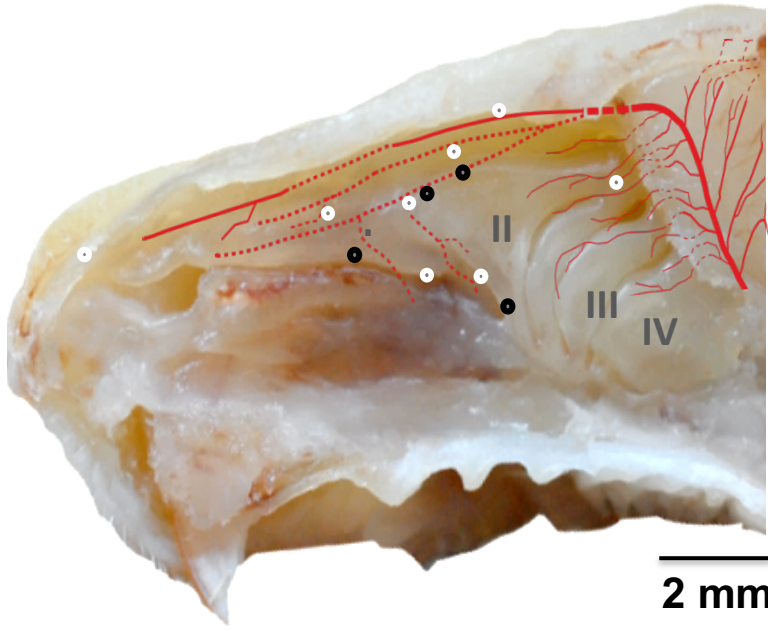
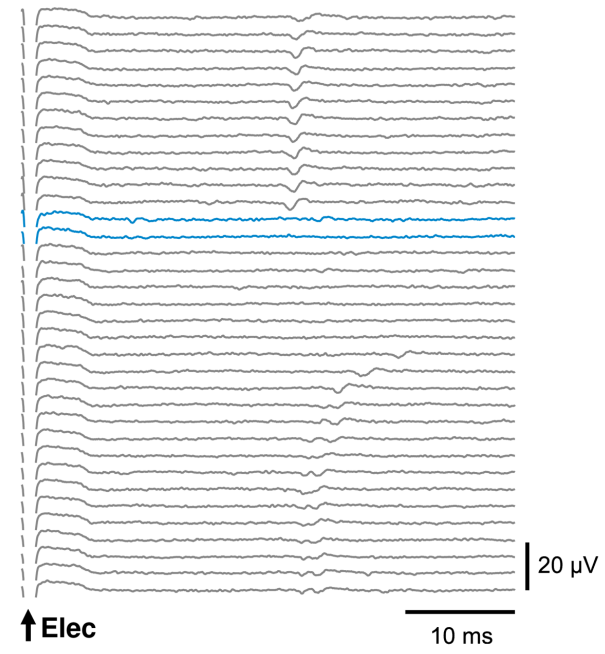
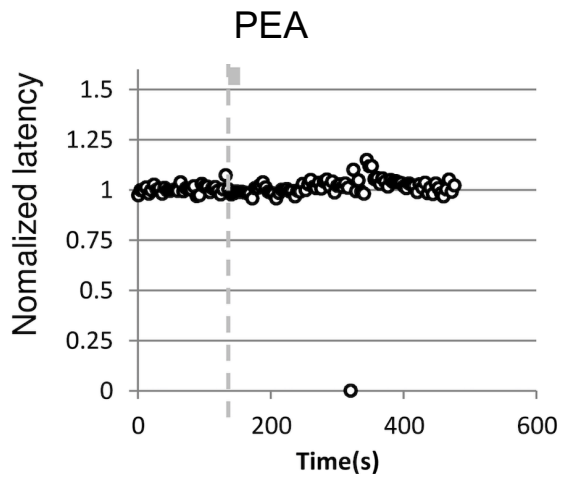
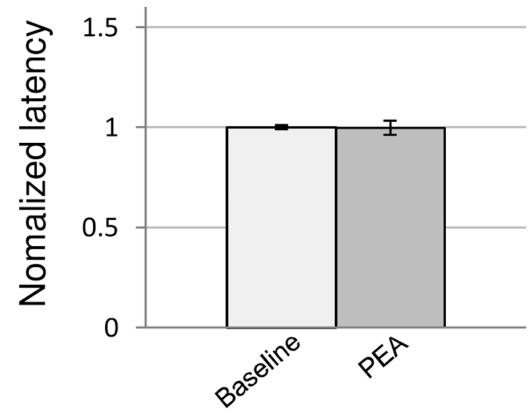
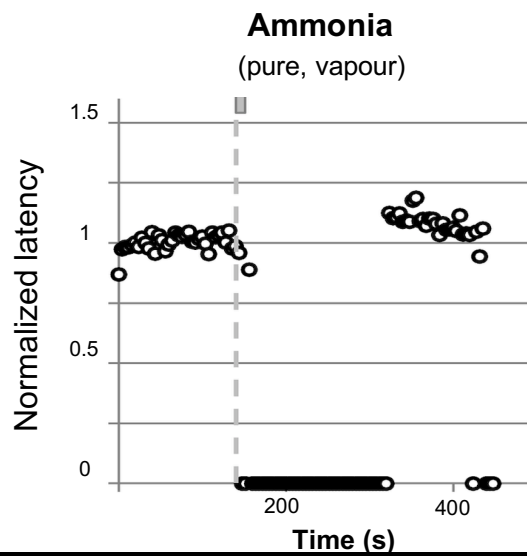
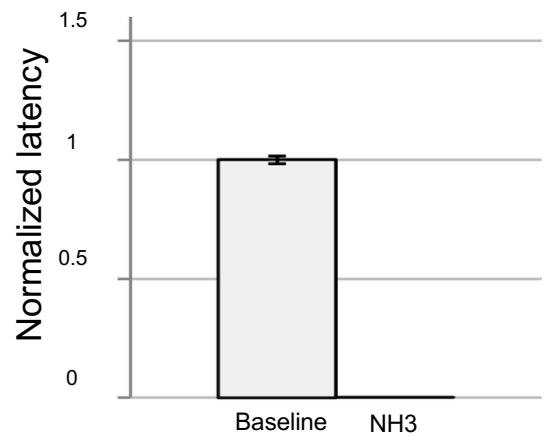
A**B****C****D****E****F**

Figure 14: Chemosensitivity of trigeminal afferents within the nasal epithelium.

A: Mapping individual sensory trigeminal axon responding to electrical (white markers) or mechanical (black markers) stimuli co-activated by chemical substances applied in the recording bath. Anterior ethmoidal nerve projections are represented in red. Scale bar = 2 mm. Background adapted from Barrios et al. 2014.

B: Example of an electrically evoked response disappearing during chemical co-activation of the trigeminal axon. Each line corresponds to an electrical stimulation. Vertical scale bar = 20 μ V ; horizontal bar = 10 ms.

C: Normalized latency of a trigeminal response to repeated electrical stimuli before, during and after PEA co-application. Each marker corresponds to the latency of a trigeminal action potential response.

D: Comparison of normalized latencies of individual trigeminal action potential responses before and during PEA co-stimulation for 6 axons tested.

E: Representative example of changes in electrical response latency of individual trigeminal axons during application of ammonia vapour in the nasal cavity

F: corresponding pooled data for latency changes (n = 4).

Phenylethyl alcohol was applied pure as a vapour to the air exposed nasal epithelium using a syringe and was without effect on the electrical response latency of trigeminal axons (Fig. 14, panel C), for any of the 6 units tested (Fig. 14, panel D, n = 6, t-test, p = 0.769).

Ammonia

Ammonia (NH₃) is a pungent substance present in household detergents. This noxious volatile chemical has been shown to elicit calcium responses in mice sensory neurons via the activation of transient receptor potential channels such as TRPV1 and TRPA1, involved in heat and pain perception (Dhaka *et al.*, 2009). Ammonia was applied as a pressurized air pulse to the air exposed nasal epithelium and activated all 4 trigeminal units tested (Fig. 14, panel E, F).

TRPV1 agonists

The transient receptor potential vanilloid 1 is involved in heat and pain perception (Caterina *et al.*, 1997). TRPV1 agonists capsaicin (250nM, Fig.15, panel A, left) and cyclohexanone (1% v/v, Fig. 15, panel B, left) were applied to the solution perfusing the recording chamber.

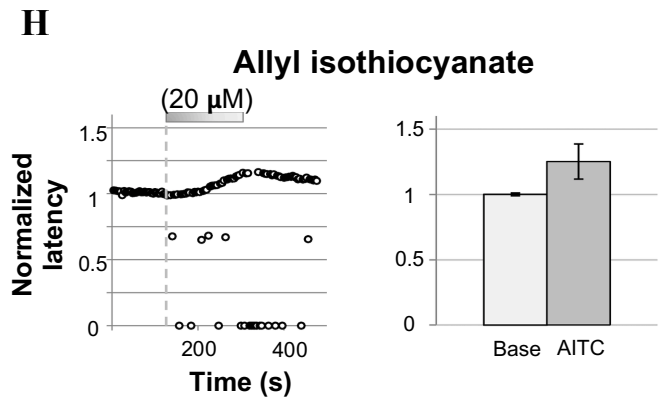
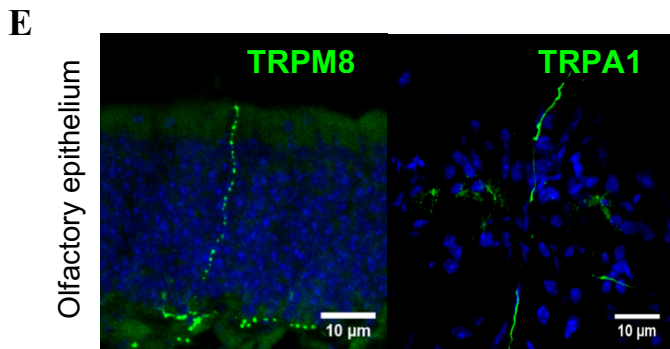
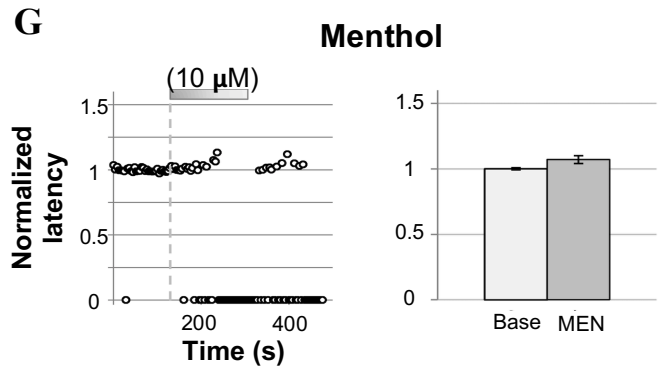
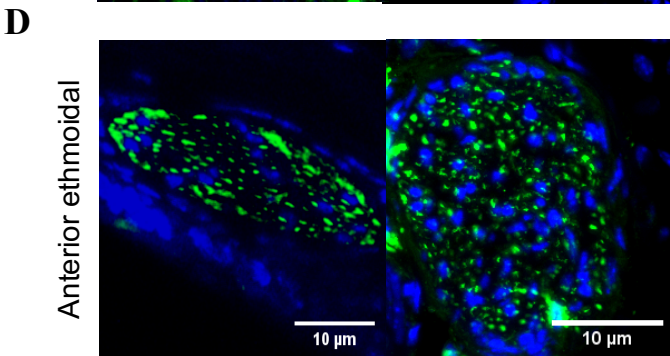
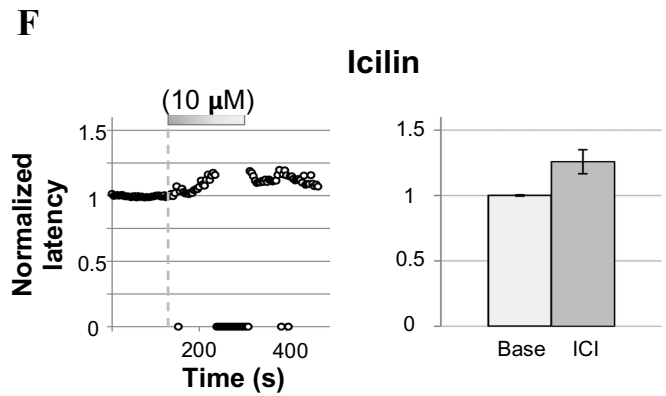
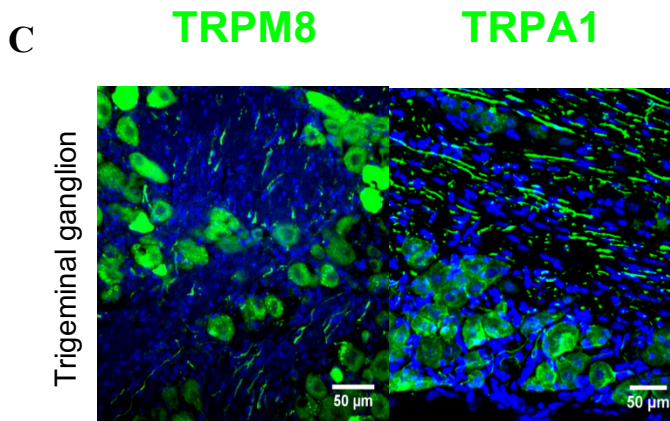
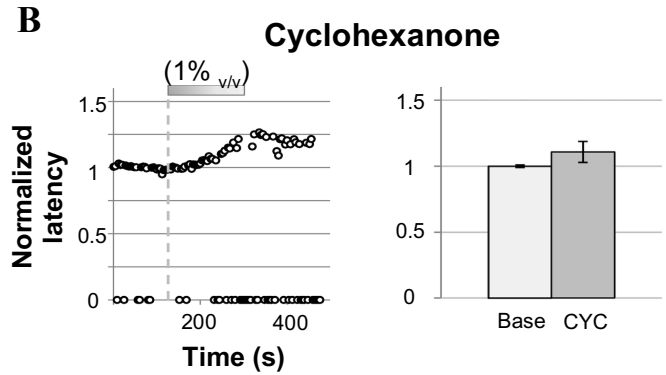
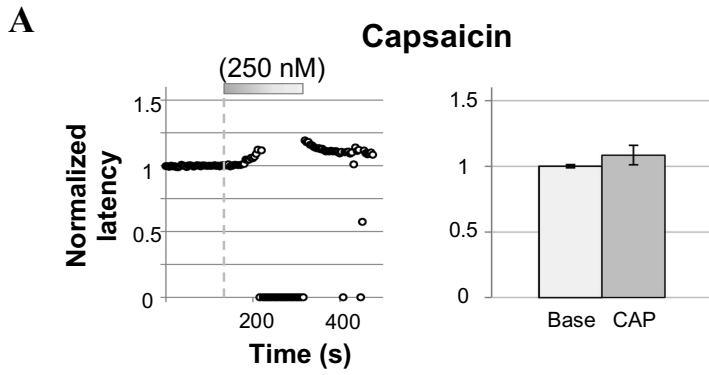


Figure 15: TRP channels transduce nasal trigeminal chemesthesis.

A & B: Representative examples of changes in electrical response latency of individual trigeminal axons during application of TRPV1 agonists in the nasal cavity (left panels) and corresponding pooled data for latency changes in response to capsaicin (250 nM, n = 2), and cyclohexanone (1%; n = 5).

C: Cellular bodies TRPM8 (green, left) and TRPA1 (green, right, Maurer et al., 2019, data acquired and kindly offered by Nunzia Papotto, Center for Organismal Studies) positive neurons in trigeminal ganglia sections. Cell nuclei are labelled with DAPI. Scale bar = 50 μ m.

D: Axon bundles TRPM8 (green, left) and TRPA1 (green, right, Maurer et al., 2019, data acquired and kindly offered by Nunzia Papotto, Center for Organismal Studies) positive axons in coronal sections of the anterior ethmoidal nerve. Cell nuclei are labelled with DAPI. Scale bar = 10 μ m.

E: TRPM8-positive individual axon passing through the olfactory epithelium and ending in the mucus layer (left). TRPA1-positive individual axon passing through the olfactory epithelium (right). Cell nuclei are labelled with DAPI. Scale bar = 10 μ m.

F & G: Representative examples of changes in electrical response latency of individual trigeminal axons during application of TRPM8 agonists in the nasal cavity (left panels) and corresponding pooled data for latency changes in response to (-)-menthol (10 μ M, n = 1) and icilin (10 μ M, n = 2).

H: Representative example of changes in electrical response latency of individual trigeminal axons during application of the TRPA1 agonist in the nasal cavity (left panels) and

Out of 5 receptive fields exposed, 2 afferents responded to the hot compound of chilli peppers capsaicin added to the recording bath (Fig. 15, panel A, right, norm. latency_{baseline} = 1.00 \pm 0.01 norm.latency_{CAP} = 1.08 \pm 0.07). Likewise, 1% v/v cyclohexanone induced a delay in action potential latency for 5 receptive fields out of 10 (Fig. 15, panel B, right, norm. latency_{baseline} = 1.00 \pm 0.01, norm.latency_{CYC} = 1.11 \pm 0.08). Noticeably, most units tested for TRPV1 agonists sensitivity did not recover completely after exposure to the TRPV1 agonist.

TRPM8 agonists

Cold perception is mainly mediated by activation of the transient receptor potential channel melastatine 8 (Bautista *et al.*, 2007). Specific subpopulations of TRP-positive fibres have been identified in diverse trigeminal structures associated with the innervation of the nasal cavity.

In a TRPM8-eGFP mouse model previously characterized (Dhaka *et al.*, 2008), the reporter green fluorescent protein could be observed in cell bodies within the trigeminal ganglion and in axon bundles in coronal sections of the anterior ethmoidal nerve (Fig. 15, panels C, D, left panels). Moreover, sections of the nasal cavity revealed individual eGFP labelled axon terminals crossing the olfactory epithelium from the lamina propria to the apical surface (Fig. 15, panel E, left panel). Several cold-mimicking substances, such as menthol or icilin, can activate TRPM8 channels (McKemy, Neuhausser and Julius, 2002). Functionally, both trigeminal afferents tested were activated by icilin (10 μ M, Fig. 15, panel F, norm. latency_{baseline} = 1.00 ± 0.003 , norm.latency_{ICI} = 1.26 ± 0.09) while menthol evoked an increase in latency in 1 out of 3 units recorded (10 μ M, Fig. 15, panel G, norm. latency_{baseline} = 1.00 ± 0.01 , norm.latency_{MEN} = 1.07 ± 0.03).

TRPA1 agonist

The transient receptor potential ankyrin 1, named after the repeated ankyrin domains forming the N-terminal side of the protein, is controversially thought to be involved in noxious cold perception (Reid, 2005). Alike TRPM8, somata and fibres of trigeminal neurons expressing transient receptor potential channels TRPA1 were labelled and identified in the trigeminal ganglion and the anterior ethmoidal nerve using immunostaining techniques (Fig. 15, panel C, D, right panels, Maurer *et al.*, 2019, data acquired and kindly offered by Nunzia Papotto, Center for Organismal Studies). In the nasal cavity, afferent somatosensory axons were also identified crossing the olfactory epithelium from the lamina propria towards the apical surface (Fig. 15, panel E, right panel). However, no axonal ending could be discerned. TRPA1 is activated by agonists such as allyl isothiocyanate (AITC), a pungent constituent of wasabi also named mustard oil (Jordt *et al.*, 2004). AITC elicited delays in conduction latency for 2 out of 4 receptive fields exposed to the substance in the recording bath (20 μ M, Fig. 15, panel H, norm. latency_{baseline} = 1.00 ± 0.01 , norm.latency_{MEN} = 1.25 ± 0.13).

3. The sodium voltage gated channel 1.8 is expressed within an OSN subpopulation

An unexpected observation was made during imaging of the nasal cavity in Scn10a-Cre:tdTomato-OMP-hChR2Venus transgenic mice. The fluorescent reporter TdTomato expressed under the promoter of the Na_v 1.8 gene, namely Scn10a, was detected in a subpopulation of olfactory sensory neurons recognized by Venus-tagged olfactory marker proteins.

Axonal and dendritic projections were also labelled within the nasal epithelium of Scn10a-Cre:tdTomato-OMP-hChR2Venus mice. Specifically, bundles of sensory tdTomato positive axons could be observed in the lamina propria, under the epithelium (Fig. 16, panel A). Moreover, OSNs expressing Na_v 1.8 sent ca. 15 μ m long projections through the epithelium towards the apical surface where knob-like terminals could be discerned (Fig. 16, panel B, arrows).

TdTomato-labelled OSN cell bodies were located in the lower part of the epithelium, although not in the lowest cell layer, including basal cells differentiating in OSNs (Fig. 16, panel A, B). In an attempt to functionally verify the presence of Na_v 1.8 isoforms within OSNs we took advantage of the optogenetic properties of resistance of the OMP-hChR2Venus mouse line expressing the light-sensitive channel rhodopsin 2 (ChR2), under the promoter for OMP, in the plasma membrane with exception of OSN cilia (Genovese *et al.*, 2016). Electro-olfactogram recordings of OSN field potentials were thus performed in submersed hemi-sected skull preparations, and biphasic EOG responses were recorded at the surface of the second endoturbinat in response to 470 nm light pulses applied on the same epithelial area (Fig. 16, panel C). Stimulus durations varying by 5 to 15ms resulted in EOG signals with significant differences in amplitude. The maximal field potential recorded, corresponding to a highly synchronous OSN activation, was observed for 10 ms stimuli (Fig.16 panel C). Therefore, this duration was selected for pharmacology experiments. Each light stimulus was repeated 4 consecutive times during exposure to any chemical applied in the recording bath.

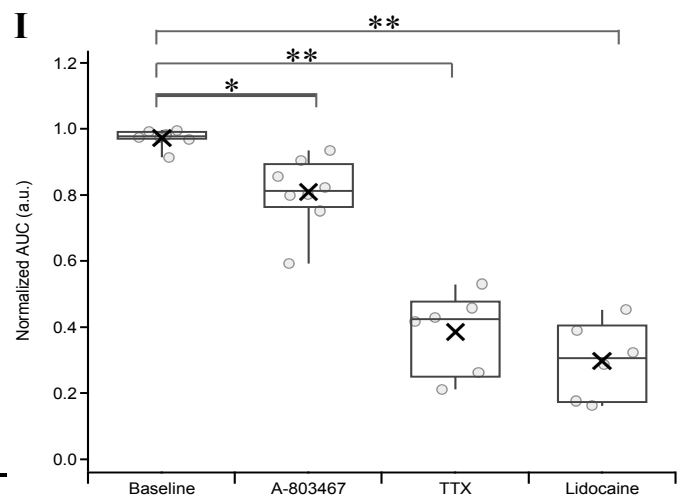
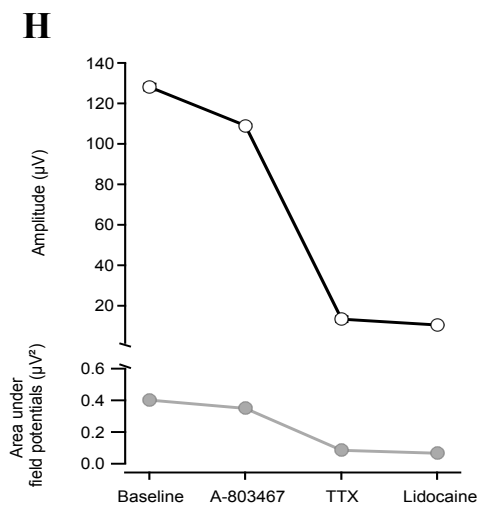
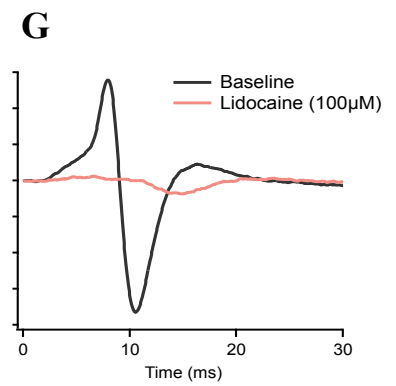
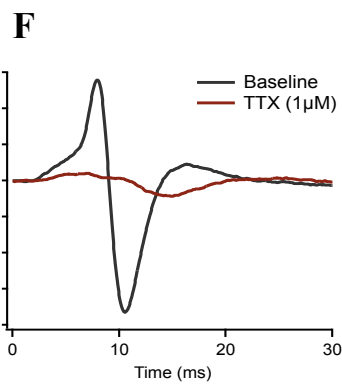
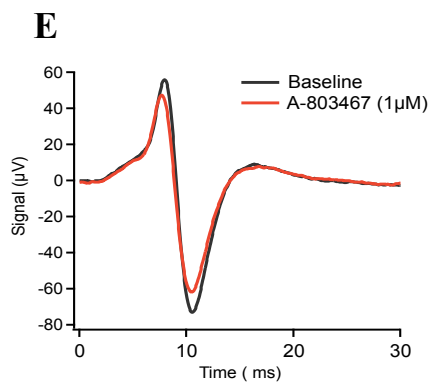
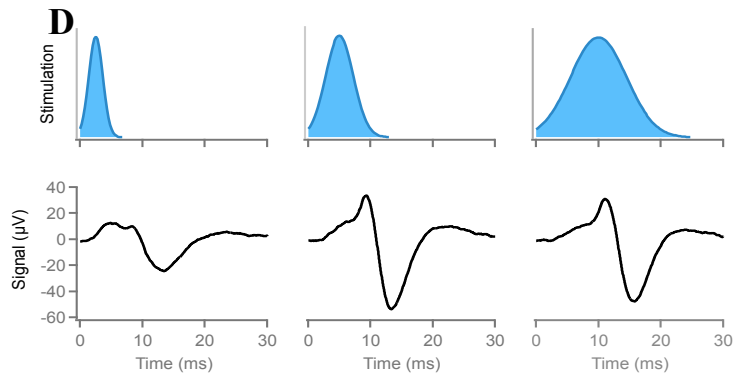
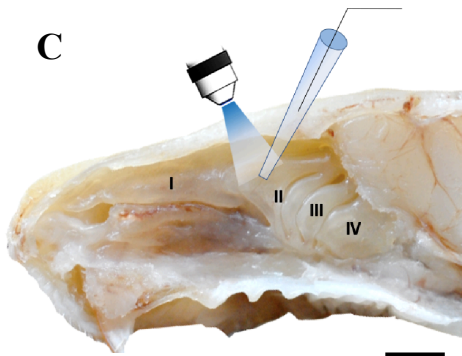
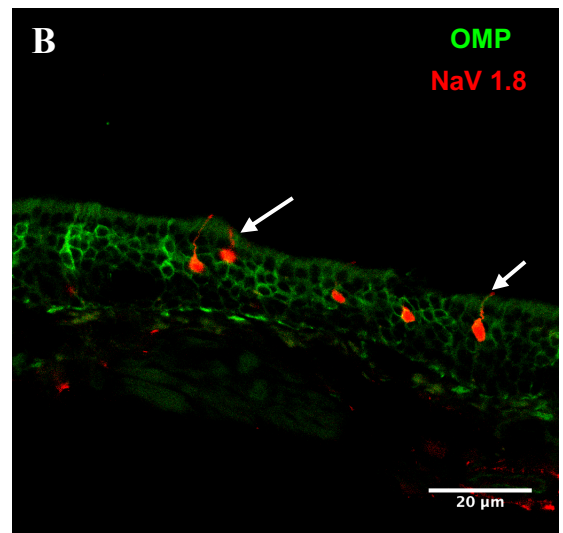
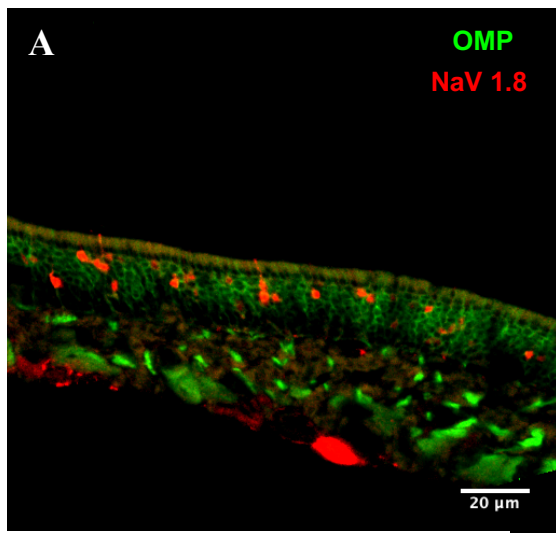


Figure 16: Nav 1.8 sodium voltage-gated channel is expressed in a subpopulation of OSNs

A: Sensory cellular bodies and projections identified within the olfactory epithelium of Scn10A-TdTomato-OMP-EYFP mice. Scale bar = 20 μ m.

B: Example of Nav1.8 expressing sensory cells observed at a higher magnification surrounded by OSNs. Sensory projections reach the apical surface of the epithelium (arrow). Scale bar = 20 μ m.

C: Ex-vivo half skull preparation used to record OSN field potentials on the middle part of the endoturbinates II following light stimulation. Scale bar = 2 mm. Roman number correspond to nasal endoturbinates.

D: Field potentials (black traces) evoked by 5 ms, 10 ms or 20 ms light pulses (blue traces) in OMP-hChr2Venus mice. Signals with a maximal amplitude were obtained with 10 ms stimuli.

E-G: Representative example of field potential recorded before (grey trace, "baseline") and after application of 1 μ M of the Nav1.8 channel inhibitor A-803467 (E, red trace), 1 μ M TTX (F, dark red trace), and 100 μ M lidocaine (G, light red trace).

H: Decrease in the relative amplitude (upper) following the application of 1 μ M A-803467 (reduction of 14.9 ± 1.5 %), 1 μ M TTX (reduction of 87.6 ± 1.4 %) and 100 μ M lidocaine (reduction of 91.7 ± 0.3 %). Values were averaged for 4 consecutive light stimuli. Decrease in the total area under field potentials (lower) following the application of 1 μ M A-803467 (reduction of 12.8 ± 1.5 %), 1 μ M TTX (reduction of 75.1 ± 1.1 %) and 100 μ M lidocaine (reduction of 83.3 ± 0.9 %) (values were averaged for 4 consecutive light stimuli).

I: Box and whisker plot representing normalized area under field potentials (AUC) in arbitrary units (a.u.). In comparison to control (min = 0.91, Q1 = 0.97, mediane = 0.98, Q3 = 0.99, max = 0.99, average = 0.97, SD = 0.02), light-evoked field potential AUC were significantly reduced after application of 1 μ M A-803467 (min = 0.59, Q1 = 0.77, mediane = 0.81, Q3 = 0.89, max = 0.94, average = 0.80, SD = 0.10; paired t-test, $p = 0.0034$), 1 μ M TTX (min = 0.08, Q1 = 0.21, mediane = 0.42, Q3 = 0.48, max = 0.53, average = 0.39, SD = 0.12; paired t-test, $p < 0.001$) and 100 μ M lidocaine (min = 0.16, Q1 = 0.17, mediane = 0.30, Q3 = 0.40, max = 0.45, average = 0.29, SD = 0.11; paired t-test, $p < 0.001$).

Upon addition of 1 μ M of the Nav 1.8-specific channel blocker A-803467 (Jarvis *et al.*, 2007), light-induced OSN responses decreased (a representative example is shown in Fig. 16, panel E) and the relative amplitude of EOG responses, averaged over 4 consecutive light stimulations, decreased of 14.9 ± 1.5 % (Fig. 16, panel H, upper section). The area under EOG signals, another measure for OSN activity less dependent on synchronization, was also reduced following the application of A-

803467 (Fig. 16, panel H, lower section ; reduction of 12.8 ± 1.5 %). Six OMP-hChR2Venus mouse hemisected skulls were successively exposed to 1 μ M TTX and 100 μ M lidocaine, added to the recording bath solution. Signals were largely suppressed by both toxins (examples are shown in Fig. 16, panel F, G), characterized with reduced amplitudes (Fig. 16, panel H, upper section ; TTX: reduction of 87.6 ± 1.4 % ; Lidocaine: reduction of 91.7 ± 0.3 %) and area measured under EOG signals (Fig. 16, panel H, lower section ; TTX: reduction of 75.1 ± 1.1 % ; Lidocaine: reduction of 83.3 ± 0.9 %). Quantitative evaluation revealed a significant reduction of the normalized area under OSN field potentials in the presence of A-803467 (Fig. 16, panel I; 1 μ M, n = 8 , min = 0.59 , Q1 = 0.77, mediane = 0.81, Q3 = 0.89 , max = 0.94 , average = 0.80, SD = 0.10, paired t-test, p = 0.0034) in comparison to control light-evoked responses (Fig. 16, panel I ; “baseline”, n = 8, min = 0.91 , Q1 = 0.97, mediane = 0.98, Q3 = 0.99 , max = 0.99 , average = 0.97, SD = 0.02) . In contrast, TTX (Fig. 16, panel I; 1 μ M, n = 6, min = 0.08 , Q1 = 0.21, mediane = 0.42, Q3 = 0.48 , max = 0.53 , average = 0.39, SD = 0.12) and lidocaine (Fig. 16, panel I; 100 μ M, n = 6, min = 0.16 , Q1 = 0.17, mediane = 0.30, Q3 = 0.40 , max = 0.45 , average = 0.29, SD = 0.11) largely weakened field potentials. These results suggest a significant role of Nav1.8 channels in the electrical excitation of the olfactory neuroepithelium.

B. The odorant PEA mitigates trigeminal-induced nocifensive behaviour in mice

1. Assessment of cross-modal interaction between olfactory and trigeminal systems in mice

The influence of concomitant OSNs activation on nasal trigeminal signal processing was assessed in mice using a behavioural index measured during a forced choice water preference test. The paradigm was established by offering animals two identical water bottles within their individual isolated ventilated cages. Since the sources of water were physically identical and mice were able to drink freely from either, the consumption of water from one bottle over another was taken of as an index of preference.

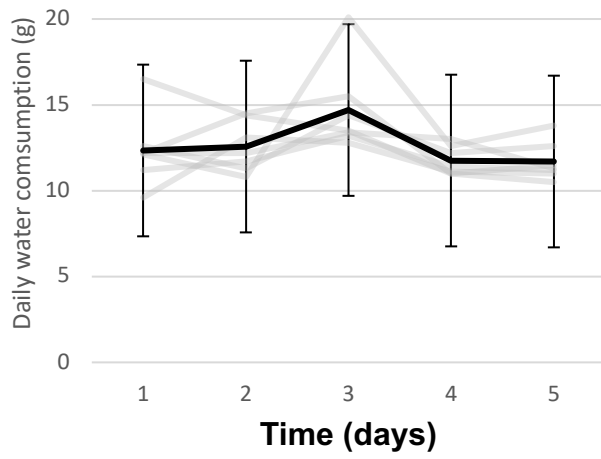
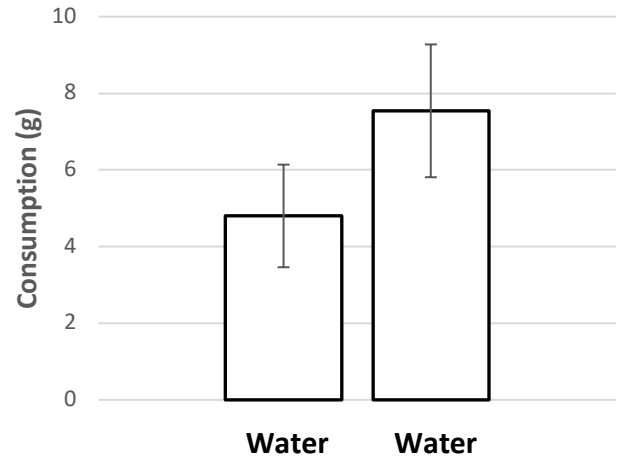
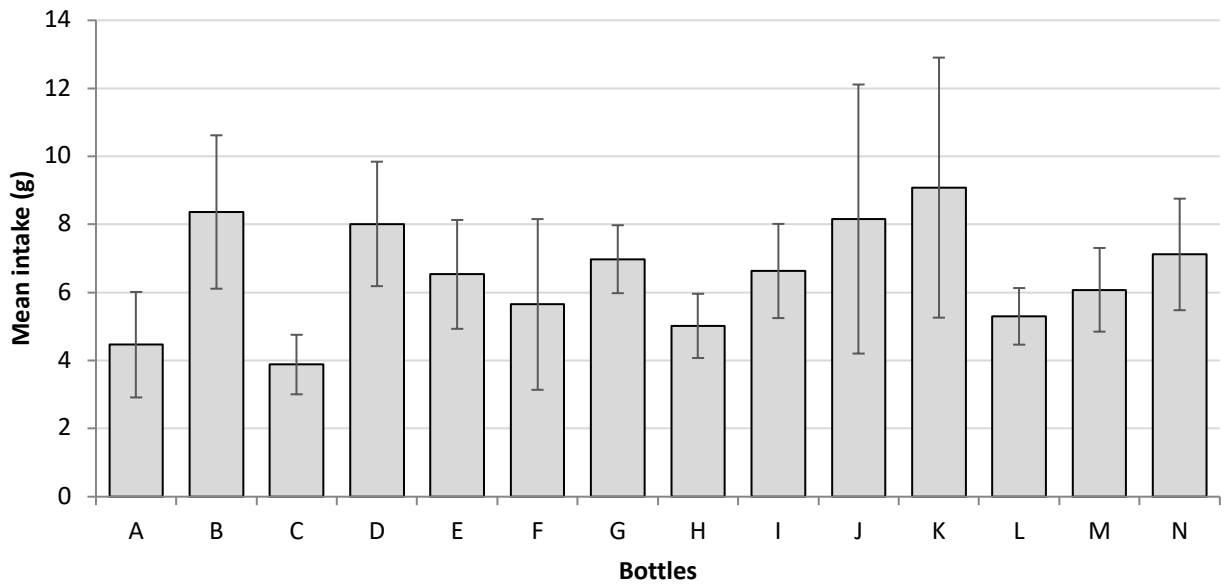
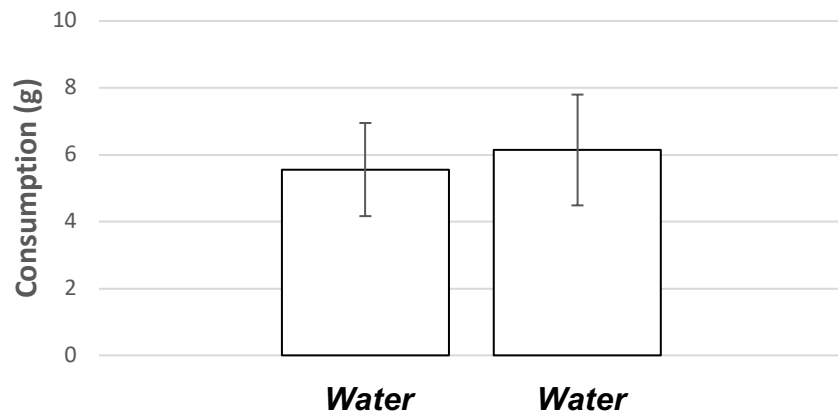
A**Daily water consumption****B****Water preference****C****Bottle consumption****D****Water preference**

Figure 17: Baseline water consumption depends on bottle

A: Daily water consumption in grams for each of the 8 mice tested over 6 days (grey curves). The black curve represents averaged daily consumption.

B: Water consumption during a forced choice behavioral test showing a preference for the water source placed on the right side of the cage (paired t-test, $p = 0.02$, $n = 7$).

C: Mean water intake over 24 hours for each bottle used to assess water source preference.

D: Water consumption during the repeated forced choice behavioral test using new bottles. In this assay, no preference could be determined for any of the water source used (paired t-test, $p = 0.61$, $n = 7$)

a. Water bottle flow and sipping tube diameter influence two bottle preference test measures

The forced choice water preference test paradigm relies on the initial observation that under control conditions, in the absence of any volatile or gustatory stimulus and without any pre-existing bias, mice drank equally from the two water sources. To establish this condition, several tests were performed with the aim to find the right configuration leading to a similar water consumption, independent of the type of bottles. Initially, bottles sipping spouts were cleaned using 70% ethanol and rinsed with water. Mice were presented clean bottles daily, in a randomized order. After an acclimatization period of 5 days, during which the average daily intake was comprised between 14.79 ± 3.36 and 11.70 ± 1.12 g per animal (Fig. 17, panel A), the preference towards one of the 2 drinking source presented was measured. Surprisingly, mice did not drink equally from both bottles (Fig. 17. Panel B ; $n = 7$, paired t-test, $p = 0.02$). A rapid quantification of the averaged intake per bottle revealed bottles leaking, leading to an increased consumption and high variability in intake (an example is shown in Fig 17, panel C, Bottle "J", average consumption = 8.1 ± 3.9 g), and clogged sipping spouts, reducing the amount of water accessible for the animal (examples shown in Fig. 17, panel C, Bottle "C", average consumption = 3.9 ± 0.9 g). The acclimatization period was therefore repeated with new bottles (ACBT0152, Tecniplast, Hohenpeissenberg, Germany) and the water consumption over 24h was measured. In

presence of new bottles with less differences in water flow, mice drank equivalent amounts from each water sources presented in the cage (Fig. 17. Panel D, $n = 7$, paired t-test, $p = 0.61$).

b. Aversion to volatile trigeminal irritants is mitigated by co-application of the pure odorant PEA in WT mice

Having settled upon 20 bottles, behavioural experiments were carried out on mice in cohorts of 10. Mice were initially acclimatized to the presence of an empty aluminium housing placed closely around sipping spouts. Water consumption was measured daily during this 7-day period to establish baseline conditions and assess any basal bias. At the end of the acclimatization phase, the amount of water consumed from each bottle was not significantly different across mice (Fig. 18, panel A, $n = 10$, paired t-test, $p = 0.60$).

i. Exposure to PEA does not evoke preference nor aversion during the forced choice test

The water preference behavioural test was first used to assess the influence of purely olfactory stimuli. Therefore, the pure odorant phenylethyl alcohol (PEA), exhaling a rose scent, was added to the odour chamber around one of the two water-dispensing bottles. For this purpose, a piece of felt was soaked in pure PEA and the soaked felt was subsequently placed in the aluminium annular housing. A similar piece of felt, soaked with distilled water (dH_2O) was placed in the olfactory chamber around the opposite sipping tube, enabling the aroma to emanate close to the drinking source. Addition of the odorant PEA to one sipping tube reduced the total amount of water consumed within a given cage (Fig. 18, panel B, upper right, $n = 10$, paired t-test, $p < 0.01$) but did not result in a preference for either bottle within each cage (Fig. 18, panel B, $n = 10$, ANOVA interaction time*PEA $F(1,9) = 2.12$, $p = 0.15$). The effect of PEA on total consumption indicates that the pure odorant PEA is perceived by freely moving mice in an IVC cage. However, the pure odorant does not seem to elicit any preference nor aversion in mice tested.

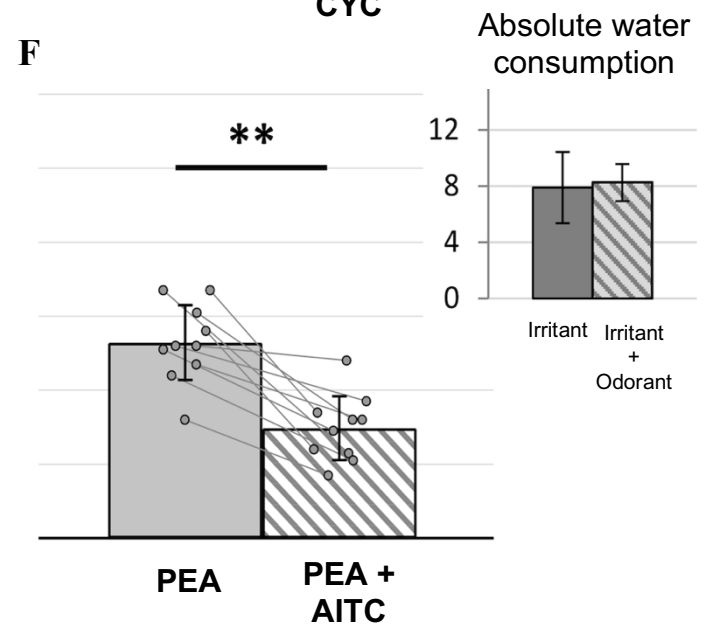
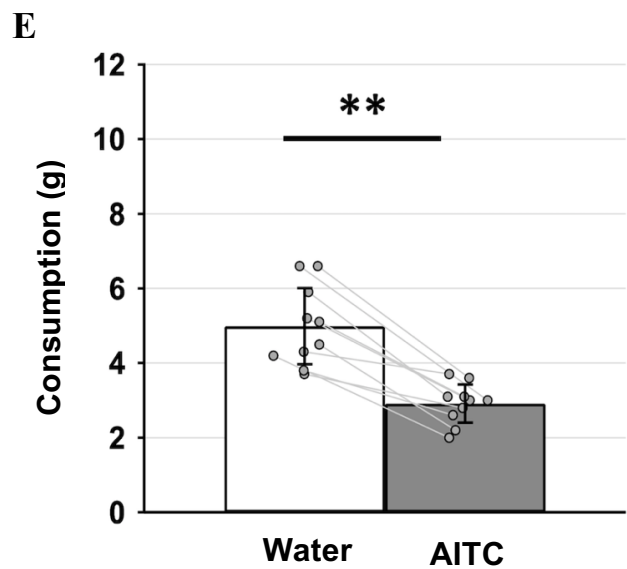
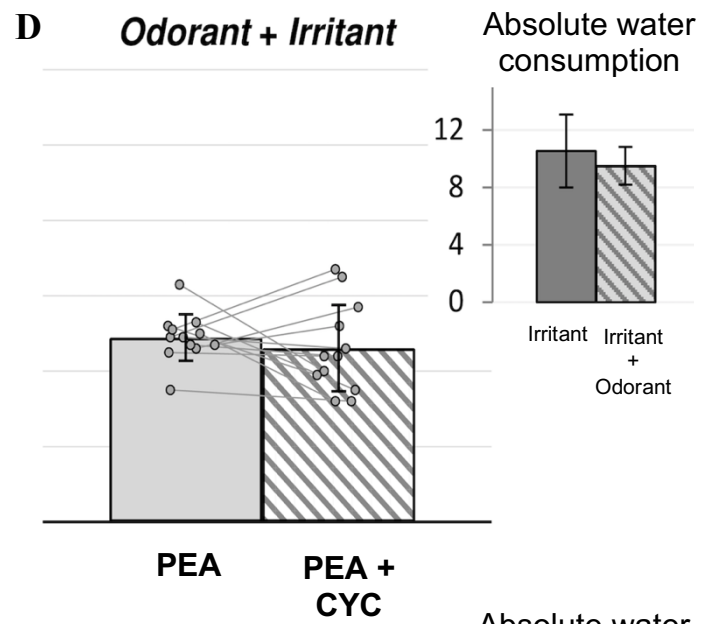
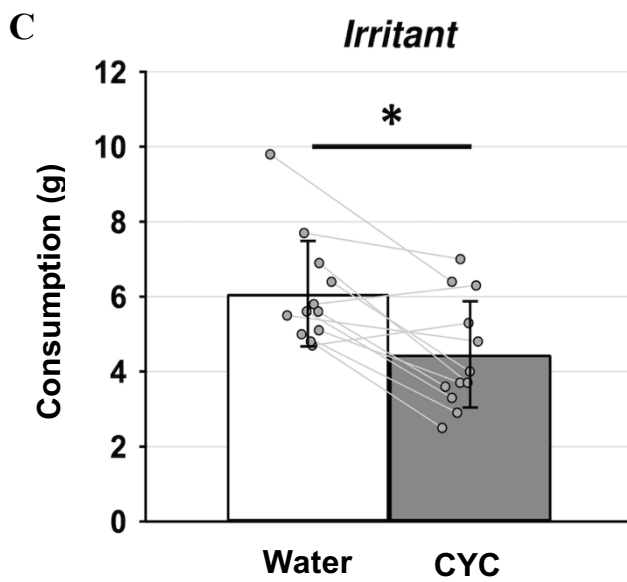
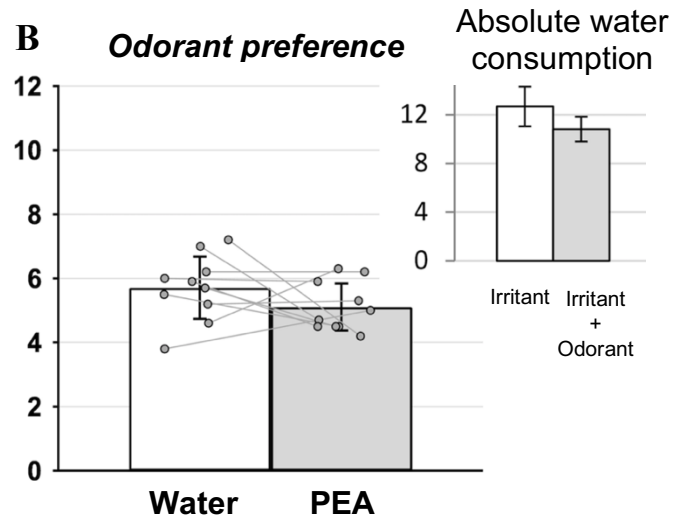
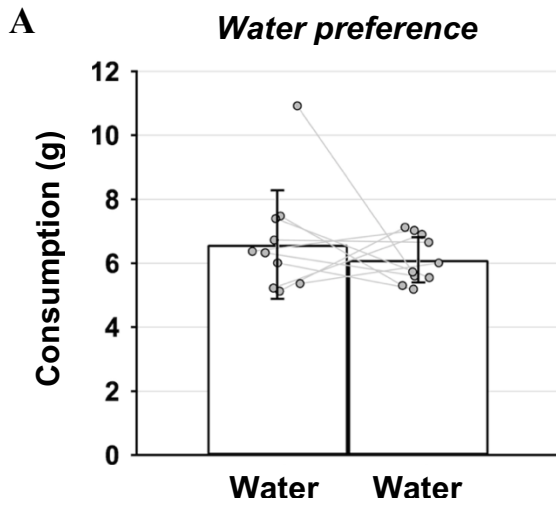


Figure 18: Concomitant exposure to the odorant PEA mitigated the aversion evoked by the volatile irritant cyclohexanone.

A: Water consumption from each of two bottles. In the absence of irritant or odorant there was no bottle preference (paired t-test, $n = 10$, $p = 0.60$).

B: Similarly, there was no drinking preference bottles with pure odorant PEA and vehicle (paired t-test, $n = 10$, $p = 0.26$).

Upper right: Absolute water consumption was diminished by the introduction of PEA (paired t-test, $n = 10$, $p < 0.01$).

Specific aversion caused by cyclohexanone can be mitigated by the odorant PEA.

C: Mice showed aversion to the volatile irritant cyclohexanone (2-way ANOVA, factor cyclo, $p < 0.05$, post hoc Tukey HSD, water vs cyclo, $p = 0.01$).

D: This aversion was mitigated with the addition of PEA to both housings (2-way ANOVA, factor cyclo, $p < 0.05$, post hoc Tukey HSD, PEA vs PEA+cyclo, $p = 0.94$) although absolute water consumption did not change (inset upper right corner: paired t-test, $n = 12$, $p = 0.16$).

E: Mice showed aversion to the volatile irritant AITC (2-way ANOVA, factor AITC, $p < 0.01$, post hoc Tukey HSD, water vs AITC, $p < 0.01$).

F: This aversion persisted with the addition of PEA to both housings (2-way ANOVA, factor AITC, $p < 0.01$, post hoc Tukey HSD, PEA vs PEA + AITC, $p < 0.01$). Absolute water consumption did not change (inset upper right corner: paired t-test, $n = 10$, $p = 0.40$).

ii. The odorant PEA mitigates the aversion evoked by the volatile TRPV1 cyclohexanone in WT mice

A lack of bottle preference in the presence of PEA provided an opportunity to explore the effect of combined olfactory and trigeminal stimuli. Initially, the effect of trigeminal activation alone on drinking preference was examined using volatile irritant substances. Alike the forced choice experiment using the pure odorant PEA, pieces of felt were soaked with volatile irritants and the effect of cyclohexanone and AITC on drinking preference was tested against water. While mice did not show neither a preference nor aversion to water coupled with PEA, the presence of volatile irritants lead to a significant decrease in the amount of water consumed (Fig. 18, panels C, E). The presence of the TRPV1 agonist cyclohexanone (Silver *et al.*, 2006) around one bottle

resulted in reduced consumption in 12 mice (Fig. 18, panel C, 2-way ANOVA, factor CYC, $n = 12$, $p < 0.05$, post hoc Tukey HSD, water vs CYC, $p = 0.01$). To examine the interaction of olfactory and trigeminal stimuli, PEA was added to the odour chambers around the sipping tubes of both water sources. The addition of PEA to both odour sources did not change the absolute amount of water consumed (Fig. 18, panel D, upper right, paired t-test, $n = 12$, $p = 0.16$) but PEA mitigated the aversive influence of cyclohexanone (Fig. 18, panel D, post-hoc Tukey HSD PEA vs PEA+CYC, $n = 12$, $p = 0.94$). However, the interaction between PEA and cyclohexanone did not reach a statistical significance (ANOVA, interaction PEA*CYC $F(1,11)=3.44$, $n = 12$, $p=0.07$). This behavioural effect consolidated the hypothesis that odorant olfactory stimuli can affect the perception of volatile irritants in freely behaving mice.

iii. PEA does not reduce the aversion evoked by the undiluted TRPA1 agonist allyl isothiocyanate

The same experimental protocol was used to assess allyl isothiocyanate, a volatile TRPA1 agonist (Takaya *et al.*, 2015) present in mustard and wasabi. Similar to cyclohexanone, mice showed an aversion to the water source with AITC in the odour chamber around the sipping tube (Fig. 18, panel E, 2-way ANOVA, factor AITC, $p < 0.01$, post hoc Tukey HSD, water vs AITC, $p < 0.01$). Consistent with the control experiments with cyclohexanone, addition of PEA to both chambers did not cause a difference in the absolute amount of water consumed (Fig. 18, panel F, upper right, paired t-test, $n = 10$, $p = 0.40$). However, there was an aversion to a pure solution of AITC and this was not mitigated by the addition of the pure odorant PEA (Fig. 18, panel F, 2-way ANOVA, factor AITC, $p < 0.01$, post hoc Tukey HSD, PEA vs PEA + AITC, $p < 0.01$).

iv. Nocifensive behaviour caused by milder concentrations of AITC can be mitigated by the addition of PEA

To examine the possibility that the high concentration of AITC might mask a PEA mitigation, allyl isothiocyanate was diluted to 10, 30 or 60 %. Each AITC dilution was tested in a group of 3 male wild type C57BL/6N mice. Similar to pure AITC, avoidance of the water source paired with AITC alone was observed for each dilution and the magnitude of the aversion correlated with the purity of the irritant, specifically at 60 % (Fig. 19, panel A, mean_{water} = 4.70 ± 0.60 ; mean_{AITC 60%} = 2.40 ± 0.53 ; $n = 3$), 30 % (Fig. 19, panel C, mean_{water} = 4.77 ± 0.81 ; mean_{AITC 30%} = 2.30 ± 0.40 ; $n = 3$) and

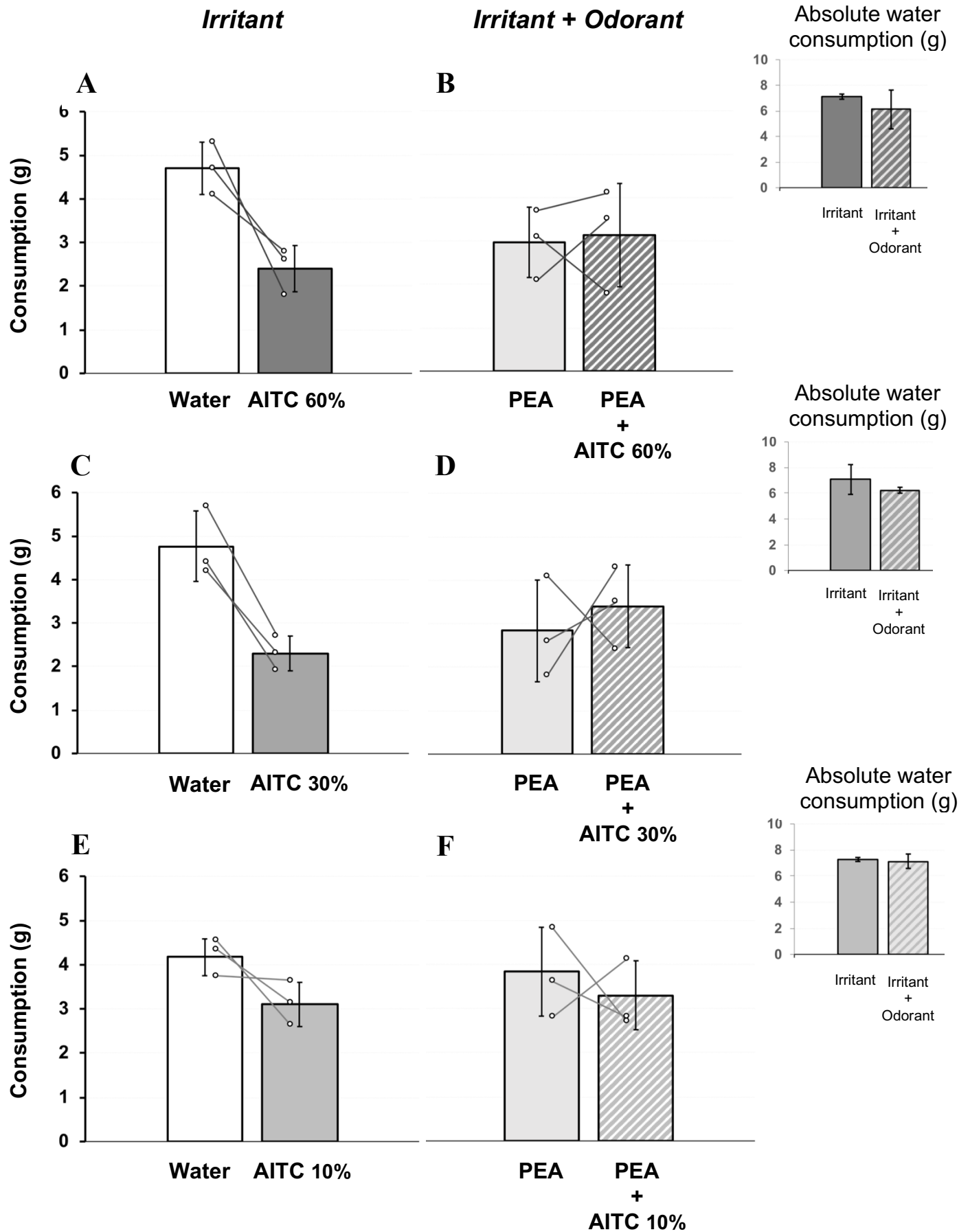


Figure 19: Concomitant exposure to the odorant PEA mitigated the aversion evoked by diluted solutions of the volatile irritant allyl isothiocyanate.

A: Mice avoided to drink from a water source paired with the volatile irritant allyl isothiocyanate diluted at 60% in physiological solution (mean_{water} = 4.70 ± 0.60; mean_{AITC 60%} = 2.40 ± 0.53; n = 3).

B: This aversion was mitigated with the addition of PEA to both housings (mean_{PEA} = 2.97 ± 0.81 ; mean_{PEA+AITC 60%} = 3.13 ± 1.19; n = 3) although absolute water consumption did not change (inset upper right corner: mean_{water/AITC60%} = 7.10 ± 0.20; mean_{PEA/PEA+AITC 60%} = 6.10 ± 1.51; n = 3).

C: Mice avoided to drink from a water source paired with the volatile irritant allyl isothiocyanate diluted at 30% in physiological solution (mean_{water} = 4.77 ± 0.81; mean_{AITC 30%} = 2.30 ± 0.40; n = 3).

D: This aversion was mitigated with the addition of PEA to both housings (mean_{PEA} = 2.83 ± 1.17 ; mean_{PEA+AITC 30%} = 3.40 ± 0.95; n = 3) although absolute water consumption did not change (inset upper right corner: mean_{water/AITC30%} = 7.07 ± 1.16; mean_{PEA/PEA+AITC 30%} = 6.23 ± 0.23; n = 3).

E: Mice avoided to drink from a water source paired with the volatile irritant allyl isothiocyanate diluted at 10% in physiological solution (mean_{water} = 4.17 ± 0.42; mean_{AITC 10%} = 3.10 ± 0.50; n = 3).

F: This aversion was mitigated with the addition of PEA to both housings (mean_{PEA} = 3.83 ± 1.01 ; mean_{PEA+AITC 10%} = 3.30 ± 0.78; n = 3) although absolute water consumption did not change (inset upper right corner: mean_{water/AITC10%} = 7.27 ± 0.15; mean_{PEA/PEA+AITC 10%} = 7.13 ± 0.55; n = 3).

10 % (Fig. 19, panel E, mean_{water} = 4.17 ± 0.42; mean_{AITC 10%} = 3.10 ± 0.50; n = 3). Also consistent with previous observations, the presence of PEA alone in the chambers of both bottles did not alter the absolute amount of water consumed by any group (Fig. 19, panel B, upper right corner, mean_{water/AITC60%} = 7.10 ± 0.20; mean_{PEA/PEA+AITC 60%} = 6.10 ± 1.51; n = 3 ; panel D, upper right corner, mean_{water/AITC30%} = 7.07 ± 1.16; mean_{PEA/PEA+AITC 30%} = 6.23 ± 0.23; n = 3 ; and panel F, upper right corner, mean_{water/AITC10%} = 7.27 ± 0.15; mean_{PEA/PEA+AITC 10%} = 7.13 ± 0.55; n = 3). However, contrary to the results with pure AITC, addition of the odorant PEA reduced the aversion seen with milder concentrations of 60% (Fig. 19, panel B, mean_{PEA} = 2.97 ± 0.81 ; mean_{PEA+AITC 60%} = 3.13 ± 1.19; n = 3) or 30% (Fig. 19, panel D, mean_{PEA} = 2.83 ± 1.17 ; mean_{PEA+AITC 30%} = 3.40 ± 0.95;

n = 3) of AITC. In presence of low concentrations of AITC, avoidance was reduced and similarly the ability of PEA to neutralize this avoidance increased (Fig. 19, panel F, mean_{PEA} = 3.83 ± 1.01 ; mean_{PEA+AITC 10%} = 3.30 ± 0.78; n = 3).

In this forced-choice water consumption test, mice avoided water sources surrounded by either cyclohexanone or AITC, respectively volatile TRPV1 and TRPA1 irritants. This aversion could be mitigated by the presence of the pure odorant PEA, confirming an interaction between the olfactory and trigeminal systems.

2. Assessment of cross-modal interaction between olfactory and trigeminal systems in humans

To assess the possibility of a cross-modal interaction between the olfactory and the trigeminal system in humans, a psychophysical test was realized. Participants were asked to rate the pungency and olfactory potency of volatile substances, including irritants and odorants, presented in the vicinity of their nostrils. In addition to ammonia (1 M), known to be a pungent volatile substance contained in smelling salts (Cometto-Muniz and Hernandez, 1990), irritant test chemicals were chosen by virtue of their ability to act as ligands for distinct classes of channels of the transient receptor potential (TRP) channel family. Specifically, menthol (MEN, (1S,2R,5S)-(+)-Menthol, 1 mM) and icilin (IC, 10 μM) were chosen for their agonist action at TRPM8 (McKemy, Neuhauser and Julius, 2002; Chuang, Neuhauser and Julius, 2004), *trans*-cinnamaldehyde (CIN, pure) as a TRPA1 agonist (Bandell *et al.*, 2004) and cyclohexanone (CYC, pure) as TRPV1 agonist (Silver *et al.*, 2006). The pure odorant phenylethyl alcohol (PEA) was also added to the list of test substances (Doty, 1975).

a. Variation of olfactory and pungency perception in humans

The intensity of perception for the odorant and irritant stimuli were compared between 4 “control” participants, with olfactory and pain perceptions unaltered, and 3 patients presenting different degrees of insensitivity to pain. This psychophysical experiment was realized in collaboration with Dr Roman Rukwied (Department of Anesthesiology, Heidelberg University, Medical Faculty, Mannheim, Germany).

i. Control participants

The control group comprised 2 women (“F1” and “F2”) and 2 men (“M1” and “M2”) with ages ranging between 30 and 50 years old. F1 and M1 subjects were healthy participants belonging to a Chinese family including congenital insensitivity to pain patients, while F2 and M2 were both living in Germany and were not related by blood. Each participant was asked to rate the pungency and odorant intensity of the test substances on a scale ranging from 0 (substance not detected) to 10 (maximum odour or pain intensity). Volatile chemicals were presented only once to each participant in a random order. Both olfactory and pungency ratings varied between participants.

Distilled water

Distilled water (dH₂O) was presented amongst test substances to determine a negative control for which no volatile chemical would be detected. F1 and M1 expectedly did not detect any odour (Fig.20, panel A, “dH₂O”, olfactory rating F1 = 0 / 10 , olfactory rating M1 = 0 / 10) nor pungency (Fig. 20, panel B, “dH₂O”, pungency rating F1 = 0 / 10 , pungency rating M1 = 0 / 10) for distilled water. However, multiple factors, such as ambient airflow or remaining scent from previous test substances can influence olfactory and pungency ratings and must be kept in mind while observing psychophysical tests results. Interestingly, both participants tested in Germany perceived an odour in the 50 ml Falcon tube with dH₂O (Fig.20, panel A, “dH₂O”, olfactory rating F2 = 2.5 / 10, olfactory rating M2 = 2 / 10). Moreover, one of these subjects described dH₂O as slightly pungent (Fig.20, panel B, “dH₂O”, pungency rating M2 = 2 / 10). These results might indicate a difference in experimental procedure between Chinese and German participants.

Phenylethyl alcohol

In this psychophysical experiment, PEA (pure) was detected by all 4 participants with medium (Fig.20, panel A, “PEA”, olfactory rating F1 = 4 / 10 , olfactory rating M1 = 4 / 10, olfactory rating M2 = 5 / 10) to high (Fig.20, panel A, “PEA”, olfactory rating F2 = 7 / 10) olfactory intensities. Phenylethyl alcohol has been shown to remain mostly undetected by patients suffering from an inability to perceive olfactory stimuli called anosmia (Doty, 1975), leading to its characterization as “pure” odorant. Accordingly, pungency ratings for this substance was moderate (Fig.20, panel B, “PEA”, pungency rating F2 = 4 / 10 , pungency rating M1 = 4 / 10) to undetected (Fig.20, panel B, “PEA”, pungency rating F1 = 0 / 10 , pungency rating M2 = 0 / 10).

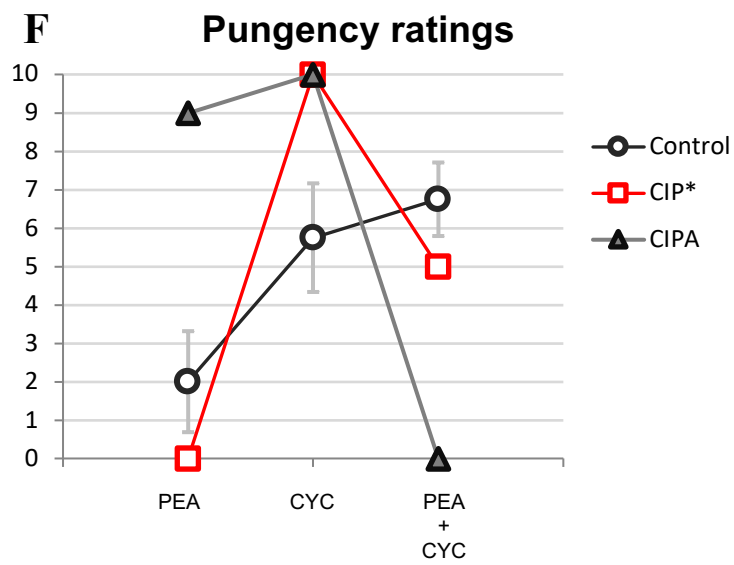
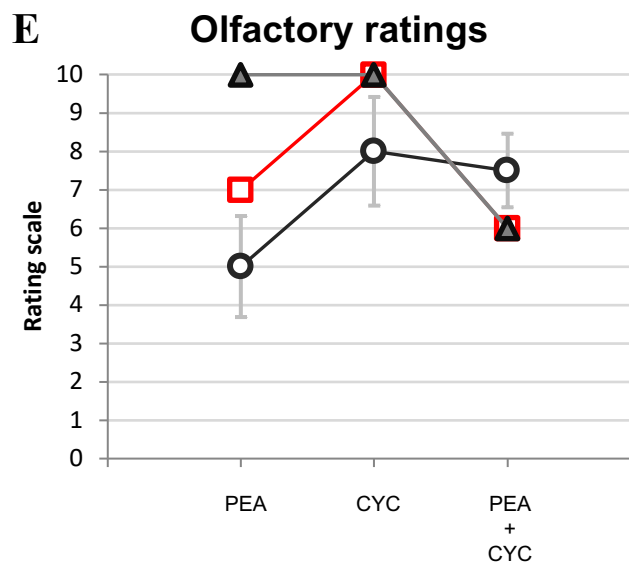
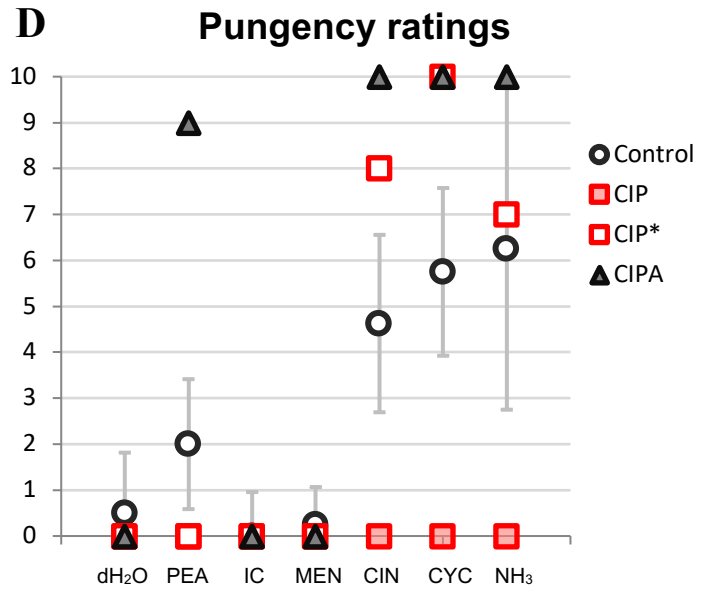
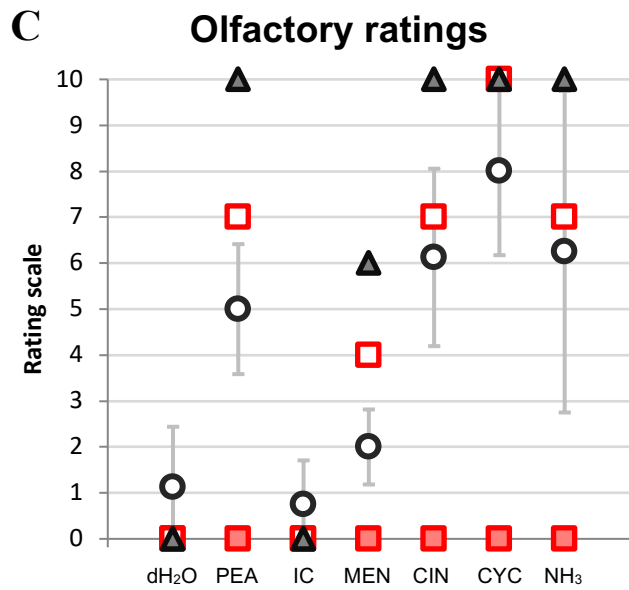
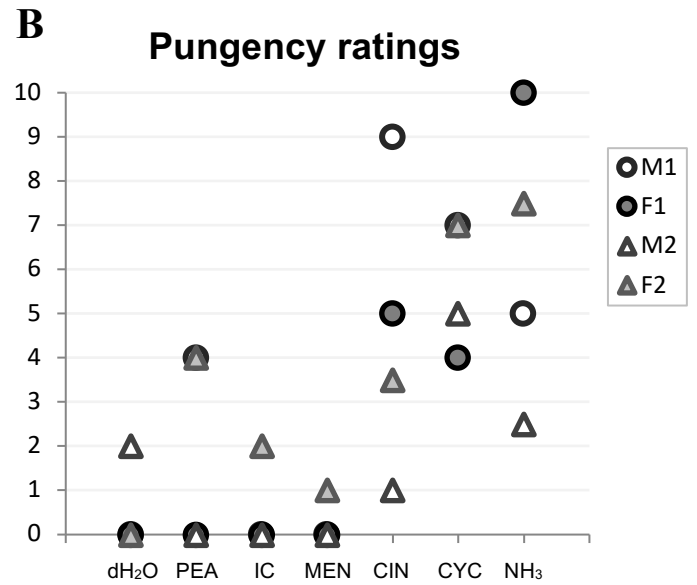
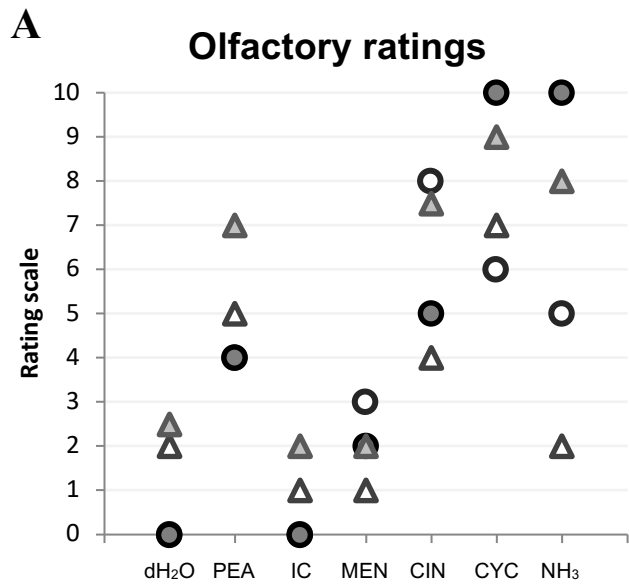


Figure 20: Psychophysical test on healthy subjects and patients show no effect of PEA on volatile irritant pungency ratings.

A: Olfactory ratings of 4 control subjects (M1,M2, F1 and F2) after exposure to distilled water (dH₂O) , the pure odorant phenylethyl alcohol (PEA), icilin (IC, 10 μM), menthol (MEN, 100 μM), cinnamaldehyde (CIN), cyclohexanone (CYC), and ammonia (NH₃).

B: Pungency ratings of 4 control subjects (M1,M2, F1 and F2) after exposure to distilled water (dH₂O) , the pure odorant phenylethyl alcohol (PEA), icilin (IC, 10 μM), menthol (MEN, 100 μM), cinnamaldehyde (CIN), cyclohexanone (CYC), and ammonia (NH₃).

C: Averaged olfactory ratings of control subjects compared to olfactory ratings of patients suffering from congenital insensitivity to pain (CIP) or congenital insensitivity to pain with anhidrosis (CIPA) or CIP recovered (CIP*) after exposure to distilled water (dH₂O) , the pure odorant phenylethyl alcohol (PEA), icilin (IC, 10 μM), menthol (MEN, 100 μM), cinnamaldehyde (CIN), cyclohexanone (CYC), and ammonia (NH₃).

D: Averaged pungency ratings of control subjects compared to olfactory ratings of patients suffering from congenital insensitivity to pain (CIP) or congenital insensitivity to pain with anhidrosis (CIPA) or CIP recovered (CIP*) after exposure to distilled water (dH₂O) , the pure odorant phenylethyl alcohol (PEA), icilin (IC, 10 μM), menthol (MEN, 100 μM), cinnamaldehyde (CIN), cyclohexanone (CYC), and ammonia (NH₃).

E: Olfactory ratings of average control subjects, congenital insensitivity to pain with anhidrosis (CIPA) and the patient recovered from congenital insensitivity to pain after exposure to PEA and CYC alone or in combination.

F: Pungency ratings of average control subjects, congenital insensitivity to pain with anhidrosis (CIPA) and the patient recovered from congenital insensitivity to pain after exposure to PEA and CYC alone or in combination.

TRPM8 agonists

Cold-mimicking substances can activate the temperature-sensitive transient receptor potential channel melastatine 8. Icilin and menthol were used in this psychophysical experiment to assess the olfactory and pungent potencies of TRPM8 agonists in humans (McKemy, Neuhausser and Julius, 2002; Chuang, Neuhausser and Julius, 2004). Alike icilin (10 μM) , menthol (1 mM) elicited moderate olfactory ratings ranging from undetected to 3 / 10 (Fig.20, panel A, “IC” & “MEN”). The

pungency perceived by control subjects was also limited with ratings inferior or equivalent to 2 / 10 for both TRPM8 agonists (Fig. 20, panel B, "IC" & "MEN").

TRPA1 agonist

TRPA1 can be activated by a wide range of volatile chemicals such as the pungent compound of wasabi, allyl isothiocyanate, or garlic-like substances containing allicin (Macpherson *et al.*, 2005). According to calcium imaging experiment realized on transfected cell lines, cinnamaldehyde, a cinnamon extract, is one of the most specific agonists for the ankyrin 1 channel (Bandell *et al.*, 2004). Pure cinnamaldehyde solutions was detected by all 4 participants and evoked olfactory ratings ranging between 4 and 8 / 10 (Fig. 20, panel A, "CIN"). Both German participants perceived cinnamaldehyde as mildly pungent (Fig.20, panel B, "CIN", pungency rating F2 = 3.5 / 10, pungency rating M2 = 1 / 10). However, Chinese subjects had higher pungency ratings (Fig.20, panel B, "CIN", pungency rating F1 = 5 / 10, pungency rating M1 = 9 / 10). This difference in perception might be due to cultural differences.

TRPV1 agonist

Capsaicin is a canonical agonist for the heat-sensing channel TRPV1 extracted from hot chili peppers (Caterina *et al.*, 1997). This compound is characterized by a low vapor pressure of 1.32×10^{-8} mmHg at 25°C (National Center for Biotechnology Information. "PubChem Compound Summary for CID 1548943, Capsaicin" *PubChem*) which indicates that a low amount of substance is present in the gaseous phase within the test Falcon tube. Therefore, cyclohexanone, another TRPV1 agonist with an odour reminiscent of peppermint and acetone and a vapor pressure of 5.2 mmHg at room temperature (National Center for Biotechnology Information. "PubChem Compound Summary for CID 7967, Cyclohexanone" *PubChem*) was used. Most control participants rated cyclohexanone (pure) as the most potent odorant (Fig.20, panel A, "CYC", olfactory rating F1 = 10 / 10 , olfactory rating F2 = 9 / 10 , olfactory rating M2 = 7 / 10) while pungency ratings ranged from 4 to 7 / 10 (Fig. 20, panel B, "CYC"), confirming the irritant properties of cyclohexanone.

Ammonia

Ammonia (NH₃) is a volatile chemical known for its pungent attributes (Cometto-Muniz and Hernandez, 1990). NH₃ vapours elicited a broad range of olfactory ratings, between 2 (Fig. 20, panel A, "NH₃", M2) and the highest 10 / 10 (Fig. 20, panel A, "NH₃", F1). Likewise, ammonia exposure resulted in the highest variability in pungency ratings between the 4 control subjects (Fig. 20, panel B, "NH₃"). Interestingly, each participant gave similar olfactory and pungency ratings values for ammonia, certainly suggesting the difficulty to distinguish the difference between odour and pungency for irritant compounds such as NH₃.

ii. Patients suffering from insensitivity to pain conditions

Akin to the testing procedure performed using control subjects, three subjects (2 boys and 1 girl, age 6 - 14 years old) affected by insensitivity to pain conditions were asked to rate olfactory intensity and pungency for distilled water, phenylethyl alcohol (pure), icilin (10 µM), menthol (1 mM), cinnamaldehyde (pure) cyclohexanone (pure) and ammonia (1 M). All patients have been discovered and characterized by Prof. Xianwei Zhang in the Department of Anesthesiology of Tongji Hospital (Tongji Medical College, Huazhong University of Science and Technology, Wuhan, China). The results obtained were compared with the average ratings collected for all control subjects.

Congenital insensitivity to pain (CIP)

Congenital insensitivity to pain (CIP) is a pathology characterized by the absence of perception of painful stimuli (Van Ness Dearborn, 1932). This condition has been linked to mutation on the SCN9A gene, leading to a loss of function of the voltage gated sodium channels 1.7 (Nav 1.7), present in both nociceptors and olfactory sensory neurons (Cox *et al.*, 2006). Therefore, SCN9A mutations can also lead to anosmia, an inability to detect odorants (Weiss *et al.*, 2011). During the psychophysical test realized in China, a CIP patient could be tested for olfactory and pungency perception. The 8-year-old girl suffering from CIP presented 2 mutations, namely c.850delG and c.129_141delTGAAGAAGCCCCA, resulting in a truncated non-functional Nav 1.7 protein. None of the test substances odour nor pungency was detected by this patients, confirming both the anosmia and insensitivity to volatile irritants characteristic of the CIP condition (Fig. 20, panel C,

D, "CIP", olfactory ratings = 0 /10 for all test substances ; pungency ratings = 0/10 for all tested substances).

Congenital insensitivity to pain re-gain of function

A second Chinese patient, previously diagnosed with a CIP condition, had recovered pain sensitivity for 6 years. During the psychophysical experiment, this patient detected most test substances with ratings similar to these of control subjects (Fig. 20, panel C, D, "CIP re-gain"). Unlike distilled water (Fig. 20, panel C, "CIP re-gain", olfactory rating = 0 /10 ; panel D, "CIP re-gain", pungency rating = 0 / 10), PEA evoked an olfactory potency (Fig. 20, panel C, "CIP re-gain", olfactory rating = 7/10 ; panel D, "CIP re-gain", pungency rating = 0 / 10). Menthol (1 mM) was the only TRPM8 agonist to be perceived at the olfactory level (Fig. 20, panel C, "CIP re-gain", olfactory rating = 4 / 10) while icilin (10 μ M) remained undetected (Fig. 20, panel C, "CIP re-gain", olfactory rating = 0 /10 ; panel D, "CIP re-gain", pungency rating = 0 / 10). In contrast, the pure TRPA1 agonists cinnamaldehyde evoked both high olfactory (Fig. 20, panel C, "CIP re-gain", olfactory rating = 7 / 10) and high pungency ratings (Fig. 20, panel D, "CIP re-gain", pungency rating = 8 / 10). Maximal olfactory and pungency intensities were rated for the TRPV1 agonist cyclohexanone (pure) (Fig. 20, panel C, "CIP re-gain", olfactory rating = 10 / 10 ; Fig. 20, panel D, "CIP re-gain", pungency rating = 10 / 10).

Congenital insensitivity to pain with anhidrosis (CIPA)

The last Chinese patient participating to the psychophysical study was the older brother of the CIP patient, suffering from congenital insensitivity to pain with anhidrosis (CIPA). Although CIP and CIPA patients share a common lack of pain perception, the second condition is also characterized by an inability to sweat, reflecting that both sensory and autonomic nervous systems are impacted in this pathology (Gillespie and Perucca, 1960). Mutations on the NTRK1 gene, encoding the nerve growth factor (NGF) receptor TrkA have been found to be causative of CIPA phenotypes (Mardy *et al.*, 1999). The patient suffering from CIPA did not detect distilled water nor icilin (10 μ M) (Fig. 20, panel C, D, "CIPA"). For test substances perceived, both odorant and irritant ratings were superior to control subjects' ratings. The pure odorant PEA was evaluated with high olfactory (Fig. 20, panel C, "CIPA", olfactory rating = 10 / 10) and pungency

potencies (Fig. 20, panel D, "CIPA", pungency rating = 9 / 10). Alike ammonia, both TRPA1 and TRPV1 evoked maximal olfactory and pungency ratings (Fig. 20, panel C, D, "CIPA").

b. PEA does not reduce pungency ratings in human subjects

i. Control participants

The possibility of a cross modal interaction between olfactory and trigeminal systems was assessed using PEA and cyclohexanone alone or in combination. Given her inability to perceive pungent volatile substances nor odorants, the patient suffering from CIP was not asked to participate to this experiment. Control participants considered that the irritant cyclohexanone (pure) to be more odorant (Fig. 20, panel E, "CYC", olfactory rating = 8 / 10) than pure PEA alone (Fig. 20, panel E, "PEA", olfactory rating = 5 / 10). The mixture of both volatile substances mildly diminished the olfactory intensity perceived for cyclohexanone alone (Fig. 20, panel E, "CYC + PEA", olfactory rating = 7.5 / 10). Expectedly, cyclohexanone (pure) was perceived with a higher pungency (Fig. 20, panel F, "CYC", pungency rating = 5.75 / 10) than the odorant PEA (pure, Fig. 20, panel F, "PEA", pungency rating = 2 / 10). Unlike the observation in mice behavioural experiments, the addition of the pure odorant did not mitigate the pungency evoked by the irritant cyclohexanone for human subjects (Fig. 20, panel F, "CYC + PEA", pungency rating = 6.75 / 10).

ii. Patients suffering from insensitivity to pain conditions

Interestingly, for the patient who recovered pain and odorant perception (CIP re-gain), both the olfactory and pungency potencies of cyclohexanone alone (Fig. 20, panel E, "CYC", olfactory rating = 10 / 10 ; panel F, pungency rating : 10 /10) were reduced after addition of PEA (Fig. 20, panel E, "CYC+PEA", olfactory rating = 6 / 10 ; panel F, "CYC+PEA", pungency rating = 5 / 10).

A similar observation was made for CIPA patient for whom cyclohexanone pungency (Fig. 20, panel F, "CYC", pungency rating = 10 / 10) was completely abolished by the addition of PEA to the test substance Falcon tube (Fig. 20, panel F, "CYC+ PEA", olfactory rating = 0 / 10).

C. Photoactivation of olfactory sensory neurons revealed that the mitigation observed at the behavioural level in mice does not happen within the OE

Behavioural studies in mice showed a modulation of the perception of irritants by concomitant application of a pure odorant. In an attempt to ascertain the location of this cross-modal interaction the nasal cavity comprising both the olfactory and trigeminal afferents, was investigated. In the absence of a direct activation of trigeminal afferents by the pure odorant PEA (see section III. A. 2. B. iv.) the hypothesis of an activation of olfactory sensory neurons affecting action potential conduction in trigeminal afferents was explored. To dissociate trigeminal and olfactory chemosensory systems, non-chemical stimulation techniques were adopted. Specifically, a mouse model previously characterized by Genovese et al., (Genovese *et al.*, 2016), and expressing a channel rhodopsin under the promoter of the olfactory marker protein, specific for OSNs, was used (Fig.21, panel A, Maurer et al., 2019, data acquired and kindly offered by Nunzia Papotto, Center for Organismal Studies) to photo-stimulate the entire population of olfactory sensory neurons synchronously. To establish initially, the optimal parameters for photostimulation of OSNs, electro-olfactogram surface potentials were recorded in response to light stimuli (470 nm) of different pulse durations (2 - 100ms). From this series, sinusoidal light pulses of 10 ms duration evoked EOG response with a maximal amplitude (see section II. F. 2. b. ; Fig. 9, panel C- E) indicating the most synchronous activation. Therefore, this duration was selected as a standard stimulus with which the effect of OSN activation on trigeminal axonal conduction could be examined. Using the standard recording configuration detailed above, electrically evoked trigeminal afferents responses were identified in the anterior ethmoidal nerve and while stimulating regularly at 0.25 Hz. Every third electrical stimulus was coupled with a 10 ms light stimulation of the olfactory epithelium (Fig. 21, panel B). Seven trigeminal units were monitored during OSNs photo-activation (Fig. 21, panel C) and in all 7 cases, the electrical responses latency was not altered (Fig. 21, panel B).

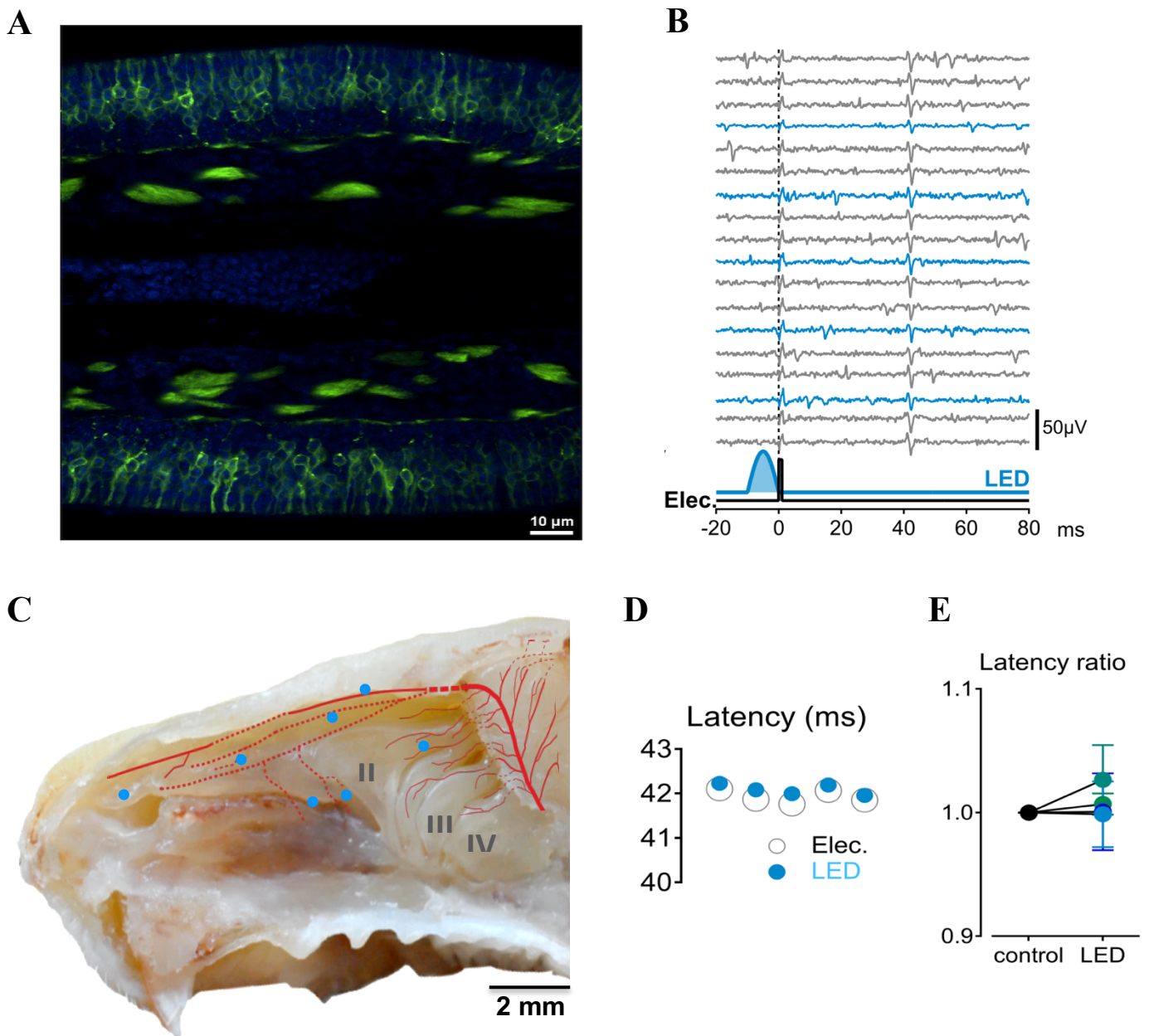


Figure 21: Effect of optogenetic stimulation of OSNs on trigeminal conduction velocity in the nose.

A: Coronal section of the septum in an OMP-ChR2-EYFP mouse model. OSNs are marked in green in the epithelium surrounding the septum. Nuclei are labelled with DAPI. Scale bar = 10 μm . (Maurer et al., 2019, data acquired and kindly offered by Nunzia Papotto, Center for Organismal Studies).

B: Example of an electrically-evoked trigeminal response (grey traces) during OSN concomitant photo-activation (blue traces).

C: Electrical receptive field locations for seven trigeminal afferents (blue markers) recorded in OMP/ChR2-YFP mice with simultaneous OSN photo-activation. Scale bar = 2 mm. Background adapted from Barrios *et al.* 2014.

D: Averaged response latency to electrical stimulation alone (open grey markers) compared to the electrical response latency during light co-stimulation (blue markers).

E: Pooled latency ratios of responses in trigeminal afferents for electrical stimuli ("control") and with photostimulation ("LED") for seven units.

To assess this dataset, 4 consecutive electrically evoked latencies were averaged (Fig. 21, panel D, grey markers) and compared to latency of the next electrically evoke response occurring during olfactory photo-stimulation (Fig. 21, panel D, blue markers). The ratio of these latencies did not reveal any significant difference (paired t-test, $n=7$, $p= 0.29$) for the seven units tested (Fig. 21, panel E). Based on this data, the possibility of localizing the cross-modal interaction between olfactory and trigeminal systems within the nasal cavity seems unlikely.

IV. Discussion

A. Characterization of trigeminal afferents within the nasal cavity

1. Trigeminal axons forming the anterior ethmoidal nerve innervate the olfactory epithelium

Trigeminal sensory innervation is responsible for mechanical, thermal and chemical detection in the tissues of the face and neck, including innocuous and nociceptive signalling. Trigeminal innervation of the nose has been known for several decades (Finger *et al.*, 1990). Indeed, carbocyanine dye Di-13 tracing experiments in rodents have shown projections of the ophthalmic branch into the nasal cavity (Silverman and Kruger, 1989; Schaefer *et al.*, 2002; Damann *et al.*, 2006). Anterograde tracing along the anterior ethmoidal nerve in rats, performed by Dr. Schüler (Institute for Physiology and Pathophysiology, Friedrich-Alexander University, Erlangen, Germany), corroborated the presence of trigeminal axons within the medio-dorsal part of the nasal cavity and revealed trigeminal projections crossing the cribiform plate to innervate the olfactory epithelium within endoturbinates II-IV (Fig.10, panel B). Using a *Scn10a*-Cre:tdTomato mouse line, that expresses the fluorescent reporter protein tdTomato under the promoter of the *Scn10a* gene encoding the alpha subunit of the sodium channel Nav 1.8, the presence of Nav 1.8-positive sensory neurons in the trigeminal ganglion and in nerve bundles in the nasal septum was confirmed (Fig.11, panel A-D). However, single trigeminal axon terminals that had previously been described using fluorescent tracing techniques could not be identified within the olfactory epithelium of transgenic mice (Silverman and Kruger, 1989; Silver and Finger, 2009). *Prima facie*

this suggests that the olfactory epithelium is devoid of Nav 1.8 expressing somatosensory axons. However, it is also possible that detection of Nav 1.8 axons was compromised by methodological limitations. To confirm that image resolution was sufficient to detect single axons expressing tdTomato, cornea from *Scn10a-Cre:tdTomato* mice were imaged. The cornea is innervated by nerve terminals with myelinated A δ - and unmyelinated C-fibre axons forming the ciliaris longus nerve of the first trigeminal division, namely the ophthalmic nerve (Giraldez, Geijo and Belmonte, 1979; Belmonte, Acosta and Gallar, 2004). Nerve bundles enter the cornea in the limbus. Within the corneal stroma, individual axons divert their course at almost 90 ° to perforate Bowman's membrane and enter the corneal epithelium. Although all axons within the cornea are devoid of ensheathing myelin, A δ -fibre axons branch within the basal epithelium, resulting in projections running parallel to the epithelial surface. C-fibre axons project radially towards the superficial epithelial layers where axonal endings arborise (Tavakoli, Petropoulos and Malik, 2012; Ivanusic, Wood and Brock, 2013).

The TTX-resistant channel Nav 1.8 was originally reported to be present in small diameter neurons with C-fibres (Akopian, Sivilotti and Wood, 1996; Pinto, Derkach and Safronov, 2008) but recent evidences using *Scn10a-Cre* mouse line suggest that expression extends also to some 40 % of DRG neurons with myelinated A-fibre axons (Shields *et al.*, 2012). In a separate *Scn10a-Cre:tdTomato* mice cornea, fluorescent sub epithelial fascicles in the stromal layer and ramified bundles in the sub-basal plexus were evident (Fig. 22, panel A-C). However, individual tdTomato fluorescent nerve terminal endings were not detectable within the nasal epithelium. This was surprising since single axons expressing cold sensitive channels TRPM8 and TRPA1 were found within the olfactory epithelium, confirming the ability to observe these structures (Fig. 15, panel E). Moreover, the examination of nasal epithelium from adult transgenic mice revealed the presence of a specific subpopulation of OSNs expressing Nav 1.8 (see section III.A.3). Using the same confocal microscopy technique, cellular structures such as dendrites and sensory knobs were observed in tdTomato-labelled Nav 1.8-positive OSNs (Fig. 16, panels A,B). Therefore, the absence of sensory axons within the OE is unlikely to be due to an insufficient imaging resolution to detect tdTomato labelling.

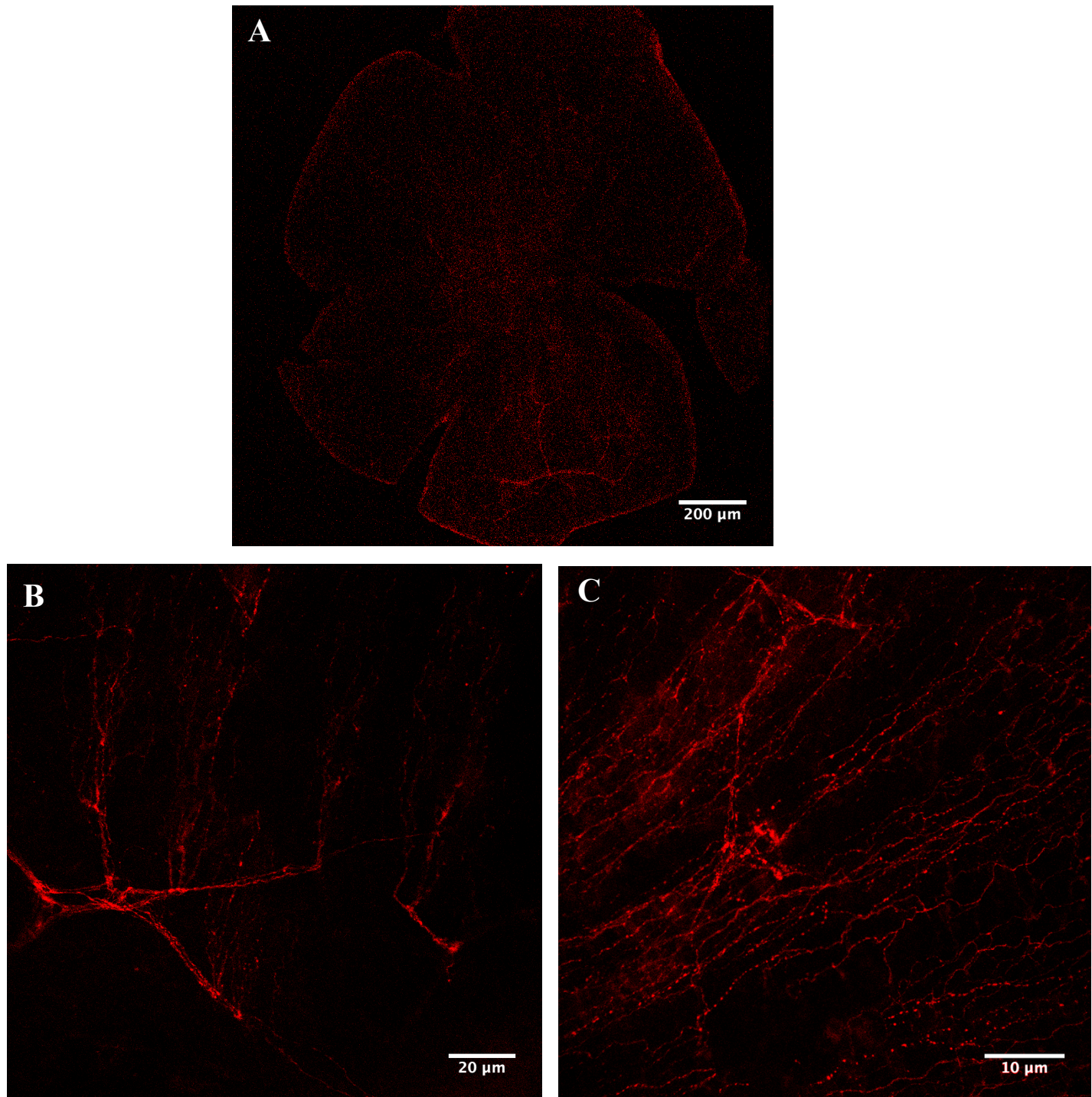


Figure 22: **Sensory innervation of mouse cornea**

A: Flat mount of the cornea of an *Scn10a*-Cre:tdTomato mouse showing Nav 1.8 positive labelling. Scale bar = 200 μm .

B: Detail of unmyelinated Nav 1.8 positive nerve fascicles (arrow) with axons turning at 90 $^\circ\text{C}$ to innervate superficial layers of the cornea. Scale bar = 20 μm .

C: Details of unmyelinated Nav 1.8 positive nerve fascicles arborization within *Scn10a*-Cre:tdTomato mouse cornea. Scale bar = 10 μm .

However, low expression levels of Nav 1.8 might explain the difficulty to identify axons within the pigmented olfactory epithelium in comparison to the cornea which is a transparent tissue.

2. Nasal trigeminal afferents are mostly polymodal A δ - and C-fibre

Extracellular signals were recorded from individual trigeminal afferents coursing in the anterior ethmoidal nerve and innervating the nasal epithelium. Axons were characterized using electrical, mechanical, thermal and chemical stimuli. Functional mapping of trigeminal afferents in the nasal cavity revealed a low density of innervation for the MOE, in accordance with previous reports for sensory axons labelled using calcitonin gene-related peptide immunoreactivity (Silverman and Kruger, 1989).

a. Conduction velocity of nasal trigeminal afferents

Due to their homologous functions and complementary innervation territories, TG and DRG neurons have been extensively compared (Manteniotis *et al.*, 2013; Lopes, Denk and McMahon, 2017). Both systems comprise pseudo-unipolar sensory neurons with a single axon extending from the soma and subsequently bifurcating into a peripheral collateral innervating skin, muscle and deeper tissues, and a central collateral which synapses onto second order neurons in the medullary or spinal dorsal horn (Purves *et al.*, 2004; Le Pichon and Chesler, 2014). Although differences have been observed in primary culture from rodent and human DRG (Zhang *et al.*, 2017), sensory neurons are canonically characterized by the conduction velocity measured along their peripheral axon. Moreover, conduction velocities have been positively correlated with the diameter of DRG neurons in rodents (Harper and Lawson, 1985). Eighty-two receptive fields have been identified with electrical or mechanical stimuli to characterize nasal trigeminal afferents. Most axons innervating the nasal cavity had conduction velocities ranging between 0.2 and 1.5 m.s⁻¹, corresponding to C-fibres while 11 presented conduction velocities in the range of A δ -fibres (Fig.12, panel B). This observation is consistent with previous reports describing a predominance of C-type trigeminal afferents innervating the cornea alongside few myelinated A δ - axons (McIver and Tanelian, 1993; Yang, Chow and Liu, 2018). In contrast, the intracranial dura, also innervated

by trigeminal axons, revealed a preponderance of myelinated axons with conduction velocity in the range of A δ -fibres (Levy and Strassman, 2002). Similar observations were made for DRG sensory afferents innervating hairy skin via the saphenous or sural nerves (Koltzenburg, Stucky and Lewin, 1997) and for primary sensory afferents within the glabrous skin, also dominated by myelinated fibres (Cain, Khasabov and Simone, 2001). This discrepancy in axon type innervation underlies further differences in sensitivity to different modalities.

b. Nasal trigeminal afferents respond to mechanical, thermal and chemical stimuli

Primary sensory fibres are conventionally characterized by their innervation territory, axonal conduction velocity, and sensitivity to different stimuli modalities such as mechanical pressure, temperature and chemicals (Le Pichon and Chesler, 2014). Alike DRG neurons, trigeminal nasal afferents were activated by a broad range of stimuli.

i. Mechano-sensitivity

The presence of mechanoreceptive fibres in the anterior ethmoidal nerve innervating the nose has been previously described *in vivo* on guinea pigs after upper airways occlusion or using negative pressure applied to the entire nostril (Sekizawa and Tsubone, 1996). Further experiments in cats have shown anterior ethmoidal responses elicited by mechanical stimuli applied in the vestibule and in the superior meatus, indicating an uneven distribution of mechanoreceptors within the nasal epithelium (Wallois *et al.*, 1991). In this project, a total of 45 nasal trigeminal axons responded to ca. 1.47 mN force mechanical stimuli delivered locally with a servo-driven device. Mechanical activation thresholds were ranged from 0.8 to 8.6 mN which is commensurate with the range of mechanical thresholds previously reported for trigeminal innervation of the dura (De Col, Messlinger and Carr, 2012). However, the proportion of mechano-sensitive trigeminal sensory afferents (ca. 70 %) (Levy and Strassman, 2002) was higher in dura preparation when compared to the nasal epithelium (55 %). Moreover, in contrast with AEN recordings, dural trigeminal afferents activation revealed a bigger proportion of A δ -fibres in comparison to C-type axons (Levy and Strassman, 2002). These differences might underly the different role of both structures. Indeed, in addition to mechanical pressure and thermal changes, chemesthesis takes

place within the nasal cavity. This feature is mainly supported by unmyelinated C-fibres (Roper, 2014).

Functional recordings of the anterior ethmoidal nerve revealed that mechano-sensitive trigeminal afferents are preferentially located in the respiratory epithelium, present in rostral and dorsal areas of the nasal cavity (Fig.12, panel C). The physiological role of nasal mechanoreceptors is likely to be multifaceted. While their primary role as a first line of defence for the detection and initiation of the subsequent behavioural response to foreign bodies in the nose, nasal mechano-sensitive axons may play a role in sensing airflow during inhalation (Sekizawa and Tsubone, 1994). However, this hypothesis has been challenged by results showing changes in sensitivity to air pressure sensitivity depending on intranasal temperature, indicating a role for thermoreceptors in airflow sensing (Eccles and Jones, 1983; Clarke, Jones and Jones A S, 1992). In our data, mechano-sensitive fibres presented conduction velocities ranging from 0.2 to 5.2 m.s⁻¹ corresponding to both A δ - and C-fibres. Both fibre classes can respond to thermal stimuli. Moreover, 12 of the mechanically-activated trigeminal axons responded either to cooling or heating. The presence of these polymodal axons has been observed previously and supports the hypothesis of a contribution of both thermal and mechanical modalities in airflow sensing (Sant'ambrogio, Tsubone and Sant'ambrogio, 1995).

ii. Sensitivity to heating

In this study, 21 individual axons in the nasal epithelium responded to slow changes in temperature of the fluid perfusing the recording bath. The heat-sensitive channel TRPV1 is involved in temperature detection is extensively distributed in nerve terminals (Caterina *et al.*, 1997) and keratinocytes in the skin (Denda *et al.*, 2001; Lee and Caterina, 2005). TRPV1 is activated by temperatures above approximately 42 °C (Caterina *et al.*, 1997). However, in the present study, the average heat detection threshold found in nasal trigeminal axons was 34.7 \pm 6.2 °C (Fig. 13, panel D). This observation suggests the implication of additional warm-sensing channels in thermal responses in the nose such as TRPV3, another isoform of the vanilloid sub-family, expressed in trigeminal ganglia and with heat activation thresholds ranging from 22 to 38

°C (Peier *et al.*, 2002; Xu *et al.*, 2002). Indeed, there is significant redundancy in the detection of heat in mice, which requires the triple deletion of TRPV1, TRPA1 and TRPM3 for a complete loss of sensitivity to noxious heat (Singh, 2019).

iii. Sensitivity to cooling

In contrast, thermo-sensitive trigeminal afferents in the nose presented similar average cold temperature thresholds around 24 °C (Fig.13, panel C). TRPM8 and TRPA1 channels have been implicated in cold temperature perception (Bautista *et al.*, 2007; Laursen *et al.*, 2015) with evidence for the latter being somewhat controversial (Knowlton *et al.*, 2010). Using chemical agonists, we found evidence for both TRPA1 and TRPM8 in afferents in the nasal epithelium (Fig.15, panel G, H). While some evidences indicate that TRPA1 is specifically activated by noxious cold, TRPM8 plays a role in the detection of innocuous temperatures below approximately 27 °C (Madrid *et al.*, 2009). This difference suggests that the threshold observed for trigeminal afferents in the nasal cavity is more likely to depend on the activation of TRPM8 channels. In the nose, TRPM8 is also involved in mechanisms preventing the nasal epithelium from drying up (Liu *et al.*, 2017). Indeed, TRPM8 activation in trigeminal afferents at 24 °C induces an increase in the expression of the mucus protein MUC5AC, the principal mucin secreted by goblet cells in the respiratory epithelium (Liu *et al.*, 2017). The detailed mechanism through which trigeminal afferents communicate with goblet cells remains unknown. Interestingly, 2 thermo-sensitive axons were activated by both innocuous cold and warm stimuli. This surprising result had already been observed in C-type fibres innervating hairy (Koltzenburg, Stucky and Lewin, 1997) and glabrous (Cain, Khasabov and Simone, 2001) skin in mice. Likewise, in humans, C2 receptors have been shown to respond to innocuous changes above and below basal skin temperature (Campero *et al.*, 2009). However, most thermally-sensitive endings in the nose were selective in the response to cooling or heating, consistent with a largely distinct pattern of expression for heat sensing TRPV1 or cold sensing TRPM8 channels previously described in primary sensory neurons (Kobayashi *et al.*, 2005).

iv. Chemesthesis

In addition to mechanical and thermal sensitivity, many trigeminal neurons are chemo-sensitive. The chemosensitivity of sensory afferents, also known as chemesthesis, often reflects allosteric activation of TRP channels (Viana, 2011). Trigeminal afferents in the nasal epithelium have been shown to respond to a variety of chemicals (Damann *et al.*, 2006). This observation was confirmed in sixteen individual axons exposed to chemicals in solution (Fig.14, panel A-B). In addition, irritating substances such as ammonia delivered as vapor directly in the nose also activated individual trigeminal afferents consistent with previous reports illustrating the ability of odorants to activate trigeminal afferents at high concentration (Cometto-Muñiz and Cain, 1991). Interestingly, the pure odorant PEA did not evoke trigeminal afferents activity when applied in the recording bath (Fig.14, panel C,D).

TRPV1 is often expressed in peptidergic nociceptors and can be activated by a range of chemical compounds including capsaicin, the spicy compound of hot chili pepper, and cyclohexanone, a cyclic ketone present in cigarette smoke (Caterina *et al.*, 1997; Silver *et al.*, 2006; Willis *et al.*, 2011). Both substances evoked responses in nasal trigeminal afferents, indicative of the presence of TRPV1-positive fibres within the nasal epithelium (Fig.15, panel A,B). Repeated applications of heat and capsaicin (Caterina *et al.*, 1997) are known to result in desensitization of TRPV1 via PKA (Mohapatra and Nau, 2003). Similarly, 3 out of 5 fibres that initially responded to cyclohexanone (1% v/v) were either not activated by subsequent applications or no longer electrically activated.

Calcium-imaging experiments have shown that TRPA1 is co-expressed in 60 % of TRPV1-positive trigeminal neurons (Jordt *et al.*, 2004). In our experiments, 7 trigeminal axons that responded to either capsaicin or cyclohexanone were not co-activated by TRPA1 agonists. (Fig.15, panel E). TRPA1 is also associated with noxious cold detection. While noxious heat 44 °C activated one of the two axons sensitive to AITC innervating the nose, none of the TRPA1-expressing axons recorded during electrophysiological experiments were activated by cooling from 32 °C into the noxious range (below 10°C).

v. Polymodal C-fibres

Most somatosensory nociceptors can respond to several stimulus modalities and are therefore characterized as polymodal (Bessou and Perl, 1969). A recent controversial study, using in situ calcium imaging of neuronal somata in transgenic mice DRGs suggested that polymodality was not a common feature (Emery *et al.*, 2016). This has been heavily criticized and the present electrophysiological experiments also provide evidences for nasal trigeminal afferents being primarily polymodal in nature. Indeed, 72 % of trigeminal afferents were confirmed to be polymodal, responding to two or more stimulus modalities including mechanical pressure, temperature changes and volatile chemicals (Fig. 12, panel D). This distribution corresponds to the proportion of polymodal neurons previously reported in DRG nociceptors (Lawson *et al.*, 2008) and suggests methodological concerns with the calcium imaging experiments of Emery *et al.* (Emery *et al.*, 2016)). Although polymodality implies a single neuron to respond to different types of stimuli, mechanical, thermal and chemically-induced pain are still distinguished at the level of perception. While this distinction has not yet been explained, several hypotheses were suggested including firing frequency (Campero, Serra and Ochoa, 1996), differences in post-synaptic receptor expression observed in *C. Elegans* (Mellem *et al.*, 2002) or specific transducing channel arrangement requiring the present of the TRP channel Painless in *Drosophila melanogaster* (Stockand and Eaton, 2013). Interestingly a very recent study describing detection of warm stimuli revealed the necessity of both activated and silenced TRP channel mediated signals to encode innocuous temperature increase in polymodal fibres (Paricio-Montesinos *et al.*, 2020). Albeit the complete mechanisms underlying stimuli discrimination in neurons responding to several stimulus modalities remains unknown, these hypotheses participate to the understanding of polymodal sensory fibres encoding.

3. Nav 1.8 in mature OSNs

An unexpected observation in our experiments was the presence of fluorescent signal in a small number (ca. 6%) of OSNs in mature *Scn10a*-Cre:tdTomato mice (Fig.16, panel A,B). These structures were considered olfactory sensory neurons with cell bodies located in the middle and

upper part of the epithelium and sending a projection to the apical surface ending in a dendritic knob (Barrios *et al.*, 2014). Scn10a gene encodes the α -subunit of the voltage-gated sodium channel Na_v 1.8 which is expressed in sensory neurons (Cummins *et al.*, 1999). Of the nine voltage-gated sodium channel isoforms, five isoforms including the tetrodotoxin-resistant isoform Na_v 1.5 have been detected using immunohistochemistry techniques on OSNs (Ahn *et al.*, 2011; Weiss *et al.*, 2011; Zufall *et al.*, 2012; Frenz *et al.*, 2014). However, while residual TTX-resistant sodium current suggesting the presence of Na_v 1.5, Na_v 1.8 or Na_v 1.9 isoforms had already been shown in nasal trigeminal neurons (Damann *et al.*, 2006), the two latter had not previously been reported in OSNs. Using RT-PCR we established Scn10a mRNA within the olfactory epithelium (Papotto *et al.*, under revision). The identity of Na_v 1.8-expressing OSNs was confirmed by tdTomato and YFP co-labelling in a transgenic mouse line obtained by crossing *Scn10A-Cre:tdTomato* with OMP-hChR2Venus mice in collaboration with Nunzia Papotto (Centre for Organismal Studies, Heidelberg, Germany) (Fig.16, panel C) (Papotto *et al.*, under revision). About 30% of OSNs expressed Na_v 1.8 and represents a large sub-population when compared to the proportion of OSNs expressing one of the 900 identified olfactory receptors in mice (Malnic, Gonzalez-Kristeller and Gutiyama, 2010).

The function of Na_v 1.8 channels in mature OSNs is not currently understood. To explore its role in OSN responses light-evoked electro-olfactogram responses were recorded from the olfactory epithelium over the second endoturbinat in OMP-hChR2Venus mice. Application of the Na_v 1.8-specific blocker A-803467 (1 μ M) reduced the EOG amplitude by 15%, suggesting that Na_v 1.8 contributed to action potential signalling in OSNs (Fig.16, panel D). Olfactory neurons project axons to the main olfactory bulb in an odorant-specific manner and each OB glomerulus receives converging axonal projections from OSNs expressing one and the same odorant receptor (Ressler, Sullivan and Buck, 1993; Vassar *et al.*, 1994). Na_v 1.8 expressing OSN axons were observed in all glomeruli of the main olfactory bulb, suggesting a glomerular distribution independent of Na_v 1.8 (Papotto *et al.*, under revision). In somatosensory neurons Na_v 1.8 has been shown to be involved in the initiation propagation of sensory signals at low temperature (Akopian, Sivilotti and Wood, 1996; Zimmermann *et al.*, 2007). It is thus reasonable to speculate that Na_v 1.8 may serve a similar role in OSNs. Electrophysiological characterization of Na_v 1.8 has shown high voltage activation

thresholds and rapid inactivation kinetics (Akopian, Sivilotti and Wood, 1996) potentially enabling high frequency discharge in OSNs in particular during sustained chemically mediated depolarization. In addition to the olfactory epithelium, Na_v 1.8-positive OSNs were observed in the Grüneberg ganglion and the vomeronasal organ, nasal structures involved in pheromone detection in rodents (Fleischer *et al.*, 2006; Mucignat-Caretta, 2010). This finding corroborates the hypothesis of a subset of olfactory neurons present in every OSN subpopulation, independent of the olfactory receptor expressed and dedicated to sense volatile compounds in specific thermal and concentration conditions. However, further experiments such as electrophysiological recordings on Na_v 1.8-positive OSNs are required to unravel the exact role supported by this voltage-gated sodium channel in olfaction.

B. Modulation of nasal trigeminal signalling by olfactory stimuli

Our sense of smell derives from odorant signals via the olfactory system and from irritant information transduced by trigeminal afferents (Hummel and Livermore, 2002). Most odorants can act as irritants at a high concentration (Cometto-Muniz and Hernandez, 1990). Likewise, volatile irritants are associated with a specific odour (Doty, 1975). While the effect of concomitant trigeminal activation on odorant perception is well documented (Jacquot, Monnin and Brand, 2004; Brand, 2006; Daiber *et al.*, 2013), the possible interaction in the reverse direction, i.e. odorants affecting irritant perception, remains obscure. We explored possible modulation of trigeminal responses by concomitant olfactory activation and the mechanisms underlying any potential cross-modal interaction in the nose of mice.

1. Pure odorants alter volatile irritant perception in mice

a. PEA mitigates irritant-evoked nocifensive behaviour in mice

The interaction between trigeminal and olfactory modalities in the nose was examined using a forced choice behavioural assay in which mice had access to 2 separate sources of water, one of which was surrounded by a volatile chemical, in this case the volatile TRPV1 agonist cyclohexanone a cyclic ketone. Cyclohexanone is characterized by a high vapour pressure V_p (5

mmHg at 25°C, National Center for Biotechnology Information, PubChem Database) and is more volatile than capsaicin ($V_p = 1.32 \times 10^{-8}$ mmHg at 25°C, National Center for Biotechnology Information, PubChem Database). In the present forced choice assay, mice rapidly developed a strong aversion to the water source coupled with cyclohexanone (Fig.18, panel C). This behaviour was mitigated by the addition of phenylethyl alcohol, the rose scent considered a “pure” odorant which alone did not elicit any nocifensive behaviour (Fig.18, panel B). The degree to which cyclohexanone is a specific TRPV1 agonist is not unequivocally established. TRPV1 knock-out mice do however display an albeit reduced but nevertheless persistent aversion to cyclohexanone in behavioural assays (Saunders *et al.*, 2013). The pure odorant phenylethyl alcohol also mitigated Irritant-evoked aversion to the TRPA1 agonist allyl isothiocyanate at 60 % dilution but not 100%. (Fig.18, panel E,F). Interestingly, both cyclohexanone and allyl isothiocyanate decreased light-induced EOG responses indicating their ability to affect olfactory neurons directly (suppl.Fig. S3). At such high concentrations it is certainly possible that unspecific effects on other transduction or voltage-gated channels contribute to this effect. Modulation of nocifensive responses by volatile irritants is not restricted to olfactory neurons with a previous report indicating that cyclohexanone respiratory irritation in the nose was decreased by menthol and eugenol both of which are TRPM8 agonists (Willis *et al.*, 2011).

b. Pungency modulation in normosmic and CIP patients

Olfactory and trigeminal perception can also be investigated in humans. While subjects able to perceive both olfactory and irritant components of volatile substances are referred to as “normosmic”, abnormalities in olfactory perception and detection are recognized clinically. Symptomatic profiles can range from the perception of many odours as unpleasant, called “cacosmia”, to the complete insensitivity to pure odorants, namely “anosmia” (Doty, 1975). Psychophysical ratings experiments are used to assess olfactory capacity in people. Using this method, Doty *et al.* generated a ranking order of chemical substances from “pure” odorant to “pure” irritant for this purpose. (Doty *et al.*, 1978).

i. Control subjects

Adopting the Doty (1978) odorant-pungency scale, cross-modal interactions between olfactory and trigeminal signalling was assessed in control normosmic subjects. In contrast with pungent substances, icilin and menthol, two TRPM8 agonists inducing cooling responses, which elicited were low olfactory and trigeminal ratings, TRPV1 and TRPA1 agonists were perceived as highly pungent. Moreover, substances rated with high pungency, such as ammonium bicarbonate, cyclohexanone or the TRPA1 agonist cinnamaldehyde, also evoked an olfactory rating superior to 5 / 10 (Fig.20, panel A,B), confirming the odorant potency reported for most irritant volatile substances (Doty, 1975). Participants were recruited in Germany and China, two countries with different cultural backgrounds. Owing to this, as previously reported (Ferdenzi *et al.*, 2013), a certain degree of variation in odorant ratings attributable to gender and cultural differences as was expected in our experiments. Indeed, differences in chemicals ratings could vary between 1 to 8 arbitrary units on a scale from 0 to 10 (Fig. 20, panel A, B).

ii. CIP patient

Despite variation in the control population, meaningful differences in olfaction were observed in patients with congenital insensitivity to pain (CIP). Congenital insensitivity to pain patients are characterized by an inability to feel painful stimuli and anosmia (Van Ness Dearborn, 1932). This condition has later been linked with mutations on the SCN9A gene encoding the voltage-gated sodium channel Nav 1.7 (Herzog *et al.*, 2003; Cox *et al.*, 2006; Weiss *et al.*, 2011). One Chinese CIP patient carrying a deletion of a guanine in position 850 (c.850delG) (Fig. 6, panel A, "1") and a 13 base pair deletion c.129_141delTGAAGAAGCCCCA, resulting in a truncated Nav 1.7 protein close to the N-terminus (Fig. 6, panel A, "2") was unable to detect any of the test substances presented at the olfactory nor pungency level (Fig.20, panel C,D).

A second Chinese patient previously diagnosed with CIP by Prof. Zhang (Department of anaesthesiology, Tongji Hospital, Tongji Medical College, Huazhong University of Science and Technology, Wuhan, China) and requalified as "recovered" 6 years before the experiment was assessed. Both olfactory and pungency ratings given by this patient were in adequation with the previous ratings gathered from control subjects (Fig. 20, panel C, D)

iii. CIPA patient

In addition, a patient diagnosed with congenital insensitivity to pain with anhidrosis (CIPA) by Prof. Zhang (Department of anaesthesiology, Tongji Hospital, Tongji Medical College, Huazhong University of Science and Technology, Wuhan, China) participated to the psychophysical experiment. CIPA is characterized by an absence of pain perception and autonomic deficits leading to the inability to sweat due to a mutation in the NTRK1 gene encoding TrkA receptor, involved in nerve growth (Swanson, 1963; Indo *et al.*, 1996). Besides dH₂O and Icilin (1 μM), olfactory and pungency ratings given by the CIPA patient were 2 to 5 arbitrary units higher than the mean rating from normosmic subjects calculated for each test substance (Fig. 20, panel C, D). These results suggest a hypersensitivity to olfactory and pungent chemicals for CIPA patient. However, it is interesting to notice that this patient could still rate the pungency of some of the compounds that were presented, since CIPA is characterized by the absence of painful sensations. Moreover, TrkA knockout mice were insensitive to noxious volatile stimuli (Indo, 2002). A closer look to pungency ratings for this patient reveals very similar scores to olfactory ratings (Fig. 20, panel C, D). It is therefore highly possible that the results observed during this experiment arise solely from olfactory perception. Moreover, it is important to keep in mind that, despite the translation of the protocol in Chinese, the description of terms such as “pungency” might be challenging when addressing a patient insensitive to painful stimuli. This difficulty might therefore lead to misunderstandings during the experiment and erroneous ratings.

iv. Cross-modal interaction between olfactory and trigeminal systems in humans

To assess the possibility of a cross-modal interaction between trigeminal and olfactory signal, normosmic subjects were asked to rate PEA and cyclohexanone presented together. Unlike CIPA and CIP-recovered patients who both showed reduced olfactory and pungency ratings of cyclohexanone in the presence of PEA, control subjects perceived the mix equally or even more pungent than the individual components, suggesting that odorants may amplify irritant pungency (Fig.20, panel E-F). The discrepancy between mouse and human data could arise from the experimental settings. During the psychophysical test, volatile compounds were presented in a randomized manner and some of the substances pre-selected could influence trigeminal perception. Indeed, chemicals such as menthol, applied in the nasal cavity, have been found to

diminish respiratory responses to cyclohexanone-induced trigeminal activation (Willis *et al.*, 2011). More importantly, although some studies have shown that both species display similar odorant preferences, rodents and humans express different sets of olfactory receptors resulting in different levels of sensitivity to volatile compounds (Mandairon *et al.*, 2009; Sarrafchi *et al.*, 2013; McGann, 2017). A lower sensitivity to PEA could explain the lack of effect of the “pure” odorant on cyclohexanone pungency ratings in normosmic subjects. Indeed, both the CIPA and CIP-recovered patient, ranked PEA with higher olfactory scores, i.e. a decrease of cyclohexanone pungency when presented in combination with the pure odorant phenylethyl alcohol. Therefore, further experiments using diverse “pure” odorants such as vanillin or decanoic acid might result in a mitigation of volatile irritant perception (Doty *et al.*, 1978).

2. Mouse trigeminal signalling is not affected by olfactory co-activation in the nose

Recent studies in people have suggested that the addition of pure odorants to a volatile irritant stimulus enhanced the ability to localize irritant stimuli presented unilaterally in the nose (Tremblay and Frasnelli, 2018). In contrast, in mice irritant related avoidance behaviour was reduced in the presence of the pure odorant PEA (see section IV.B.1.a). There is a precedent for the observation in the mouse indicating that trigeminal activation can influence olfaction. Specifically, since Olfactory sensory neurons and trigeminal nerve terminals reside in parallel within the nasal epithelium (Schaefer *et al.*, 2002; Silver and Finger, 2009) and many of the trigeminal endings are peptidergic. Peptidergic trigeminal axons have large dense cored vesicles that contain substance P and calcitonin-gene related peptide (Finger *et al.*, 1990; Lucero, 2013) and these can be released in response to noxious stimuli or via axon-reflex signals. Neuropeptides have paracrine effects on epidermal cells within the skin such as keratinocytes, and also possibly on second order neurons within the olfactory bulb (Genovese *et al.*, 2017). However, whether activation of olfactory neurons might affect trigeminal signalling remains an open question. We tested this directly in mice by recording from individual trigeminal axons innervating the olfactory epithelium and combining this with light-induced olfactory activation (Fig.21, panel B). Optical stimulation of OSNs did not modulate individual trigeminal axon responses (Fig. 21, panel D, E). Therefore, it is unlikely that the mitigation of irritant-induced nocifensive behaviour by odorants

is due to a paracrine modulation of trigeminal afferents by OSNs within the nasal epithelium. The possibility of other cell types to be involved in this cross-modal interaction cannot be ruled out. Indeed, volatile odorants and irritants can also activate other chemosensory cells located within the main olfactory epithelium, such as solitary chemosensory cells which, akin to OSNs, express TRPM5 (Lin, Ogura, *et al.*, 2008). Solitary chemosensory cells, located in the vicinity of trigeminal axons, comprise the machinery necessary for acetyl choline vesicular release and could therefore act as a paracrine modulator of trigeminal signalling (Saunders *et al.*, 2014). The possibility that olfactory signals can impact nociceptive processing within the central nervous system is also possible.

V. Conclusion

The detection and identification of odorants and irritants in the surrounding environment is essential for several behavioural processes including protective reflexes against noxious volatile substances. These physiological functions rely on nasal olfaction and chemesthesis, two modalities residing in parallel within the nose (Doty *et al.*, 1978). Evidences of interactions between both modalities have been described at the level of the central nervous system and for pathological conditions such as congenital insensitivity to pain (Boyle *et al.*, 2007; Weiss *et al.*, 2011). Moreover, olfactory modulations induced by trigeminal activation has been reported (Bouvet *et al.*, 1987; Daiber *et al.*, 2013). This thesis aims to interrogate the cross-modal interaction between the olfactory and the trigeminal system and to explore the effect of olfactory stimulation on trigeminal perception.

In mice, aversive behaviour evoked by an irritant was mitigated by co-application of the odorant phenylethyl alcohol. These observations suggest an interaction between nasal trigeminal chemesthetic and olfactory pathways at a level sufficient to affect behaviour. However, these results could not be reproduced in a psychophysical test on a small group of normosmic and anosmic human subjects, using the same chemical combination. In mice, nasal trigeminal innervation supplied by the anterior ethmoidal nerve was characterized, confirming the presence of C—type polymodal trigeminal axons crossing the nasal epithelium to reach its apical surface where they can be activated by volatile irritants. Direct recordings from the AEN during concomitant olfactory and trigeminal stimuli application refute the possibility of a cross-talk between both systems at the level of the olfactory epithelium.

Finally, the immunohistochemical examination of nasal trigeminal innervation in mice revealed a specific subset of olfactory sensory neurons expressing the voltage-gated sodium channel Nav1.8. Further experiment will be necessary to determine the precise role of this OSN sub-population.

Supplementary figures

Psychophysical experiment – Olfactory test

Date:	Room temperature: °C
Patient:	

Protocol:



Substances	Detection		Olfactory intensity	Pungency
	yes	no	Scale: 0 (no odor) to 10 (strong odor)	Scale: 0 (no discomfort) to 10 (painful)
1				
2				
3				
4				
5				
6				
7				
8				

Supplementary figure S1: **Psychophysical test form - English version -**

Psychophysical experiment – Olfactory test

心理物理实验 - 嗅觉测试

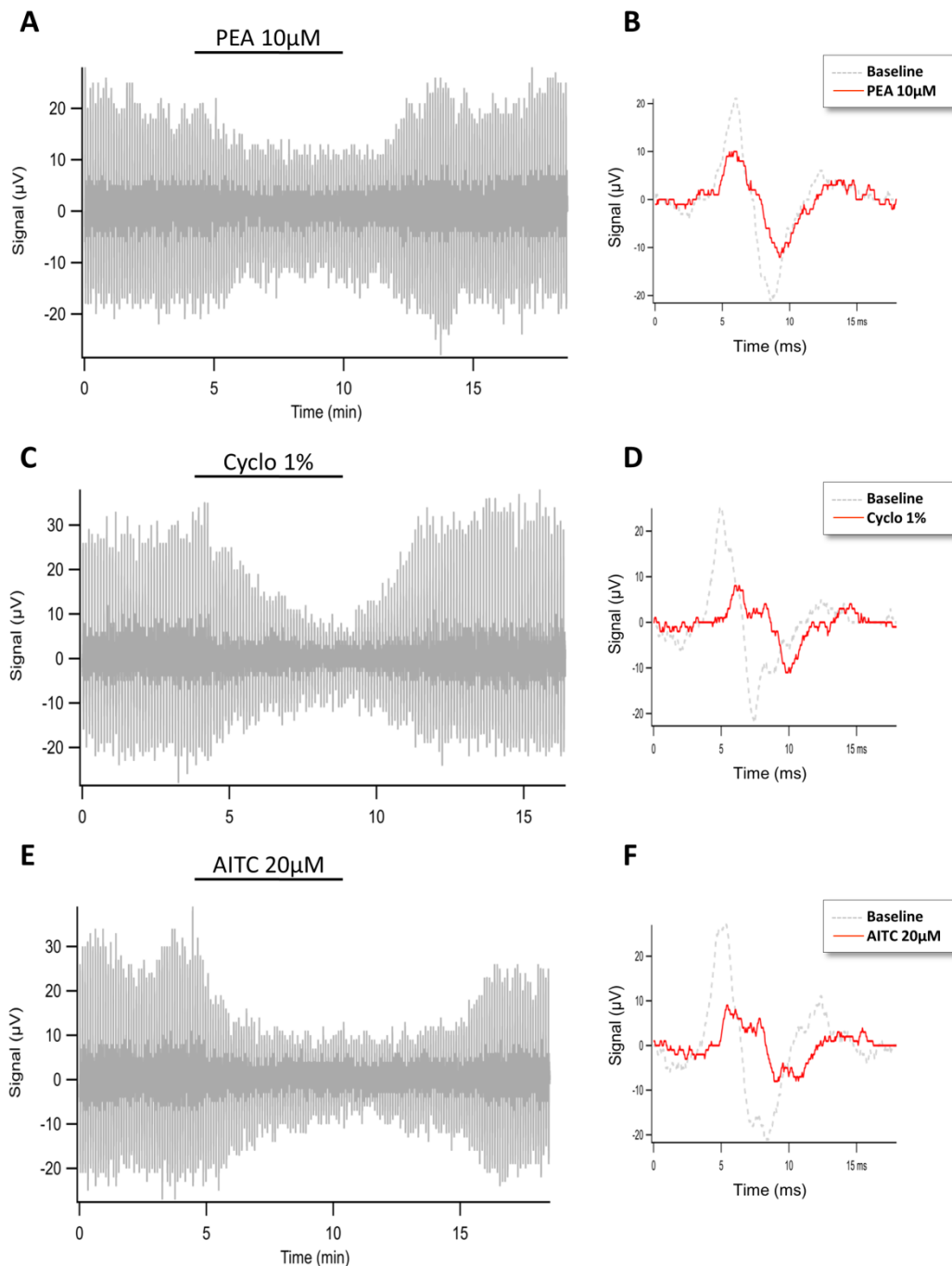
Date 日期:	Room temperature 室温:
Patient 病人:	

操作规程:



Substances 物质	检出		嗅觉强度	刺激性
	Yes 是	No 否	等级: 0 无味到等级 10 强烈气味	等级: 0 没有不适感 到等级 10 痛苦
1				
2				
3				
4				
5				
6				
7				
8				

Supplementary figure S2: Psychophysical test form - Chinese version -



Supplementary figure S3: Alike the pure odorant PEA, volatile irritants activate olfactory sensory neurons.

A: PEA (10 μ M) perfused in the recording bath solution induced a decrease in the amplitude of EOG responses induced by 10ms light pulses delivered repeatedly with a 10s interval.

B: Examples of light-induced EOG responses before (gray, dashed) and during (red) phenylethyl alcohol application.

C: Cyclo (1%) perfused in the recording bath solution induced a decrease in the amplitude of EOG responses induced by 10ms light pulses delivered repeatedly with a 10s interval.

D: Examples of light-induced EOG responses before (gray, dashed) and during (red) cyclohexanone application.

E: AITC (20 μ M) perfused in the recording bath solution induced a decrease in the amplitude of EOG responses induced by 10ms light pulses delivered repeatedly with a 10s interval.

F: Examples of light-induced EOG responses before (gray, dashed) and during (red) AITC application.

Date	Stimulus	Unit	Latency (s)	Distance to recording electrode (mm)	Conduction velocity (m.s ⁻¹)	Fiber class	Heat threshold	Cooling threshold	PEA	Capsaicin	MEN	AITC	CYC	IC	NH3
03/03/2017	Electrical	U1	0,054	26,00	0,48	C							+		
	Electrical	U2	0,012	23,01	1,92	Ad									
	Electrical	U4	0,027	16,64	0,62	C							+		
09/03/2017	Electrical	U5	0,044	22,75	0,52	C	38,000								
	Electrical	U5	0,040	22,75	0,57	C									
14/03/2017	Electrical	U6	0,035	14,56	0,42	C									
	Electrical	U7	0,017	21,19	1,25	C									
	Electrical	U7	0,020	21,19	1,06	C									
16/03/2017	Electrical	U8	0,035	13,65	0,39	C	35,000						+		
21/03/2017	Electrical	U9	0,035	11,96	0,34	C									
22/03/2017	Electrical	U10	0,030	12,87	0,43	C									
29/03/2017	Electrical	U11	0,009	5,33	0,59	C									
	Electrical	U11	0,011	5,33	0,48	C									
	Electrical	U11	0,014	5,33	0,38	C									
	Electrical	U12	0,021	8,19	0,39	C									
	Electrical	U13	0,013	7,02	0,54	C									
	Electrical	U13	0,019	7,02	0,37	C	39,000								
	Electrical	U14	0,014	6,24	0,45	C						+			
06/04/2017	Electrical	U15	0,009	6,37	0,71	C									
	Electrical	U15	0,014	6,37	0,46	C									
	Electrical	U15	0,016	6,37	0,40	C									
	Electrical	U16	0,016	13,91	0,87	C									
	Electrical	U16	0,021	13,91	0,66	C									
13/04/2017	Electrical	U17	0,021	11,70	0,56	C									
	Electrical	U17	0,023	11,70	0,51	C									
	Electrical	U18	0,012	11,57	0,96	C									
	Electrical	U18	0,026	11,57	0,45	C									
	Electrical	U19	0,018	13,52	0,75	C	39								
	Electrical	U19	0,024	13,52	0,56	C	39,000							+	
20/04/2017	Electrical	U20	0,040	12,35	0,31	C							+		
30/05/2017	Electrical	U21	0,026	12,09	0,47	C									
	Electrical	U22	0,014	10,53	0,75	C			x						
18/10/2017	Mechanical	M1	0,008	20,80	2,60	Ad									
	Mechanical	M2	0,01	20,80	2,08	Ad									
	Mechanical	M3	0,006	20,80	3,47	Ad									
	Mechanical	M4	0,020	20,80	1,04	C									
	Mechanical	M5	0,004	20,80	5,20	Ad									
	Mechanical	M6	0,009	20,80	2,31	Ad			x						+
	Mechanical	M6	0,013	20,80	1,60	Ad			24°						
30/01/2018	Mechanical	M6	0,019	20,80	1,09	C	41,000								+
30/01/2018	Mechanical	M10	0,032	18,46	0,58	C	31,000	x	0						
	Mechanical	M11	0,015	4,42	0,29	C									
31/01/2018	Mechanical	M12	0,020	10,14	0,51	C									
	Mechanical	M13	0,013	11,31	0,87	C	25,000	x							
	Mechanical	M14	0,009	14,30	1,59	Ad									
01/02/2018	Mechanical	M14	0,022	14,30	0,65	C									
	Mechanical	M15	0,012	14,30	1,19	C						24°C			
	Mechanical	M16	0,040	19,89	0,50	C						24°C			
06/02/2018	Mechanical	M17	0,043	9,23	0,21	C									
	Mechanical	M18	0,034	10,66	0,31	C									
07/02/2018	Mechanical	M19	0,039	10,79	0,28	C									
	Mechanical	M20	0,014	21,06	1,50	C									
	Mechanical	M20	0,02	21,06	1,05	C									
13/02/2018	Mechanical	M20	0,041	21,06	0,51	C									
	Mechanical	M21	0,026	10,01	0,39	C									
	Mechanical	M22	0,011	11,57	1,05	C						24°C			
14/02/2018	Mechanical	M23	0,035	11,44	0,33	C									
	Mechanical	M24	0,040	11,44	0,29	C									
23/03/2018	Mechanical	M25	0,010	10,14	1,01	C									
	Mechanical	M25	0,020	10,14	0,51	C									
	Mechanical	M26	0,007	8,71	1,24	C	27								
	Mechanical	M26	0,015	8,71	0,58	C						+			
	Mechanical	M26	0,022	8,71	0,40	C						22°C			
29/03/2018	Mechanical	M30	0,011	16,77	1,52	Ad									
	Mechanical	M30	0,016	16,77	1,05	C						24°C			
04/04/2018	Mechanical	M31	0,029	20,28	0,70	C									
	Mechanical	M31	0,040	20,28	0,51	C									
	Mechanical	M32	0,038	10,92	0,29	C									
14/04/2018	Mechanical	M33	0,006	12,61	2,10	Ad									+
	Mechanical	M33	0,015	12,61	0,84	C	28	24°C							
	Mechanical	M33	0,020	12,61	0,63	C									
23/11/2017	Mechanical	ME1	0,017	18,46	1,09	C									+
	Mechanical	ME2	0,030	22,62	0,75	C									+
27/04/2018	Electrical	U01	0,040	8,97	0,22	C									
18/05/2018	Electrical	U02	0,037	8,71	0,24	C	31	26°C							
	Electrical	U03	0,034	10,53	0,31	C							+		+
	Electrical	U04	0,014	4,16	0,30	C							+		
22/05/2018	Electrical	U05	0,028	9,75	0,35	C									
04/05/2016	Electrical	U7	0,017	10,380	0,61	C									
	Electrical	Nase1a/U8	0,006	6,00	1,00	C									+
10/05/2016	Electrical	Nase1a/U8	0,003	6,00	2,00	Ad									+
	Electrical	Nase2/U9	0,016	6,80	0,43	C	44						+		

Supplementary figure S4: Summary of single trigeminal afferents recorded within the murine nasal epithelium.

References

- Agarwal, N., Offermanns, S. and Kuner, R. (2004) 'Conditional gene deletion in primary nociceptive neurons of trigeminal ganglia and dorsal root ganglia', *Genesis*, 38(3), pp. 122–129. doi: 10.1002/gene.20010.
- Ahmad, S. *et al.* (2007) 'A stop codon mutation in SCN9A causes lack of pain sensation', *Human Molecular Genetics*. Oxford University Press, 16(17), pp. 2114–2121. doi: 10.1093/hmg/ddm160.
- Ahn, H. S. *et al.* (2011) 'Nav1.7 is the predominant sodium channel in rodent olfactory sensory neurons', *Molecular Pain*, 7. doi: 10.1186/1744-8069-7-32.
- Al Ain, S. and Frasnelli, J. A. (2017) 'Intranasal Trigeminal Chemoreception', in *Conn's Translational Neuroscience*. Elsevier Inc., pp. 379–397. doi: 10.1016/B978-0-12-802381-5.00030-0.
- Akopian, A. N. *et al.* (1999) 'The tetrodotoxin-resistant sodium channel SNS has a specialized function in pain pathways', *Nature*, 2(6), pp. 541–548. doi: 10.1038/9195.
- Akopian, A. N., Sivilotti, L. and Wood, J. N. (1996) 'A tetrodotoxin-resistant voltage-gated sodium channel expressed by sensory neurons', *Nature*, 379(6562), pp. 257–262. doi: 10.1038/379257a0.
- Amaya, F. *et al.* (2006) 'The voltage-gated sodium channel Nav1.9 is an effector of peripheral inflammatory pain hypersensitivity', *Journal of Neuroscience*, 26(50), pp. 12852–12860. doi: 10.1523/JNEUROSCI.4015-06.2006.
- Andersson, D. A. *et al.* (2008) 'Transient receptor potential A1 is a sensory receptor for multiple products of oxidative stress', *Journal of Neuroscience*, 28(10), pp. 2485–2494. doi: 10.1523/JNEUROSCI.5369-07.2008.
- Anton, F. and Peppel, P. (1991) 'Central projections of trigeminal primary afferents innervating the nasal mucosa: A horseradish peroxidase study in the rat', *Neuroscience*, 41(2–3), pp. 617–628. doi: 10.1016/0306-4522(91)90354-q.
- Arvidson, B. (1979) 'Distribution of intravenously injected protein tracers in peripheral ganglia of adult mice', *Experimental Neurology*, 63(2), pp. 388–410. doi: 10.1016/0014-4886(79)90134-1.
- Ashwell, K. (2012) 'The olfactory system', in *The Mouse Nervous System*. Elsevier Inc., pp. 653–660. doi: 10.1016/B978-0-12-369497-3.10026-3.
- Bandell, M. *et al.* (2004) 'Noxious cold ion channel TRPA1 is activated by pungent compounds and bradykinin', *Neuron*, 41(6), pp. 849–857. doi: 10.1016/s0896-6273(04)00150-3.
- Bane, V. *et al.* (2014) 'Tetrodotoxin: Chemistry, toxicity, source, distribution and detection', *Toxins*. MDPI AG, pp. 693–755. doi: 10.3390/toxins6020693.
- Barrios, A. W. *et al.* (2014) 'Anatomy, histochemistry, and immunohistochemistry of the

- olfactory subsystems in mice', *Frontiers in Neuroanatomy*. doi: 10.3389/fnana.2014.00063.
- Barrios, A. W., Sánchez-Quinteiro, P. and Salazar, I. (2014) 'Dog and mouse: Toward a balanced view of the mammalian olfactory system', *Frontiers in Neuroanatomy*. Frontiers Media S.A., 8(SEP). doi: 10.3389/fnana.2014.00106.
- Barrios, A. W., Sanchez Quinteiro, P. and Salazar, I. (2014) 'The nasal cavity of the sheep and its olfactory sensory epithelium', *Microscopy Research and Technique*. Wiley-Liss Inc., 77(12), pp. 1052–1059. doi: 10.1002/jemt.22436.
- Bautista, D. M. *et al.* (2007) 'The menthol receptor TRPM8 is the principal detector of environmental cold', *Nature*. Nature Publishing Group, 448(7150), pp. 204–208. doi: 10.1038/nature05910.
- Beech, D. J., Muraki, K. and Flemming, R. (2004) 'Non-selective cationic channels of smooth muscle and the mammalian homologues of Drosophila TRP', *Journal of Physiology*, 559(3), pp. 685–706. doi: 10.1113/jphysiol.2004.068734.
- Beitz, A. J. *et al.* (1987) 'The nuclei of origin of brainstem enkephalin and cholecystokinin projections to the spinal trigeminal nucleus of the rat', *Neuroscience*, 20(2), p. 409425. doi: 10.1016/0306-4522(87)90101-1.
- Belmonte, C., Acosta, M. C. and Gallar, J. (2004) 'Neural basis of sensation in intact and injured corneas', *Experimental Eye Research*. Academic Press, 78(3), pp. 513–525. doi: 10.1016/j.exer.2003.09.023.
- Bennett, D. L. *et al.* (2019) 'The role of voltage-gated sodium channels in pain signaling', *Physiological Reviews*, 99(2), pp. 1079–1151. doi: 10.1152/physrev.00052.2017.
- Bessou, P. and Perl, E. R. (1969) 'Response of cutaneous sensory units with unmyelinated fibers to noxious stimuli', *Journal of Neurophysiology*, 32(6), pp. 1025–1043. doi: 10.1152/jn.1969.32.6.1025.
- Binshtok, A. M. *et al.* (2008) 'Nociceptors are interleukin-1 β sensors', *Journal of Neuroscience*, 28(52), pp. 14062–14073. doi: 10.1523/JNEUROSCI.3795-08.2008.
- Bisogno, T. *et al.* (2001) 'Molecular targets for cannabidiol and its synthetic analogues: effect on vanilloid VR1 receptors and on the cellular uptake and enzymatic hydrolysis of anandamide', *British Journal of Pharmacology*, 134, p. 852. doi: 10.1038/sj.bjp.0704327.
- Black, J. A. *et al.* (1996) 'Spinal sensory neurons express multiple sodium channel α -subunit mRNAs', *Molecular Brain Research*, 43, pp. 117–131. doi: 10.1016/S0169-328X(96)00163-5.
- Black, J. A. and Waxman, S. G. (2002) 'Molecular identities of two tetrodotoxin-resistant sodium channels in corneal axons', *Experimental Eye Research*. Academic Press, 75(2), pp. 193–199. doi: 10.1006/exer.2002.2014.
- Blair, N. T. and Bean, B. P. (2003) 'Cellular/molecular role of tetrodotoxin-resistant Na current slow inactivation in adaptation of action potential firing in small-diameter dorsal root ganglion

- neurons', *Journal of Neuroscience*, 23(32), pp. 10338–10350. doi: 10.1523/JNEUROSCI.23-32-10338.2003.
- Blednov, Y. A. *et al.* (2001) 'Potassium channels as targets for ethanol: studies of G-protein-coupled inwardly rectifying potassium channel 2 (GIRK2) null mutant mice', *J Pharmacol Exp Ther*, 298(2), pp. 521–530. Available at: <http://jpet.aspetjournals.org>.
- Bolz, F. *et al.* (2017) 'Organization and plasticity of sodium channel expression in the mouse olfactory and vomeronasal epithelia', *Frontiers in Neuroanatomy*. Frontiers Media S.A., 11:28. doi: 10.3389/FNANA.2017.00028.
- Bongenhielm, U. *et al.* (2000) 'Expression of sodium channel SNS/PN3 and ankyrinG mRNAs in the trigeminal ganglion after inferior alveolar nerve injury in the rat', *Experimental Neurology*. Academic Press Inc., 164(2), pp. 384–395. doi: 10.1006/exnr.2000.7437.
- Bouvet, J. F. *et al.* (1987) 'Olfactory receptor cell function is affected by trigeminal nerve activity', *Neuroscience Letters*, 77, pp. 181–186. doi: 10.1016/0304-3940(87)90583-0.
- Boyle, J. A. *et al.* (2007) 'Cross-modal integration of intranasal stimuli: A functional magnetic resonance imaging study', *Neuroscience*, 149(1), pp. 223–231. doi: 10.1016/j.neuroscience.2007.06.045.
- Bozza, T. C. and Kauer, J. S. (1998) 'Odorant response properties of convergent olfactory receptor neurons', *Journal of Neuroscience*, 18(12), pp. 4560–4569. doi: 10.1523/JNEUROSCI.18-12-04560.1998.
- Brand, G. (2006) 'Olfactory/trigeminal interactions in nasal chemoreception', *Neuroscience and Biobehavioral Reviews*, 30(7), pp. 908–917. doi: 10.1016/j.neubiorev.2006.01.002.
- Brann, J. H. and Firestein, S. J. (2014) 'A lifetime of neurogenesis in the olfactory system', *Frontiers in Neuroscience*. Frontiers Research Foundation. doi: 10.3389/fnins.2014.00182.
- Breer, H., Boekhoff, I. and Tareilus, E. (1990) 'Rapid kinetics of second messenger formation in olfactory transduction', *Nature*, 3(345), pp. 65–68. doi: 10.1038/345065a0.
- Breer, H., Fleischer, J. and Strotmann, J. (2006) 'The sense of smell: Multiple olfactory subsystems', in *Cellular and Molecular Life Sciences*, pp. 1465–1475. doi: 10.1007/s00018-006-6108-5.
- Brock, J. A., McLachlan, E. M. and Belmonte, C. (1998) 'Tetrodotoxin-resistant impulses in single nociceptor nerve terminals in guinea-pig cornea', *Journal of Physiology*, 512, pp. 211–217. doi: 10.1111/j.1469-7793.1998.211bf.x.
- Buck, L. and Axel, R. (1991) 'A novel multigene family may encode odorant receptors: a molecular basis for odor recognition', *Cell*, 65, pp. 175–187. doi: 10.1016/0092-8674(91)90418-x.
- Bushdid, C. *et al.* (2014) 'Humans can discriminate more than 1 trillion olfactory stimuli', *Science*. American Association for the Advancement of Science, 343(6177), pp. 1370–1372. doi:

10.1126/science.1249168.

Cain, D. M., Khasabov, S. G. and Simone, D. A. (2001) 'Response properties of mechanoreceptors and nociceptors in mouse glabrous skin: an in vivo study', *Journal of Neurophysiology*, 85(4), pp. 1561–1574. doi: 10.1152/jn.2001.85.4.1561.

Cain, D. P. and Bindra, D. (1972) 'Responses of amygdala single units to odors in the rat', *Experimental Neurology*, 35, pp. 98–110. doi: 10.1016/0014-4886(72)90062-3.

Caldwell, J. H. *et al.* (2000) 'Sodium channel Na v 1.6 is localized at nodes of Ranvier, dendrites, and synapses', *PNAS*, 97(10), pp. 5616–5620. doi: 10.1073/pnas.090034797.

Campero, M. *et al.* (2009) 'Human cutaneous C fibres activated by cooling, heating and menthol', *Journal of Physiology*, 587(23), pp. 5633–5652. doi: 10.1113/jphysiol.2009.176040.

Campero, M., Serra, J. and Ochoa, J. L. (1996) 'C-polymodal nociceptors activated by noxious low temperature in human skin', *Journal of Physiology*, (2), pp. 565–572. doi: 10.1113/jphysiol.1996.sp021789.

Cardoso-Cruz, H. *et al.* (2013) 'Prefrontal cortex and mediodorsal thalamus reduced connectivity is associated with spatial working memory impairment in rats with inflammatory pain', *Pain*. Elsevier B.V., 154(11), pp. 2397–2406. doi: 10.1016/j.pain.2013.07.020.

Cardoso, F. C. and Lewis, R. J. (2018) 'Sodium channels and pain: from toxins to therapies', *British Journal of Pharmacology*, 175, p. 2138. doi: 10.1111/bph.v175.12/issuetoc.

Carr, R. W. *et al.* (2003) 'Effects of heating and cooling on nerve terminal impulses recorded from cold-sensitive receptors in the guinea-pig cornea', *Journal of General Physiology*, 121(5), pp. 427–439. doi: 10.1085/jgp.200308814.

Caterina, M. J. *et al.* (1997) 'The capsaicin receptor: a heat-activated ion channel in the pain pathway', *Nature*, 389. doi: 10.1038/39807.

Catterall, W. A. (2000) 'From ionic currents to molecular review mechanisms: The structure and function of voltage-gated sodium channels', *Neuron*, 26, pp. 13–25. doi: 10.1016/S0896-6273(00)81133-2.

Ćetković, M. *et al.* (2020) 'Arterial supply of the trigeminal ganglion, a micromorphological study', *Folia Morphologica (Poland)*. Via Medica, 79(1), pp. 58–64. doi: 10.5603/FM.a2019.0062.

Chai, Y. *et al.* (2014) 'Somatotopic organization of trigeminal ganglion: Three-dimensional reconstruction of three divisions', *Journal of Craniofacial Surgery*. Lippincott Williams and Wilkins, 25(5), pp. 1882–1884. doi: 10.1097/SCS.0000000000000994.

Challis, R. C. *et al.* (2015) 'An olfactory cilia pattern in the mammalian nose ensures high sensitivity to odors', *Current Biology*. Cell Press, 25(19), pp. 2503–2512. doi: 10.1016/j.cub.2015.07.065.

- Chapuis, J. *et al.* (2013) ‘Lateral entorhinal modulation of piriform cortical activity and fine odor discrimination’, *Journal of Neuroscience*, 33(33), pp. 13449–13459. doi: 10.1523/JNEUROSCI.1387-13.2013.
- Chaput, M. A. (2000) ‘EOG responses in anesthetized freely breathing rats’, *Chemical Senses*, 25, pp. 695–701. doi: 10.1093/chemse/25.6.695.
- Cheng, W., Sun, C. and Zheng, J. (2010) ‘Heteromerization of TRP channel subunits: Extending functional diversity’, *Protein and Cell*. Higher Education Press, 1(9), pp. 802–810. doi: 10.1007/s13238-010-0108-9.
- Chesler, A. and Szczot, M. (2018) ‘Portraits of a pressure sensor’, *eLife*, 7, pp. e34346-undefined. doi: 10.7554/eLife.
- Chuang, H., Neuhausser, W. and Julius, D. (2004) ‘The super-cooling agent icilin reveals a mechanism of coincidence detection by a temperature-sensitive TRP channel’, *Neuron*, 43(6), pp. 859–869. doi: 10.1016/j.neuron.2004.08.038.
- Clapham, D. E. (2003) ‘TRP channels as cellular sensors’, *Nature*, 426, pp. 517–524. doi: 10.1038/nature02196.
- Clarke, R. W., Jones, A. S. and Jones A S (1992) ‘Nasal airflow receptors: the relative importance of temperature and tactile stimulation’, *Clinical Otolaryngology*, 17, pp. 388–392. doi: 10.1111/j.1365-2273.1992.tb01680.x.
- Coggeshall, R. E., Tate, S. and Carlton, S. M. (2004) ‘Differential expression of tetrodotoxin-resistant sodium channels Nav1.8 and Nav1.9 in normal and inflamed rats’, *Neuroscience Letters*, 355(1), pp. 45–48. doi: 10.1016/j.neulet.2003.10.023.
- De Col, R., Messlinger, K. and Carr, R. W. (2008) ‘Conduction velocity is regulated by sodium channel inactivation in unmyelinated axons innervating the rat cranial meninges’, *Journal of Physiology*, 586(4), pp. 1089–1103. doi: 10.1113/jphysiol.2007.145383.
- De Col, R., Messlinger, K. and Carr, R. W. (2012) ‘Repetitive activity slows axonal conduction velocity and concomitantly increases mechanical activation threshold in single axons of the rat cranial dura’, *Journal of Physiology*, 590(4), pp. 725–736. doi: 10.1113/jphysiol.2011.220624.
- Cometto-Muñiz, J. E. and Cain, W. S. (1991) ‘Nasal pungency, odor, and eye irritation thresholds for homologous acetates’, *Pharmacology, Biochemistry and Behavior*, 39(4), pp. 983–989. doi: 10.1016/0091-3057(91)90063-8.
- Cometto-Muniz, J. E. and Hernandez, S. M. (1990) ‘Odorous and pungent attributes of mixed and unmixed odorants’, *Perception & Psychophysics*, 47(4), pp. 391–399. doi: 10.3758/bf03210879.
- Cosens, D. J. and Manning, A. (1969) ‘Abnormal electroretinogram from a drosophila mutant’, *Nature*, 224, pp. 285–287. doi: 10.1038/224285a0.
- Coste, B. *et al.* (2010) ‘Piezo1 and Piezo2 are essential components of distinct mechanically

activated cation channels', *Science*. American Association for the Advancement of Science, 330(6000), pp. 55–60. doi: 10.1126/science.1193270.

Coste, B. *et al.* (2012) 'Piezo proteins are pore-forming subunits of mechanically activated channels', *Nature*, 483(7388), pp. 176–181. doi: 10.1038/nature10812.

Courtiol, E. and Wilson, D. A. (2015) 'The olfactory thalamus: Unanswered questions about the role of the mediodorsal thalamic nucleus in olfaction', *Frontiers in Neural Circuits*. Frontiers Research Foundation, 9:49. doi: 10.3389/fncir.2015.00049.

Cox, J. J. *et al.* (2006) 'An SCN9A channelopathy causes congenital inability to experience pain', *Nature*. Nature Publishing Group, 444(7121), pp. 894–898. doi: 10.1038/nature05413.

Croy, I. *et al.* (2012) 'Learning about the functions of the olfactory system from people without a sense of smell', *PLoS ONE*, 7(3). doi: 10.1371/journal.pone.0033365.

Cummins, T. R. *et al.* (1999) 'A novel persistent tetrodotoxin-resistant sodium current in SNS-null and wild-type small primary sensory neurons', *Journal of Neuroscience*, 19(6). doi: 10.1523/JNEUROSCI.19-24-j0001.1999.

D'Aniello, B. *et al.* (2017) 'The vomeronasal organ: A neglected organ', *Frontiers in Neuroanatomy*. Frontiers Media S.A., 11:70. doi: 10.3389/fnana.2017.00070.

Daiber, P. *et al.* (2013) 'Neuropeptide receptors provide a signalling pathway for trigeminal modulation of olfactory transduction', *European Journal of Neuroscience*, 37(4), pp. 572–582. doi: 10.1111/ejn.12066.

Damann, N. *et al.* (2006) 'Chemosensory properties of murine nasal and cutaneous trigeminal neurons identified by viral tracing', *BMC Neuroscience*, 7. doi: 10.1186/1471-2202-7-46.

Davies, A. M. and Lumsden, A. (1990) 'Ontogeny of the somatosensory system: Origins and early development of primary sensory neurons', *Annu. Rev. Neurosci*, 13, pp. 61–73. doi: 10.1146/annurev.ne.13.030190.000425.

Davis, J. B. *et al.* (2000) 'Vanilloid receptor-1 is essential for inflammatory thermal hyperalgesia', *Nature*, 405, pp. 183–187. doi: 10.1038/35012076.

Denda, M. *et al.* (2001) 'Immunoreactivity of VR1 on epidermal keratinocyte of human skin', *Biochemical and Biophysical Research Communications*. Academic Press Inc., 285(5), pp. 1250–1252. doi: 10.1006/bbrc.2001.5299.

Dhaka, A. *et al.* (2008) 'Visualizing cold spots: TRPM8-expressing sensory neurons and their projections', *Journal of Neuroscience*. Society for Neuroscience, 28(3), pp. 566–575. doi: 10.1523/jneurosci.3976-07.2008.

Dhaka, A. *et al.* (2009) 'TRPV1 is activated by both acidic and basic pH', *Journal of Neuroscience*, 29(1), pp. 153–158. doi: 10.1523/JNEUROSCI.4901-08.2009.

Dib-Hajj, S. *et al.* (2002) 'NaN/Nav1.9: a sodium channel with unique properties.', *Trends in*

- Neurosciences*, 25(5), pp. 253–259. doi: 10.1016/s0166-2236(02)02150-1.
- Djoughri, L. *et al.* (2003) ‘The TTX-resistant sodium channel Nav 1.8 (SNS/PN3): Expression and correlation with membrane properties in rat nociceptive primary afferent neurons’, *Journal of Physiology*, 550(3), pp. 739–752. doi: 10.1113/jphysiol.2003.042127.
- Doty, R. L. (1975) ‘Intranasal trigeminal detection of chemical vapors by humans’, *Physiology and Behavior*, 14, pp. 855–859. doi: 10.1016/0031-9384(75)90081-5.
- Doty, R. L. *et al.* (1978) ‘Intranasal trigeminal stimulation from odorous volatiles: psychometric responses from anosmic and normal humans’, *Physiology and Behavior*. Pergamon Press and Brain Research Publ, 20, pp. 175–185. doi: 10.1016/0031-9384(78)90070-7.
- Doty, R. L. *et al.* (1997) ‘Chapter 14 laterality in human nasal chemoreception’, in *Advances in Psychology*. Elsevier, pp. 497–542. doi: 10.1016/S0166-4115(97)80081-7.
- Dulac, C. (2000) ‘Sensory coding of pheromone signals in mammals’, *Current Opinion in Neurobiology*, 10, pp. 511–518. doi: 10.1016/s0959-4388(00)00121-5.
- Dulac, C. and Torello, A. T. (2003) ‘Molecular detection of pheromone signals in mammals: From genes to behaviour’, *Nature Reviews Neuroscience*, 4(7), pp. 551–562. doi: 10.1038/nrn1140.
- Dunston, D. *et al.* (2013) ‘An effective manual deboning method to prepare intact mouse nasal tissue with preserved anatomical organization’, *Journal of Visualized Experiments*, (78):50538. doi: 10.3791/50538.
- Durham, P. L. and Masterson, C. G. (2013) ‘Two mechanisms involved in trigeminal CGRP release: Implications for migraine treatment’, *Headache*, 53(1), pp. 67–80. doi: 10.1111/j.1526-4610.2012.02262.x.
- Dux, M., Rosta, J. and Messlinger, K. (2020) ‘TRP Channels in the Focus of Trigeminal Nociceptor Sensitization Contributing to Primary Headaches’, *International Journal of Molecular Sciences*, 21(1), p. 342. doi: 10.3390/ijms21010342.
- Dzeja, C. *et al.* (1999) ‘Ca²⁺ permeation in cyclic nucleotide-gated channels’, *EMBO Journal*, 18(1), pp. 131–144. doi: 10.1016/j.neuron.2005.01.012.
- Eccles, R. and Jones, A. S. (1983) ‘The effect of menthol on nasal resistance to air flow’, *Journal of Laryngology and Otology*, 97, pp. 705–709. doi: 10.1017/s002221510009486x.
- Emery, E. C. *et al.* (2016) ‘In vivo characterization of distinct modality-specific subsets of somatosensory neurons using GCaMP’, *Science Advances*, 2(11). doi: 10.1126/sciadv.1600990.
- Ennis, M., Hamilton, K. A. and Hayar, A. (2007) ‘Neurochemistry of the main olfactory system’, in Lajtha, A. and Johnson, D. A. (eds) *Handbook of Neurochemistry and Molecular Neurobiology: Sensory Neurochemistry*. Boston, MA: Springer US, pp. 137–204. doi: 10.1007/978-0-387-30374-1_6.

- Erskine, A. *et al.* (2019) ‘Mammalian olfaction is a high temporal bandwidth sense’, *bioRxiv*, p. 570689. doi: 10.1101/570689.
- Escalard, C. *et al.* (2019) ‘New detailed description of the anterior part of the cribriform plate using anatomic specimens and computed tomography’, *Surgical and Radiologic Anatomy*, 41(7), pp. 801–808. doi: 10.1007/s00276-019-02220-z.
- Fan, X. R. *et al.* (2010) ‘Blocking effect of methylflavonolamine on human NaV1.5 channels expressed in xenopus laevis oocytes and on sodium currents in rabbit ventricular myocytes’, *Acta Pharmacologica Sinica*, 31(3), pp. 297–306. doi: 10.1038/aps.2010.8.
- Fang, X. *et al.* (2002) ‘The presence and role of the tetrodotoxin-resistant sodium channel Na v 1.9 (NaN) in nociceptive primary afferent neurons’, *Journal of Neuroscience*, 22(17), pp. 7425–7433. doi: 10.1523/JNEUROSCI.22-17-07425.2002.
- Favre, J. . *et al.* (1995) ‘Blood supply of the olfactory nerve. Meningeal relationship and surgical relevance.’, *Surgical Radiologic Anatomy*, 17, pp. 133–138. doi: 10.1007/bf01627573.
- Ferdenzi, C. *et al.* (2013) ‘Variability of affective responses to odors: Culture, gender, and olfactory knowledge’, *Chemical Senses*, 38(2), pp. 175–186. doi: 10.1093/chemse/bjs083.
- Field, P. M., Li, Y. and Raisman, G. (2003) ‘Ensheathment of the olfactory nerves in the adult rat’, *Journal of Neurocytology*, 32, pp. 317–324. doi: doi:10.1023/b:neur.0000010089.37032.48.
- Finger, T. E. *et al.* (1990) ‘Ultrastructure of substance P-and CGRP-immunoreactive nerve fibers in the nasal epithelium of rodents’, *Journal Of Comparative Neurology*, 294(2), pp. 293–305. doi: 10.1002/cne.902940212.
- Firestein, S. (2001) ‘How the olfactory system makes sense of scents’, *Nature*, 413, pp. 211–218. doi: <https://doi.org/10.1038/35093026>.
- Fjell, J. *et al.* (2000) ‘Localization of the tetrodotoxin-resistant sodium channel NaN in nociceptors’, *NeuroReport*, 11(1), pp. 199–202. doi: 10.1097/00001756-200001170-00039.
- Fleischer, J. *et al.* (2006) ‘Olfactory receptors and signalling elements in the Grueneberg ganglion’, *Journal of Neurochemistry*, 98(2), pp. 543–554. doi: 10.1111/j.1471-4159.2006.03894.x.
- Frenz, C. T. *et al.* (2014) ‘Na V 1.5 sodium channel window currents contribute to spontaneous firing in olfactory sensory neurons’, *Journal of Neurophysiology*, 112, pp. 1091–1104. doi: 10.1152/jn.00154.2014.-Olfactory.
- Fuss, S. H., Omura, M. and Mombaerts, P. (2005) ‘The Grueneberg ganglion of the mouse projects axons to glomeruli in the olfactory bulb’, *European Journal of Neuroscience*, 22(10), pp. 2649–2654. doi: 10.1111/j.1460-9568.2005.04468.x.
- Gadziola, M. A. *et al.* (2015) ‘The olfactory tubercle encodes odor valence in behaving mice’, *Journal of Neuroscience*. Society for Neuroscience, 35(11), pp. 4515–4527. doi: 10.1523/JNEUROSCI.4750-14.2015.

- Gaillard, I. *et al.* (2002) ‘A single olfactory receptor specifically binds a set of odorant molecules’, *European Journal of Neuroscience*, 15, pp. 409–418. doi: 10.1046/j.0953-816x.2001.01871.x.
- Garcia-Gonzalez, D. *et al.* (2013) ‘Olfactory system and demyelination’, *Anatomical Record*, 296(9), pp. 1424–1434. doi: 10.1002/ar.22736.
- Gaudet, R. (2008) ‘TRP channels entering the structural era’, *Journal of Physiology*, 586(15), pp. 3565–3575. doi: 10.1113/jphysiol.2008.155812.
- Gavva, N. R. *et al.* (2004) ‘Molecular determinants of vanilloid sensitivity in TRPV1’, *Journal of Biological Chemistry*, 279(19), pp. 20283–20295. doi: 10.1074/jbc.M312577200.
- Genovese, F. *et al.* (2016) ‘Properties of an optogenetic model for olfactory stimulation’, *Journal of Physiology*, 594(13), pp. 3501–3516. doi: 10.1113/JP271853.
- Genovese, F. *et al.* (2017) ‘Possible role of calcitonin gene-related peptide in trigeminal modulation of glomerular microcircuits of the rodent olfactory bulb’, *European Journal of Neuroscience*, 45(4), pp. 587–600. doi: 10.1111/ejn.13490.
- Gesteland, R. C. (1964) ‘Initial events of the electro-olfactogram’, *Annals of the New York Academy of Sciences*, 116(2), pp. 440–447.
- Getchell, T. V. (1974) ‘Electrogenic sources of slow voltage transients recorded from frog olfactory epithelium’, *Journal of Neurophysiology*, 37(6), pp. 1115–1130. doi: 10.1152/jn.1974.37.6.1115.
- Giannetti, N., Saucier, D. and Astic, L. (1992) ‘Organization of the septal organ projection to the main olfactory bulb in adult and newborn rats’, *Journal of Comparative Neurology*, 323, pp. 288–298. doi: 10.1002/cne.903230211.
- Gillespie, J. B. and Perucca, L. G. (1960) ‘Congenital generalized indifference to pain (Congenital analgia)’, *American Journal of Diseases in Children*, 100, pp. 124–126. doi: 10.1001/archpedi.1960.04020040126019.
- Gingras, J. *et al.* (2014) ‘Global Nav1.7 knockout mice recapitulate the phenotype of human congenital indifference to pain’, *PLoS ONE*. Public Library of Science, 9:e105895(9). doi: 10.1371/journal.pone.0105895.
- Giraldez, F., Geijo, E. and Belmonte, C. (1979) ‘Response characteristics of corneal sensory fibers to mechanical and thermal stimulation’, *Brain Research*, 177, pp. 571–576. doi: 10.1016/0006-8993(79)90475-x.
- Goadsby, P. J., Edvinsson, L. and Ekman, R. (1990) ‘Vasoactive peptide release in the extracerebral circulation of humans during migraine headache’, *Annals of Neurology*, 28(2), pp. 183–187. doi: 10.1002/ana.410280213.
- Gold, M. S. *et al.* (2002) ‘Prostaglandin E2 modulates TTX-R I Na in rat colonic sensory neurons’, *Journal of Neurophysiology*, 88(3), pp. 1512–1522. doi: 10.1152/jn.00668.2001.

- Gold, M. S. (2005) 'Role of voltage-gated sodium channels in oral and craniofacial pain', in Coward, K. and Baker, M. D. (eds) *Sodium channels, pain and analgesia*. Basel: Birkhäuser Basel, pp. 145–164. doi: 10.1007/3-7643-7411-X.
- Goldberg, Y. P. *et al.* (2007) 'Loss-of-function mutations in the Nav1.7 gene underlie congenital indifference to pain in multiple human populations', *Clinical Genetics*. Blackwell Publishing Ltd, 71(4), pp. 311–319. doi: 10.1111/j.1399-0004.2007.00790.x.
- Golgi, C. (1875) 'Sulla fina struttura dei bulbi olfactorii.', *Rivista Sperimentale di Freniatria e Medicina Legale*, 1, pp. 405–425.
- Griffin, J. W. and Thompson, W. J. (2008) 'Biology and pathology of nonmyelinating schwann cells', *Glia*, 56(14), pp. 1518–1531. doi: 10.1002/glia.20778.
- Grosmaître, X. *et al.* (2007) 'Dual functions of mammalian olfactory sensory neurons as odor detectors and mechanical sensors', *Nature Neuroscience*, 10(3), pp. 348–354. doi: 10.1038/nn1856.
- Guo, Y. R. and Mackinnon, R. (2017) 'Structure-based membrane dome mechanism for Piezo mechanosensitivity', *eLife*, 6, pp. e33660-undefined. doi: 10.7554/eLife.33660.001.
- Han, C. *et al.* (2015) 'The domain II S4-S5 linker in Nav1.9: A missense mutation enhances activation, impairs fast inactivation, and produces human painful neuropathy', *NeuroMolecular Medicine*. Humana Press Inc., 17(2), pp. 158–169. doi: 10.1007/s12017-015-8347-9.
- Han, P. *et al.* (2018) 'Pepper with and without a sting: Brain processing of intranasal trigeminal and olfactory stimuli from the same source', *Brain Research*, 1700, pp. 41–46. doi: 10.1016/j.brainres.2018.07.010.
- Hanani, M. (2005) 'Satellite glial cells in sensory ganglia: From form to function', *Brain Research Reviews*, pp. 457–476. doi: 10.1016/j.brainresrev.2004.09.001.
- Harper, A. A. and Lawson, S. N. (1985) 'Conduction velocity is related to morphological cell type in rat dorsal root ganglion neurones', *Journal of Physiology*, 359, pp. 31–46. doi: 10.1113/jphysiol.1985.sp015573.
- Hayar, A. *et al.* (2004) 'External tufted cells: A major excitatory element that coordinates glomerular activity', *Journal of Neuroscience*, 24(30), pp. 6676–6685. doi: 10.1523/JNEUROSCI.1367-04.2004.
- Herzog, R. I. *et al.* (2003) 'Distinct repriming and closed-state inactivation kinetics of Nav1.6 and Nav1.7 sodium channels in mouse spinal sensory neurons', *Journal of Physiology*, 551(3), pp. 741–750. doi: 10.1113/jphysiol.2003.047357.
- Hockfield, S. and Gobel, S. (1982) 'An anatomical demonstration of projections to the medullary dorsal horn (trigeminal nucleus caudalis) from rostral trigeminal nuclei and the contralateral caudal medulla', *Brain Research*, 252, pp. 203–211. doi: 10.1016/0006-8993(82)90388-2.
- Hodgkin, A. L. and Huxley, A. F. (1952) 'Quantitative description of membrane current and its

application to conduction and excitation in nerve.’, *Journal of Physiology*, 117, pp. 500–544. doi: 10.1113/jphysiol.1952.sp004764.

Hofmann, T. *et al.* (2002) ‘Subunit composition of mammalian transient receptor potential channels in living cells’, *PNAS*, 28(11), pp. 7461–7466. doi: 10.1073/pnas.102596199.

Hollandsworth, M. P., DiNovo, K. M. and McCulloch, P. F. (2009) ‘Unmyelinated fibers of the anterior ethmoidal nerve in the rat co-localize with neurons in the medullary dorsal horn and ventrolateral medulla activated by nasal stimulation’, *Brain Research*, 1298, pp. 131–144. doi: 10.1016/j.brainres.2009.08.077.

Holzmann, B. (2013) ‘Antiinflammatory Activities of CGRP Modulating Innate Immune Responses in Health and Disease’, *Current Protein & Peptide Science*, 14(4), pp. 268–274. doi: 10.2174/13892037113149990046.

Huang, J. *et al.* (2014) ‘Gain-of-function mutations in sodium channel NaV1.9 in painful neuropathy’, *Brain*. Oxford University Press, 137(6), pp. 1627–1642. doi: 10.1093/brain/awu079.

Huang, L. *et al.* (2013) ‘Reciprocal connectivity between mitral cells and external plexiform layer interneurons in the mouse olfactory bulb’, *Frontiers in Neural Circuits*, 1, pp. 7–32. doi: 10.3389/fncir.2013.00032.

Hummel, T. and Livermore, A. (2002) ‘Intranasal chemosensory function of the trigeminal nerve and aspects of its relation to olfaction’, *International Archives of Occupational and Environmental Health*, 75(5), pp. 305–313. doi: 10.1007/s00420-002-0315-7.

Hursh, J. B. (1939) ‘Conduction velocity and diameter of nerve fibers’, *American Journal of Physiology*, 127(1), pp. 131–139. doi: 10.1152/ajplegacy.1939.127.1.131.

Illig, K. R. (2005) ‘Projections from orbitofrontal cortex to anterior piriform cortex in the rat suggest a role in olfactory information processing’, *Journal of Comparative Neurology*, 488(2), pp. 224–231. doi: 10.1002/cne.20595.

Imai, T. (2014) ‘Construction of functional neuronal circuitry in the olfactory bulb’, *Seminars in Cell and Developmental Biology*. Elsevier Ltd, pp. 180–188. doi: 10.1016/j.semcdb.2014.07.012.

Indo, Y. *et al.* (1996) ‘Mutations in the TRKA/NGF receptor gene in patients with congenital insensitivity to pain with anhidrosis’, *Nature Genetics*, 13(4), pp. 485–488. doi: 10.1038/ng0896-485.

Indo, Y. (2002) ‘Genetics of congenital insensitivity to pain with anhidrosis (CIPA) or hereditary sensory and autonomic neuropathy type IV: Clinical, biological and molecular aspects of mutations in TRKA(NTRK1) gene encoding the receptor tyrosine kinase for nerve growth factor’, *Clinical Autonomic Research*, Suppl 1, pp. I20–I32. doi: 10.1007/s102860200016.

Inokuchi, A., Kimmelman, C. P. and Snow, J. B. (1993) ‘Convergence of olfactory and nasotrigeminal inputs and possible trigeminal contributions to olfactory responses in the rat thalamus’, *Eur Arch Otorhinolaryngol*, 249, pp. 473–477. doi: 10.1007/BF00168858.

- Ivanusic, J. J., Wood, R. J. and Brock, J. A. (2013) 'Sensory and sympathetic innervation of the mouse and guinea pig corneal epithelium', *Journal of Comparative Neurology*, 521(4), pp. 877–893. doi: 10.1002/cne.23207.
- Jacquot, L., Monnin, J. and Brand, G. (2004) 'Influence of nasal trigeminal stimuli on olfactory sensitivity', *Comptes Rendus - Biologies*, 327(4), pp. 305–311. doi: 10.1016/j.crv.2004.02.004.
- Jarvis, M. F. *et al.* (2007) 'A-803467, a potent and selective Na^v1.8 sodium channel blocker, attenuates neuropathic and inflammatory pain in the rat', *PNAS*, 104(20), pp. 8520–8525. doi: 10.1073/pnas.0611364104.
- Jin, X. and Gereau IV, R. W. (2006) 'Acute p38-mediated modulation of tetrodotoxin-resistant sodium channels in mouse sensory neurons by tumor necrosis factor- α ', *Journal of Neuroscience*, 26(1), pp. 246–255. doi: 10.1523/JNEUROSCI.3858-05.2006.
- Johnson, D. M. G. *et al.* (2000) 'New features of connectivity in piriform cortex visualized by intracellular injection of pyramidal cells suggest that "primary" olfactory cortex functions like "association" cortex in other sensory systems', *Journal of Neuroscience*, 20(18), pp. 6974–6982. doi: 10.1523/JNEUROSCI.20-18-06974.2000.
- Jordt, S.-E. and Julius, D. (2002) 'Molecular basis for species-specific sensitivity to "hot" chili peppers', *Cell*, 108, pp. 421–430. doi: 10.1016/s0092-8674(02)00637-2.
- Jordt, S. *et al.* (2004) 'Mustard oil and cannabinoids excite sensory nerve fibres through the TRP channel ANKTM1', *Nature*, 427(6971), pp. 260–265. doi: 10.1038/nature02282.
- Kageneck, C. *et al.* (2014) 'Release of CGRP from mouse brainstem slices indicates central inhibitory effect of triptans and kynurenate', *Journal of Headache and Pain*. Springer-Verlag Italia s.r.l., 15(1). doi: 10.1186/1129-2377-15-7.
- Kamajaya, A. *et al.* (2014) 'The structure of a conserved piezo channel domain reveals a topologically distinct β sandwich fold', *Structure*. Cell Press, 22(10), pp. 1520–1527. doi: 10.1016/j.str.2014.08.009.
- Kara, C. O. (2004) 'Animal models of sinusitis: Relevance to human disease', *Current Allergy and Asthma Reports*. Current Science Ltd, pp. 496–499. doi: 10.1007/s11882-004-0018-0.
- Kedei, N. *et al.* (2001) 'Analysis of the native quaternary structure of vanilloid receptor 1', *Journal of Biological Chemistry*, 276(30), pp. 28613–28619. doi: 10.1074/jbc.M103272200.
- Kikuta, S. *et al.* (2010) 'Neurons in the anterior olfactory nucleus pars externa detect right or left localization of odor sources', *PNAS*, 107(27), pp. 12363–12368. doi: 10.1073/pnas.1003999107.
- Kim, S. E. *et al.* (2012) 'The role of Drosophila Piezo in mechanical nociception', *Nature*, 483(7388), pp. 209–212. doi: 10.1038/nature10801.
- Knowlton, W. M. *et al.* (2010) 'TRPM8, but not TRPA1, is required for neural and behavioral responses to acute noxious cold temperatures and cold-mimetics in vivo', *Pain*, 150(2), pp. 340–350. doi: 10.1016/j.pain.2010.05.021.

- Kobayashi, K. *et al.* (2005) ‘Distinct expression of TRPM8, TRPA1, and TRPV1 mRNAs in rat primary afferent neurons with A δ /C-fibers and colocalization with Trk receptors’, *Journal of Comparative Neurology*, 493(4), pp. 596–606. doi: 10.1002/cne.20794.
- Koltzenburg, M., Stucky, C. L. and Lewin, G. R. (1997) ‘Receptive properties of mouse sensory neurons innervating hairy skin’, *Journal of Neurophysiology*, 78(4), pp. 1841–1850. doi: 10.1152/jn.1997.78.4.1841.
- Kosaka, K., Heizmann, C. W. and Kosaka, T. (1994) ‘Calcium-binding protein parvalbumin-immunoreactive neurons in the rat olfactory bulb’, *Experimental Brain Research*, 99, pp. 191–204. doi: 10.1007/BF00239586.
- LaGuardia, J. J., Cohrs, R. J. and Gilden, D. H. (2000) ‘Numbers of neurons and non-neuronal cells in human trigeminal ganglia’, *Neurological Research*. Forefront Publishing Group, 22(6), pp. 565–566. doi: 10.1080/01616412.2000.11740719.
- Lapid, H. *et al.* (2009) ‘Odorant concentration dependence in electroolfactograms recorded from the human olfactory epithelium’, *Journal of Neurophysiology*. American Physiological Society, 102(4), pp. 2121–2130. doi: 10.1152/jn.91321.2008.
- Lapid, H. *et al.* (2011) ‘Neural activity at the human olfactory epithelium reflects olfactory perception’, *Nature Neuroscience*, 14(11), pp. 1455–1461. doi: 10.1038/nn.2926.
- Laska, M. (2001) ‘Perception of trigeminal chemosensory qualities in the elderly’, *Chemical Senses*, 26(6), pp. 681–689. doi: 10.1093/chemse/26.6.681.
- Laursen, W. J. *et al.* (2015) ‘Species-specific temperature sensitivity of TRPA1’, *Temperature*. Routledge, 2(2), pp. 214–226. doi: 10.1080/23328940.2014.1000702.
- Lawson, J. J. *et al.* (2008) ‘TRPV1 Unlike TRPV2 is restricted to a subset of mechanically insensitive cutaneous nociceptors responding to heat’, *Journal of Pain*, 9(4), pp. 298–308. doi: 10.1016/j.jpain.2007.12.001.
- Lee, H. and Caterina, M. J. (2005) ‘TRPV channels as thermosensory receptors in epithelial cells’, *Pflügers Archiv European Journal of Physiology*, 451(1), pp. 160–167. doi: 10.1007/s00424-005-1438-y.
- Leston, J. M. (2009) ‘Anatomie fonctionnelle du nerf trijumeau’, *Neurochirurgie*, pp. 99–112. doi: 10.1016/j.neuchi.2009.01.001.
- Letierrier, C. *et al.* (2010) ‘Voltage-gated sodium channel organization in neurons: Protein interactions and trafficking pathways’, *Neuroscience Letters*. Elsevier, 486(2), pp. 92–100. doi: 10.1016/j.neulet.2010.08.079i.
- Levy, D. and Strassman, A. M. (2002) ‘Mechanical response properties of A and C primary afferent neurons innervating the rat intracranial dura’, *Journal of Neurophysiology*. American Physiological Society, 88(6), pp. 3021–3031. doi: 10.1152/jn.00029.2002.
- Li, A. *et al.* (2014) ‘Precise detection of direct glomerular input duration by the olfactory bulb’,

- Journal of Neuroscience*. Society for Neuroscience, 34(48), pp. 16058–16064. doi: 10.1523/JNEUROSCI.3382-14.2014.
- Li, Y., Field, P. M. and Raisman, G. (2005) ‘Olfactory ensheathing cells and olfactory nerve fibroblasts maintain continuous open channels for regrowth of olfactory nerve fibres’, *Glia*, 52(3), pp. 245–251. doi: 10.1002/glia.20241.
- Liman, E. R. and Buck, L. B. (1994) ‘A second subunit of the olfactory cyclic nucleotide-gated channel confers high sensitivity to cAMP’, *Neuron*, 13, pp. 611–621. doi: 10.1016/0896-6273(94)90029-9.
- Lin, W., Ezekwe, E. A. D., *et al.* (2008) ‘TRPM5-expressing microvillous cells in the main olfactory epithelium’, *BMC Neuroscience*, 9. doi: 10.1186/1471-2202-9-114.
- Lin, W., Ogura, T., *et al.* (2008) ‘TRPM5-expressing solitary chemosensory cells respond to odorous irritants.’, *Journal of Neurophysiology*, 99(3), pp. 1451–1460. doi: 10.1152/jn.01195.2007.
- Lindberg, S., Dolata, J. and Mercke, U. (1987) ‘Stimulation of C fibers by ammonia vapor triggers a mucociliary defense reflex’, *Am Rev Respir Dis*, 135(5), pp. 1093–1098. doi: 10.1164/arrd.1987.135.5.1093.
- Liu, M. *et al.* (2019) ‘The expression of voltage-gated sodium channels in trigeminal nerve following chronic constriction injury in rats’, *International Journal of Neuroscience*. Taylor and Francis Ltd, 129(10), pp. 955–962. doi: 10.1080/00207454.2019.1595616.
- Liu, S. C. *et al.* (2017) ‘The identification of the TRPM8 channel on primary culture of human nasal epithelial cells and its response to cooling’, *Medicine (United States)*. Lippincott Williams and Wilkins, 96(31). doi: 10.1097/MD.00000000000007640.
- Lopes, D. M., Denk, F. and McMahon, S. B. (2017) ‘The molecular fingerprint of dorsal root and trigeminal ganglion neurons’, *Frontiers in Molecular Neuroscience*. Frontiers Media S.A., 10:304. doi: 10.3389/fnmol.2017.00304.
- López-Elizalde, R. *et al.* (2018) ‘Anatomy of the olfactory nerve: A comprehensive review with cadaveric dissection’, *Clinical Anatomy*. John Wiley and Sons Inc., pp. 109–117. doi: 10.1002/ca.23003.
- Lötsch, J. *et al.* (2012) ‘The human operculo-insular cortex is pain-preferentially but not pain-exclusively activated by trigeminal and olfactory stimuli’, *PLoS ONE*, 7:e34798(4). doi: 10.1371/journal.pone.0034798.
- Lowe, G. and Gold, G. H. (1991) ‘The spatial distributions of odorant sensitivity and odorant-induced currents in salamander olfactory receptor cells’, *Journal of Physiology*, 442, pp. 147–168. doi: 10.1113/jphysiol.1991.sp018787.
- Lucero, M. T. (2013) ‘Peripheral modulation of smell: Fact or fiction?’, *Seminars in Cell and Developmental Biology*. Elsevier Ltd, 24(1), pp. 58–70. doi: 10.1016/j.semcd.2012.09.001.

- Lugrin, J. *et al.* (2014) ‘The role of oxidative stress during inflammatory processes’, *Biological Chemistry*, 395(2), pp. 203–230. doi: 10.1515/hsz-2013-0241.
- Ma, M. *et al.* (2003) ‘Olfactory signal transduction in the mouse septal organ’, *Journal of Neuroscience*, 23(1), pp. 317–324. doi: 10.1523/JNEUROSCI.23-01-00317.2003.
- Macpherson, L. J. *et al.* (2005) ‘The pungency of garlic: Activation of TRPA1 and TRPV1 in response to allicin’, *Current Biology*, 15(10), pp. 929–934. doi: 10.1016/j.cub.2005.04.018.
- Madrid, R. *et al.* (2009) ‘Variable threshold of trigeminal cold-thermosensitive neurons is determined by a balance between TRPM8 and Kv1 potassium channels’, *Journal of Neuroscience*, 29(10), pp. 3120–3131. doi: 10.1523/JNEUROSCI.4778-08.2009.
- Maggi, C. A. (1995) ‘Tachykinins and calcitonine gene-related peptide (CGRP) as co-transmitter released from peripheral endings of sensory nerves’, *Progress in Neurobiology*, 45, pp. 1–99. doi: 10.1016/0301-0082(94)e0017-b.
- Maingret, F. *et al.* (2008) ‘Inflammatory mediators increase Nav1.9 current and excitability in nociceptors through a coincident detection mechanism’, *Journal of General Physiology*, 131(3), pp. 211–225. doi: 10.1085/jgp.200709935.
- Malnic, B., Gonzalez-Kristeller, D. and Gutiyama, L. . (2010) ‘Odorant receptors’, in Menini, A. (ed.) *The Neurobiology of Olfaction*. Boca Raton (FL): : CRC Press/Taylor & Francis.
- Malnic, B., Hirono, J. and Sato, T. (1999) ‘Combinatorial receptor codes for odors’, *Cell*, 96, pp. 713–723. doi: 10.1016/S0092-8674(00)80581-4.
- Mandairon, N. *et al.* (2009) ‘Humans and mice express similar olfactory preferences’, *PLoS ONE*, 4:e4209(1). doi: 10.1371/journal.pone.0004209.
- Manteniatis, S. *et al.* (2013) ‘Comprehensive RNA-Seq expression analysis of sensory ganglia with a focus on ion channels and GPCRs in trigeminal ganglia’, *PLoS ONE*, 8:e79523(11), p. undefined. doi: 10.1371/journal.pone.0079523.
- Mardy, S. *et al.* (1999) ‘Congenital insensitivity to pain with anhidrosis: Novel mutations in the TRKA (NTRK1) gene encoding a high-affinity receptor for nerve growth factor’, *American Journal of Human Genetics*, 64, pp. 1570–1579. doi: 10.1086/302422.
- Marfurt, C. F. (1981) ‘The somatotopic organization of the cat trigeminal ganglion as determined by the horseradish peroxidase technique’, *Anatomical Record*, 201, pp. 105–118. doi: 10.1002/ar.1092010113.
- Marshall, D. A. and Maruniak, J. A. (1986) ‘Masera’s organ responds to odorants’, *Brain Research*, 366, pp. 329–332. doi: 10.1016/0006-8993(86)91312-0.
- Maurer, M. *et al.* (2019) ‘Photoactivation of olfactory sensory neurons does not affect action potential conduction in individual trigeminal sensory axons innervating the rodent nasal cavity’, *PLoS ONE*. Edited by H. Matsunami. Public Library of Science, 14(8), p. e0211175. doi: 10.1371/journal.pone.0211175.

- Maxwell, D. S. (1967) 'Fine structure of the normal trigeminal ganglion in the cat and monkey', *Journal of Neurosurgery*, 26, pp. 127–131. doi: 10.3171/jns.1967.26.1part2.0127.
- McCulloch, P. F. *et al.* (2018) 'Innervation of the nose and nasal region of the rat: Implications for initiating the mammalian diving response', *Frontiers in Neuroanatomy*. Frontiers Media S.A., 12:85. doi: 10.3389/fnana.2018.00085.
- McDermott, L. A. *et al.* (2019) 'Defining the functional role of Na V 1.7 in human nociception', *Neuron*. Cell Press, 101(5), pp. 905-919.e8. doi: 10.1016/j.neuron.2019.01.047.
- McGann, J. P. (2017) 'Poor human olfaction is a 19th-century myth', *Science*. American Association for the Advancement of Science. doi: 10.1126/science.aam7263.
- McIver, B. M. and Tanelian, D. L. (1993) 'Free nerve ending terminal morphology is fiber type specific for Ad and C fibers innervating rabbit cornea epithelium', *Journal of Neurophysiology*, 69(5), pp. 1779–1783. doi: 10.1152/jn.1993.69.5.1779.
- McKemy, D. D., Neuhausser, W. M. and Julius, D. (2002) 'Identification of a cold receptor reveals a general role for TRP channels in thermosensation', *Nature*, 416. doi: 10.1038/nature719.
- McNamara, F. N., Randall, A. and Gunthorpe, M. J. (2005) 'Effects of piperine, the pungent component of black pepper, at the human vanilloid receptor (TRPV1)', *British Journal of Pharmacology*, 144(6), pp. 781–790. doi: 10.1038/sj.bjp.0706040.
- Meents, J. E. *et al.* (2019) 'The role of Nav1.7 in human nociceptors: Insights from human induced pluripotent stem cell-derived sensory neurons of erythromelalgia patients', *Pain*. Lippincott Williams and Wilkins, 160(6), pp. 1327–1341. doi: 10.1097/j.pain.0000000000001511.
- Mellem, J. E. *et al.* (2002) 'Decoding of polymodal sensory stimuli by postsynaptic glutamate receptors in *C. elegans*', *Neuron*, 36(5), pp. 933–944. doi: 10.1016/s0896-6273(02)01088-7.
- Meng, J. *et al.* (2009) 'Activation of TRPV1 mediates calcitonin gene-related peptide release, which excites trigeminal sensory neurons and is attenuated by a retargeted botulinum toxin with anti-nociceptive potential', *Journal of Neuroscience*, 29(15), pp. 4981–4992. doi: 10.1523/JNEUROSCI.5490-08.2009.
- Messlinger, K. and Russo, A. F. (2019) 'Current understanding of trigeminal ganglion structure and function in headache', *Cephalalgia*. SAGE Publications Ltd, pp. 1661–1674. doi: 10.1177/0333102418786261.
- Mikhailov, N. *et al.* (2019) 'Mechanosensitive meningeal nociception via Piezo channels: Implications for pulsatile pain in migraine?', *Neuropharmacology*. Elsevier Ltd, 149, pp. 113–123. doi: 10.1016/j.neuropharm.2019.02.015.
- Milardi, D. *et al.* (2017) 'The olfactory system revealed: Non-invasive mapping by using constrained spherical deconvolution tractography in healthy humans', *Frontiers in Neuroanatomy*. Frontiers Media S.A., 11:32. doi: 10.3389/FNANA.2017.00032.

- Miller, M. L. *et al.* (1995) ‘Microvillar cells of the olfactory epithelium: morphology and regeneration following exposure to toxic compounds’, *Brain Research*, 669, pp. 1–9. doi: 10.1016/0006-8993(94)01144-7.
- Minett, M. S. *et al.* (2014) ‘Pain without nociceptors? Nav1.7-independent pain mechanisms’, *Cell Reports*, 6(2), pp. 301–312. doi: 10.1016/j.celrep.2013.12.033.
- Minke, B., Wu, C.-F. and Pak, W. L. (1975) ‘Induction of photoreceptor voltage noise in the dark in *Drosophila* mutant’, *Nature*, 258, pp. 84–87. doi: 10.1038/258084a0.
- Mishra, S. K. and Hoon, M. A. (2010) ‘Ablation of TrpV1 neurons reveals their selective role in thermal pain sensation’, *Molecular and Cellular Neuroscience*, 43(1), pp. 157–163. doi: 10.1016/j.mcn.2009.10.006.
- Miyamoto, T. *et al.* (2009) ‘TRPV1 and TRPA1 mediate peripheral nitric oxide-induced nociception in mice’, *PLoS ONE*, 4(10), pp. e7596-undefined. doi: 10.1371/journal.pone.0007596.
- Mizumura, K. *et al.* (2009) ‘Excitation and sensitization of nociceptors by bradykinin: What do we know?’, *Experimental Brain Research*, 196(1), pp. 53–65. doi: 10.1007/s00221-009-1814-5.
- Mohapatra, D. P. and Nau, C. (2003) ‘Desensitization of capsaicin-activated currents in the vanilloid receptor TRPV1 is decreased by the cyclic AMP-dependent protein kinase pathway’, *Journal of Biological Chemistry*, 278(50), pp. 50080–50090. doi: 10.1074/jbc.M306619200.
- Mombaerts, P. (1999) ‘Seven-transmembrane proteins as odorant and chemosensory receptors’, *Science*, 286, pp. 707–711. doi: 10.1126/science.286.5440.707.
- Montani, G. *et al.* (2006) ‘Neuropeptide Y in the olfactory microvillar cells’, *European Journal of Neuroscience*, 24, pp. 20–24. doi: 10.1111/j.1460-9568.2006.04878.x.
- Montell, C. and Rubin, G. M. (1989) ‘Molecular characterization of the *Drosophila* TRP locus: A putative integral membrane protein required for phototransduction’, *Neuron*, 2(4), pp. 1313–1323. doi: 10.1016/0896-6273(89)90069-x.
- Mucignat-Caretta, C. (2010) ‘The rodent accessory olfactory system’, *Journal of Comparative Physiology A: Neuroethology, Sensory, Neural, and Behavioral Physiology*, pp. 767–777. doi: 10.1007/s00359-010-0555-z.
- Nagayama, S. *et al.* (2010) ‘Differential axonal projection of mitral and tufted cells in the mouse main olfactory system’, *Frontiers in Neural Circuits*, 4:120. doi: 10.3389/fncir.2010.00120.
- Nagayama, S., Homma, R. and Imamura, F. (2014) ‘Neuronal organization of olfactory bulb circuits’, *Frontiers in Neural Circuits*. Frontiers Research Foundation. doi: 10.3389/fncir.2014.00098.
- Nara, K. *et al.* (2011) ‘A large-scale analysis of odor coding in the olfactory epithelium’, *Journal of Neuroscience*. Society for Neuroscience, 31(25), pp. 9179–9191. doi: 10.1523/jneurosci.1282-11.2011.

- Nassar, M. A. *et al.* (2004) ‘Nociceptor-specific gene deletion reveals a major role for Na^v 1.7 (PN1) in acute and inflammatory pain’, *PNAS*, 101(34), pp. 12706–12711. doi: 10.1073/pnas.0404915101.
- Van Ness Dearborn, G. (1932) ‘A case of congenital general pure analgesia’, *The Journal of Nervous and Mental Disease*, 75(6), pp. 612–615. doi: 10.1097/00005053-193206000-00002.
- Neureither, F. *et al.* (2017) ‘Tracking of unfamiliar odors is facilitated by signal amplification through anoctamin 2 chloride channels in mouse olfactory receptor neurons’, *Physiological Reports*, 5:e13373(15). doi: 10.14814/phy2.13373.
- Nguyen, M. Q. *et al.* (2017) ‘Diversity amongst trigeminal neurons revealed by high throughput single cell sequencing’, *PLoS ONE*, 12(9), p. e0185543. doi: 10.1371/journal.pone.0185543.
- Nimura, Y. and Nei, M. (2003) ‘Evolution of olfactory receptor genes in the human genome’, *PNAS*, 100(21), pp. 12235–12240. doi: 10.1073/pnas.1635157100.
- Nilius, B. *et al.* (2005) ‘Gating of TRP channels: A voltage connection?’, *Journal of Physiology*, 567(1), pp. 35–44. doi: 10.1113/jphysiol.2005.088377.
- Nilius, B. and Appendino, G. (2013) ‘Spices: The savory and beneficial science of pungency’, *Reviews of Physiology, Biochemistry and Pharmacology*. Springer Verlag, 164, pp. 1–76. doi: 10.1007/112_2013_11.
- Nilius, B. and Owsianik, G. (2010) ‘The transient receptor potential family of ion channels’, *Genome Biology*, 12. doi: 10.1186/gb-2011-12-3-218.
- Octura, J. E. R., Maeda, K. I. and Wakabayashi, Y. (2018) ‘Structure and zonal expression of olfactory receptors in the olfactory epithelium of the goat, *Capra hircus*’, *Journal of Veterinary Medical Science*. Japanese Society of Veterinary Science, 80(6), pp. 913–920. doi: 10.1292/jvms.17-0692.
- Ong, W. Y., Stohler, C. S. and Herr, D. R. (2019) ‘Role of the prefrontal cortex in pain processing’, *Molecular Neurobiology*. Humana Press Inc., 56(2), pp. 1137–1166. doi: 10.1007/s12035-018-1130-9.
- Öngür, D. and Price, J. L. (2000) ‘The organization of network within the orbital and medial prefrontal cortex of rats, monkeys and humans’, *Cerebral Cortex*, 10(3), pp. 206–219. doi: 10.1093/cercor/10.3.206.
- Orona, E., Rainer, E. C. and Scott, J. W. (1984) ‘Dendritic and axonal organization of mitral and tufted cells in the rat olfactory bulb’, *Journal Of Comparative Neurology*, 226(3), pp. 226–346. doi: 10.1002/cne.902260305.
- Orona, E., Scott, J. W. and Rainer, E. C. (1983) ‘Different granule cell populations innervate superficial and deep regions of the external plexiform layer in rat olfactory bulb’, *Journal of Comparative Neurology*, 217, pp. 227–237. doi: 10.1002/cne.902170209.
- Osteen, J. D. *et al.* (2016) ‘Selective spider toxins reveal a role for the Nav1.1 channel in

mechanical pain', *Nature*. Nature Publishing Group, 534(7608), pp. 494–499. doi: 10.1038/nature17976.

Ottoson, D. (1954) 'Sustained potentials evoked by olfactory stimulation', *Acta Physiologica Scandinavica*, 32(4), pp. 384–386. doi: 10.1111/j.1748-1716.1954.tb01186.x.

Ottoson, D. (1958) 'Studies on the relationship between olfactory stimulating effectiveness and physico-chemical properties of odorous compounds', *Acta Physiologica Scandinavica*, 43, pp. 167–181. doi: 10.1111/j.1748-1716.1958.tb01585.x.

Padilla, F. *et al.* (2007) 'Expression and localization of the Nav1.9 sodium channel in enteric neurons and in trigeminal sensory endings: Implication for intestinal reflex function and orofacial pain', *Molecular and Cellular Neuroscience*, 35(1), pp. 138–152. doi: 10.1016/j.mcn.2007.02.008.

Paintal, A. S. (1965) 'Effects of temperature on conduction in single vagal and saphenous myelinated nerve fibres of the cat', *Journal of Physiology*. Tasaki & Frank, 180(1), pp. 20–49.

Pannese, E. (2002) 'Perikaryal surface specializations of neurons in sensory ganglia', *Internal Review of Cytology*, 220, pp. 1–34. doi: 10.1016/s0074-7696(02)20002-9.

Panneton, W. M., Gan, Q. and Juric, R. (2006) 'Brainstem projections from recipient zones of the anterior ethmoidal nerve in the medullary dorsal horn', *Neuroscience*, 141, pp. 889–906. doi: 10.1016/j.neuroscience.2006.04.055.

Panneton, W. M., Pan, B. B. and Gan, Q. (2017) 'Somatotopy in the medullary dorsal horn as a basis for orofacial reflex behavior', *Frontiers in Neurology*. Frontiers Media S.A., 8:522. doi: 10.3389/fneur.2017.00522.

Paricio-Montesinos, R. *et al.* (2020) 'The sensory coding of warm perception', *Neuron*. Cell Press, 106(5), pp. 830–841.e3. doi: 10.1016/j.neuron.2020.02.035.

Patron, V. *et al.* (2015) 'The forgotten foramina: a study of the anterior cribriform plate', *Surgical and Radiologic Anatomy*, 37, pp. 835–840. doi: 10.1007/s00276-015-1471-2.

Peier, A. M. *et al.* (2002) 'A heat-sensitive TRP channel expressed in keratinocytes', *Science*, 296(5575), pp. 2046–2049. doi: 10.1126/science.1073140.

Peterlin, Z. *et al.* (2008) 'The importance of odorant conformation to the binding and activation of a representative olfactory receptor', *Chemistry and Biology*, 15(12), pp. 1317–1327. doi: 10.1016/j.chembiol.2008.10.014.

Le Pichon, C. E. and Chesler, A. T. (2014) 'The functional and anatomical dissection of somatosensory subpopulations using mouse genetics', *Frontiers in Neuroanatomy*. Frontiers Research Foundation, 8:21. doi: 10.3389/fnana.2014.00021.

Pinto, V., Derkach, V. A. and Safronov, B. V. (2008) 'Role of TTX-sensitive and TTX-resistant sodium channels in A δ - and C-fiber conduction and synaptic transmission', *Journal of Neurophysiology*, 99(2), pp. 617–628. doi: 10.1152/jn.00944.2007.

- Premkumar, L. S. and Ahern, G. P. (2000) 'Induction of vanilloid receptor channel activity by protein kinase C', *Nature*, 408, pp. 985–990. doi: 10.1038/35050121.
- Price, T. J. and Flores, C. M. (2007) 'Critical evaluation of the colocalization between calcitonin gene-related peptide, substance P, transient receptor potential vanilloid subfamily type 1 immunoreactivities and isolectin B 4 binding in primary afferent neurons of the rat and mouse', *J Pain*, 8(3), pp. 263–272. doi: 10.1016/j.jpain.2006.09.005.
- Priest, B. T. *et al.* (2005) 'Contribution of the tetrodotoxin-resistant voltage-gated sodium channel Na V 1.9 to sensory transmission and nociceptive behavior', *PNAS*, 102(26), pp. 9382–9387. doi: 10.1073/pnas.0501549102.
- Puil, E. and Spigelman, I. (1988) 'Electrophysiological responses of trigeminal root ganglion neurons in vitro.', *Neuroscience*, 24(2), pp. 635–646. doi: [https://doi.org/10.1016/0306-4522\(88\)90357-0](https://doi.org/10.1016/0306-4522(88)90357-0).
- Purves, D. *et al.* (2004) *Neuroscience*. 3rd Edition. Edited by D. Purves et al. Sunderland: Sinauer Associates, Inc.
- Qureshi, A. I. *et al.* (2018) 'Intra-arterial modulation of the trigeminal nerve ganglion in patients with refractory trigeminal neuralgia', *Journal of Neuroimaging*. Blackwell Publishing Inc., 28(1), pp. 79–85. doi: 10.1111/jon.12476.
- Ranade, S. S. *et al.* (2014) 'Piezo2 is the major transducer of mechanical forces for touch sensation in mice', *Nature*. Nature Publishing Group, 516(729), pp. 121–125. doi: 10.1038/nature13980.
- Reid, G. (2005) 'ThermoTRP channels and cold sensing: What are they really up to?', *Pflugers Archiv European Journal of Physiology*, 451(1), pp. 250–263. doi: 10.1007/s00424-005-1437-z.
- Reisert, J. *et al.* (2005) 'Mechanism of the excitatory Cl⁻ response in mouse olfactory receptor neurons', *Neuron*. Cell Press, 45(4), pp. 553–561. doi: 10.1016/j.neuron.2005.01.012.
- Ressler, K. J., Sullivan, S. L. and Buck, L. 8 (1993) 'A zonal organization of odorant receptor gene expression in the olfactory epithelium', *Cell*, 73, pp. 597–609. doi: 10.1016/0092-8674(93)90145-g.
- Roper, S. D. (2014) 'TRPs in taste and chemesthesis', *Handbook of Experimental Pharmacology*. Springer New York LLC, 223, pp. 827–871. doi: 10.1007/978-3-319-05161-1_5.
- Roy, M. L. and Narahashi, T. (1992) 'Differential properties of tetrodotoxin-sensitive and tetrodotoxin-resistant sodium channels in rat dorsal root ganglion neurons', *Journal of Neuroscience*, 72(6), pp. 2104–2111. doi: 10.1523/JNEUROSCI.12-06-02104.1992.
- Rush, A. M. *et al.* (2006) 'A single sodium channel mutation produces hyper- or hypoexcitability in different types of neurons', *PNAS*, 103(21), pp. 8245–8250. doi: 10.1073/pnas.0602813103.
- Rybka, E. J. and McCulloch, P. F. (2006) 'The anterior ethmoidal nerve is necessary for the initiation of the nasopharyngeal response in the rat', *Brain Research*, 1075(1), pp. 122–132. doi:

10.1016/j.brainres.2005.12.112.

Salzer, J. L. (2015) ‘Schwann cell myelination’, *Cold Spring Harbor Perspectives in Biology*. Cold Spring Harbor Laboratory Press, 7(8). doi: 10.1101/cshperspect.a020529.

Samad, O. A. *et al.* (2013) ‘Virus-mediated shRNA knockdown of Na v 1.3 in rat dorsal root ganglion attenuates nerve injury-induced neuropathic pain’, *Molecular Therapy*. Nature Publishing Group, 21(1), pp. 49–56. doi: 10.1038/mt.2012.169.

Sant’ambrogio, G., Tsubone, H. and Sant’ambrogio, F. B. (1995) ‘Sensory information from the upper airway: Role in the control of breathing’, *Respiration Physiology*, 102, p. 16. doi: 10.1016/0034-5687(95)00048-i.

Saotome, K. *et al.* (2018) ‘Structure of the mechanically activated ion channel Piezo1’, *Nature*. Nature Publishing Group, 554(7693), pp. 481–486. doi: 10.1038/nature25453.

Sarrafchi, A. *et al.* (2013) ‘Olfactory sensitivity for six predator odors in CD-1 mice, human subjects, and spider monkeys’, *PLoS ONE*. Public Library of Science, 8(11). doi: 10.1371/journal.pone.0080621.

Saunders, C. J. *et al.* (2013) ‘Dissecting the role of TRPV1 in detecting multiple trigeminal irritants in three behavioral assays for sensory irritation.’, *F1000Research*, 2, p. 74. doi: 10.12688/f1000research.2-74.v1.

Saunders, C. J. *et al.* (2014) ‘Cholinergic neurotransmission links solitary chemosensory cells to nasal inflammation’, *Proceedings of the National Academy of Sciences of the United States of America*. National Academy of Sciences, 111(16), pp. 6075–6080. doi: 10.1073/pnas.1402251111.

Scanio, M. J. C. *et al.* (2010) ‘Discovery and biological evaluation of potent, selective, orally bioavailable, pyrazine-based blockers of the Nav1.8 sodium channel with efficacy in a model of neuropathic pain’, *Bioorganic and Medicinal Chemistry*, 18(22), pp. 7816–7825. doi: 10.1016/j.bmc.2010.09.057.

Schaefer, M. L. *et al.* (2002) ‘Trigeminal collaterals in the nasal epithelium and olfactory bulb: A potential route for direct modulation of olfactory information by trigeminal stimuli’, *Journal of Comparative Neurology*, 444(3), pp. 221–226. doi: 10.1002/cne.10143.

Schrenk-Siemens, K. *et al.* (2015) ‘Piezo2 is required for mechanotransduction in human stem cell-derived touch receptors’, *Nature Neuroscience*. Nature Publishing Group, 18(1), pp. 10–16. doi: 10.1038/nn.3894.

Schröder, H. (1993) *Functional anatomy of the spinal trigeminal nucleus. Brain-stem localization and function*. Edited by L. R. Caplan and H. C. Hopf. Springer, Berlin, Heidelberg. doi: 10.1007/978-3-642-78172-8_19.

Scott, J. W. *et al.* (2014) ‘Tuning to odor solubility and sorption pattern in olfactory epithelial responses’, *Journal of Neuroscience*, 34(6), pp. 2025–2036. doi: 10.1523/JNEUROSCI.3736-13.2014.

- Scott, J. W., Acevedo, H. P. and Sherrill, L. (2006) 'Effects of concentration and sniff flow rate on the rat electroolfactogram', *Chemical Senses*, 30(6), pp. 581–593. doi: 10.1093/chemse/bjj063.
- Sekizawa, S.-I. and Tsubone, H. (1994) 'Nasal receptors responding to noxious chemical irritants', *Respiration Physiology*, 96, pp. 37–48. doi: 10.1016/0034-5687(94)90104-x.
- Sekizawa, S.-I. and Tsubone, H. (1996) 'Nasal mechanoreceptors in guinea pigs', *Respiration Physiology*, 106, pp. 223–230. doi: 10.1111/j.1365-2273.1992.tb01680.x.
- Shepherd, G. M. *et al.* (2011) 'The first images of nerve cells: Golgi on the olfactory bulb 1875', *Brain Research Reviews*, pp. 92–105. doi: 10.1016/j.brainresrev.2010.09.009.
- Sherwood, C. C. (2005) 'Comparative anatomy of the facial motor nucleus in mammals, with an analysis of neuron numbers in primates', in *Anatomical Record - Part A Discoveries in Molecular, Cellular, and Evolutionary Biology*, pp. 1067–1079. doi: 10.1002/ar.a.20259.
- Shields, S. D. *et al.* (2012) 'Na v1.8 expression is not restricted to nociceptors in mouse peripheral nervous system', *Pain*, 153(10), pp. 2017–2030. doi: 10.1016/j.pain.2012.04.022.
- Silver, W. L. *et al.* (2006) 'TRPV1 receptors and nasal trigeminal chemesthesis.', *Chemical senses*, 31(9), pp. 807–12. doi: 10.1093/chemse/bjl022.
- Silver, W. L., Farley, L. G. and Finger, T. E. (1991) 'The effects of neonatal capsaicin administration on trigeminal nerve chemoreceptors in the rat nasal cavity', *Brain Research*, 561, pp. 212–216. doi: 10.1016/0006-8993(91)91597-t.
- Silver, W. L. and Finger, T. E. (2009) 'The anatomical and electrophysiological basis of peripheral nasal trigeminal chemoreception', in *Annals of the New York Academy of Sciences*. Blackwell Publishing Inc., pp. 202–205. doi: 10.1111/j.1749-6632.2009.03894.x.
- Silverman, J. D. and Kruger, L. (1989) 'Calcitonin-gene-related-peptide-immunoreactive innervation of the rat head with emphasis on specialized sensory structures', *Journal of Comparative Neurology*, 280(2), pp. 303–330. doi: 10.1002/cne.902800211.
- Simmons, P. A. and Getchell, T. V (1981) 'Physiological activity of newly differentiated olfactory receptor neurons correlated with morphological recovery from olfactory nerve section in the salamander', *Journal of neurophysiology*, 45(3). doi: 10.1152/jn.1981.45.3.529.
- Singh, G. P. (2019) 'Anatomy of trigeminal nerve', in *Handbook of Trigeminal Neuralgia*. Springer Singapore, pp. 11–22. doi: 10.1007/978-981-13-2333-1_2.
- Sittl, R. *et al.* (2012) 'Anticancer drug oxaliplatin induces acute cooling-aggravated neuropathy via sodium channel subtype Na V1.6-resurgent and persistent current', *PNAS*, 109(17), pp. 6704–6709. doi: 10.1073/pnas.1118058109.
- Smith, T. D. and Bhatnagar, K. P. (2019) 'Anatomy of the olfactory system', in Doty, R. L. (ed.) *Handbook of Clinical Neurology*. Elsevier B.V., pp. 17–28. doi: 10.1016/B978-0-444-63855-7.00002-2.

Sosulski, D. L. *et al.* (2011) ‘Distinct representations of olfactory information in different cortical centres’, *Nature*, 472(7342), pp. 213–219. doi: 10.1038/nature09868.

Spehr, M. *et al.* (2006) ‘Parallel processing of social signals by the mammalian main and accessory olfactory systems’, *Cellular and Molecular Life Sciences*, 63(13), pp. 1476–1484. doi: 10.1007/s00018-006-6109-4.

Stockand, J. D. and Eaton, B. A. (2013) ‘Stimulus discrimination by the polymodal sensory neuron’, *Communicative & Integrative Biology*, 6(2). doi: 10.4161/cib.23469.

Story, G. M. *et al.* (2003) ‘ANKTM1, a TRP-like channel expressed in nociceptive neurons, is activated by cold temperatures’, *Cell*, 112(6), pp. 819–829. doi: 10.1016/s0092-8674(03)00158-2.

Stoyanov Krastev, D. and Apostolov, A. (2013) ‘Cytoarchitectonic study of the trigeminal ganglion in humans’, *Original Research Clujul Medical*, 86(2).

Strassman, A. M. and Raymond, S. A. (1999) ‘Electrophysiological evidence for tetrodotoxin-resistant sodium channels in slowly conducting dural sensory fibers’, *Journal of Neurophysiology*, 81(2), pp. 413–424. doi: 10.1152/jn.1999.81.2.413.

Swanson, A. G. (1963) ‘Congenital insensitivity to pain with anhydrosis a unique syndrome in two male sibilings’, *Arch Neurol.*, 8, pp. 299–306. doi: 10.1001/archneur.1963.00460030083008.

Szczot, M. *et al.* (2017) ‘Cell-type-specific splicing of Piezo2 regulates mechanotransduction’, *Cell Reports*. Elsevier B.V., 21(10), pp. 2760–2771. doi: 10.1016/j.celrep.2017.11.035.

Takaya, J. *et al.* (2015) ‘A potent and site-selective agonist of TRPA1’, *Journal of the American Chemical Society*. American Chemical Society, 137(50), pp. 15859–15864. doi: 10.1021/jacs.5b10162.

Tan, Z. Y. *et al.* (2014) ‘Tetrodotoxin-resistant sodium channels in sensory neurons generate slow resurgent currents that are enhanced by inflammatory mediators’, *Journal of Neuroscience*. Society for Neuroscience, 34(21), pp. 7190–7197. doi: 10.1523/JNEUROSCI.5011-13.2014.

Tavakoli, M., Petropoulos, I. N. and Malik, R. A. (2012) ‘Assessing corneal nerve structure and function in diabetic neuropathy’, *Clinical and Experimental Optometry*, pp. 338–347. doi: 10.1111/j.1444-0938.2012.00743.x.

Thalakoti, S. *et al.* (2007) ‘Neuron-glia signaling in trigeminal ganglion: implications for migraine pathology’, *Headache*, 47(7), pp. 1008–1025. doi: 10.1111/j.1526-4610.2007.00854.x.

Thalhammer, J. G. *et al.* (1994) ‘Modality-dependent modulation of conduction by impulse activity in functionally characterized single cutaneous afferents in the rat modality-dependent modulation of conduction by impulse activity in functionally characterized single cutaneous afferents in the rat’, *Somatosensory & Motor Research*, 11(3), pp. 243–257. doi: 10.3109/08990229409051392.

Tham, W. W. P., Stevenson, R. J. and Miller, L. A. (2011) ‘The role of the mediodorsal thalamic

nucleus in human olfaction', *Neurocase*, 17(2), pp. 148–159. doi: 10.1080/13554794.2010.504728.

Toida, K. *et al.* (1994) 'Synaptic contacts between mitral/tufted cells and GABAergic neurons containing calcium-binding protein parvalbumin in the rat olfactory bulb, with special reference to reciprocal synapses between them', *Brain Research*, 650, pp. 347–352. doi: 10.1016/0006-8993(94)91804-X.

Tremblay, C. and Frasnelli, J. (2018) 'Olfactory and trigeminal systems interact in the periphery', *Chemical Senses*. Oxford University Press, 43(8), pp. 611–616. doi: 10.1093/chemse/bjy049.

Trotier, D. (2011) 'Vomeronasal organ and human pheromones', *European Annals of Otorhinolaryngology, Head and Neck Diseases*. Elsevier Masson SAS, 128(4), pp. 184–190. doi: 10.1016/j.anorl.2010.11.008.

Vassar, R. *et al.* (1994) 'Topographic organization of sensory projection to the olfactory bulb', *Cell*, 79(6), pp. 951–991. doi: 10.1016/0092-8674(94)90029-9.

Venkatachalam, K. and Montell, C. (2007) 'TRP Channels', *Annual Review of Biochemistry*, 76(1), pp. 387–417. doi: 10.1146/annurev.biochem.75.103004.142819.

Viana, F. (2011) 'Chemosensory properties of the trigeminal system', *ACS Chemical Neuroscience*, 2(1), pp. 38–50. doi: 10.1021/cn100102c.

Vit, J. P. *et al.* (2006) 'Satellite glial cells in the trigeminal ganglion as a determinant of orofacial neuropathic pain', *Neuron Glia Biology*, 2(4), pp. 247–257. doi: 10.1017/S1740925X07000427.

Voets, T. *et al.* (2004) 'The principle of temperature-dependent gating in cold-and heat-sensitive TRP channels', *Nature*, 430, pp. 748–754. doi: 10.1038/nature02732.

Voets, T. *et al.* (2005) 'Sensing with TRP channels', *Nature Chemical Biology*, 1(2), pp. 85–92. doi: 10.1038/nchembio0705-85.

Wallois, F. *et al.* (1991) 'Trigeminal nasal receptors related to respiration and to various stimuli in cats', *Respiration Physiology*, 85, pp. 111–125. doi: 10.1016/0034-5687(91)90010-G.

Wang, J., La, J. H. and Hamill, O. P. (2019) 'PIEZO1 is selectively expressed in small diameter mouse DRG neurons distinct from neurons strongly expressing TRPV1', *Frontiers in Molecular Neuroscience*. Frontiers Media S.A., 12. doi: 10.3389/fnmol.2019.00178.

Waxman, S. G., Kocsis, J. D. and Black, J. A. (1994) 'Type III sodium channel mRNA is expressed in embryonic but not adult spinal sensory neurons, and is reexpressed following axotomy', *Journal of Neurophysiology*, 72(1), pp. 466–470. doi: 10.1152/jn.1994.72.1.466.

Wei, E. T. and Seid, D. A. (1983) 'AG-3-5: a chemical producing sensations of cold', *Journal of Pharmacy and Pharmacology*, 35(2), pp. 110–112. doi: 10.1111/j.2042-7158.1983.tb04279.x.

Weiss, J. *et al.* (2011) 'Loss-of-function mutations in sodium channel Nav1.7 cause anosmia.', *Nature*. Nature Publishing Group, 472(7342), pp. 186–90. doi: 10.1038/nature09975.

Wesson, D. W., Verhagen, J. V. and Wachowiak, M. (2009) ‘Why sniff fast? The relationship between sniff frequency, odor discrimination, and receptor neuron activation in the rat’, *Journal of Neurophysiology*, 101(2), pp. 1089–1102. doi: 10.1152/jn.90981.2008.

Willis, D. N. *et al.* (2011) ‘Menthol attenuates respiratory irritation responses to multiple cigarette smoke irritants’, *FASEB Journal*. Wiley, 25(12), pp. 4434–4444. doi: 10.1096/fj.11-188383.

Wilson, D. A. and Rennaker, R. L. (2010) ‘Cortical activity evoked by odors.’, in Menini, A. (ed.) *The Neurobiology of Olfaction*. Boca Raton (FL): CRC Press/Taylor & Francis. Available at: <https://www.ncbi.nlm.nih.gov/books/NBK55970/#>.

Woo, S. H. *et al.* (2014) ‘Piezo2 is required for Merkel-cell mechanotransduction’, *Nature*. Nature Publishing Group, 509(7502), pp. 622–626. doi: 10.1038/nature13251.

Woo, S. H. *et al.* (2015) ‘Piezo2 is the principal mechanotransduction channel for proprioception’, *Nature Neuroscience*. Nature Publishing Group, 18(12), pp. 1756–1762. doi: 10.1038/nn.4162.

Xu, H. *et al.* (2002) ‘TRPV3 is a calcium-permeable temperature-sensitive cation channel’, *Nature*, 418(6894), pp. 181–186. doi: 10.1038/nature00850.

Yang, A. Y., Chow, J. and Liu, J. (2018) ‘Corneal innervation and sensation: The eye and beyond’, *Yale Journal of Biology and Medicine*, 91, pp. 13–21.

Yang, F. *et al.* (2015) ‘Structural mechanism underlying capsaicin binding and activation of the TRPV1 ion channel’, *Nature Chemical Biology*. Nature Publishing Group, 11(7), pp. 518–524. doi: 10.1038/nchembio.1835.

Yang, G. C. *et al.* (2007) ‘Numerical modeling of odorant uptake in the rat nasal cavity’, *Chemical Senses*, 32(3), pp. 273–284. doi: 10.1093/chemse/bjl056.

Yoshida, T. *et al.* (2006) ‘Nitric oxide activates TRP channels by cysteine S-nitrosylation’, *Nature Chemical Biology*. Nature Publishing Group, 2(11), pp. 596–607. doi: 10.1038/nchembio821.

Yousry, I. *et al.* (2004) ‘Detailed anatomy of the motor and sensory roots of the trigeminal nerve and their neurovascular relationships: a magnetic resonance imaging study’, *Journal of Neurosurgery*, 101, pp. 427–434. doi: 10.3171/jns.2004.101.3.0427.

Zald, D. H. and Pardo, J. V (1997) ‘Emotion, olfaction, and the human amygdala: Amygdala activation during aversive olfactory stimulation’, *PNAS*, 94(8), pp. 4119–4124. doi: 10.1073/pnas.94.8.4119.

Zhang, X. F. *et al.* (2004) ‘Differential action potentials and firing patterns in injured and uninjured small dorsal root ganglion neurons after nerve injury’, *Brain Research*, 1009(1–2), pp. 147–158. doi: 10.1016/j.brainres.2004.02.057.

Zhang, X. and Firestein, S. (2002) ‘The olfactory receptor gene superfamily of the mouse’,

Nature Neuroscience, 5(2), pp. 124–133. doi: 10.1038/nn800.

Zhang, Y. *et al.* (2017) ‘Glucose Intake Alters Expression of Neuropeptides Derived from Proopiomelanocortin in the Lateral Hypothalamus and the Nucleus Accumbens in Fructose Preference Rats’, *Neural Plasticity*. doi: 10.1155/2017/6589424.

Zimmermann, K. *et al.* (2007) ‘Sensory neuron sodium channel Nav1.8 is essential for pain at low temperatures’, *Nature*. Nature Publishing Group, 447(7146), pp. 855–858. doi: 10.1038/nature05880.

Zou, Z., Li, F. and Buck, L. B. (2005) ‘Odor maps in the olfactory cortex’, *PNAS*, 102(21), pp. 7724–7729. doi: 10.1073/pnas.0503027102.

Zozulya, S., Echeverri, ernando and Nguyen, T. (2001) ‘The human olfactory receptor repertoire’, *Genome Biology*, 2(6), p. research 0018.I-0018.I2. doi: 10.1186/gb-2001-2-6-research0018.

Zufall, F. *et al.* (2012) ‘Link between pain and olfaction in an inherited sodium channelopathy’, *Archives of Neurology*, 69(9), pp. 1119–1123. doi: 10.1001/archneurol.2012.21.

List of figures

Figure 1	Main olfactory epithelium located in the nasal cavity of rodents	5
Figure 2	MOE central projections	8
Figure 3	Olfactory sensory neuron signalling	13
Figure 4	Trigeminal anatomy	17
Figure 5	Trigeminal signalling	22
Figure 6	Psychophysical experiment in patients	37
Figure 7	Forced choice behavioral task in mice	42
Figure 8	Imaging techniques	44
Figure 9	Electro-olfactogram recordings	49
Figure 10	Electrophysiological recordings of single trigeminal afferents	53
Figure 11	TRPM8, TRPA1 and Nav 1.8 expression in trigeminal cellular bodies and projections	58
Figure 12	Trigeminal receptive fields in the nasal epithelium	60
Figure 13	Thermosensitivity of trigeminal afferents within the nasal cavity	63
Figure 14	Chemosensitivity of trigeminal afferents within the nasal epithelium	66
Figure 15	TRP channels transduce nasal trigeminal chemesthesis	68
Figure 16	Nav 1.8 sodium voltage-gated channel is expressed in a subpopulation of OSNs	71
Figure 17	Baseline water consumption depends on bottle	75
Figure 18	Concomitant exposure to the odorant PEA mitigated the aversion evoked by the volatile irritant cyclohexanone	77
Figure 19	Concomitant exposure to the odorant PEA mitigated the aversion evoked by diluted solutions of the volatile irritant allyl isothiocyanate	81
Figure 20	Psychophysical test on healthy subjects and patients show no effect of PEA on volatile irritant pungency ratings	84
Figure 21	Effect of optogenetic stimulation of OSNs on trigeminal conduction velocity in the nose	91
Figure 22	Sensory innervation of the mouse cornea	94
Figure 23	Reduction of AITC-evoked c-Fos labelling in the spinal trigeminal nucleus of the brainstem after concomitant exposure to PEA	109
Figure S1	Psychophysical test form - English version -	111
Figure S2	Psychophysical test form - Chinese version -	112
Figure S3	Alike the pure odorant PEA, volatile irritants activate olfactory sensory neurons	113
Figure S4	Summary of single trigeminal afferents recorded within the murine nasal epithelium	114

Abbreviations

A	
aa	<i>Amino acids</i>
AEN	<i>Anterior ethmoidal nerve</i>
AITC	<i>Allyl isothiocyanate</i>
ANO2	<i>Actonamin2</i>
aOB	<i>Accessory olfactory bulb</i>
aON	<i>Anterior olfactory nucleus</i>
AP	<i>Action potential</i>
B	
BC	<i>Basal cell</i>
C	
Ca ²⁺	<i>Calcium ion</i>
cAMP	<i>Cyclic adenosine monophosphate</i>
CFA	<i>Complete Freund adjuvant</i>
CGRP	<i>Calcitonine gene-related peptide</i>
ChR2	<i>Channel rhodopsin 2</i>
CIN	<i>Cinnamaldehyde</i>
CIP	<i>Congenital insensitivity to pain</i>
CIPA	<i>Congenital insensitivity to pain with anhidrosis</i>
CNG	<i>Cyclic nucleotide-gated ion channel</i>
CO ₂	<i>Carbon dioxide</i>
CYC	<i>Cyclohexanone</i>
D	
dH ₂ O	<i>Distilled water</i>
DMNT	<i>Dorsomedial nucleus of the thalamus</i>
DMSO	<i>Dimethyl sulfoxide</i>
DRG	<i>Dorsal root ganglia</i>
E	
Ea	<i>Activation energy</i>
ECx	<i>Entorhinal cortex</i>
eGFP	<i>Enhanced green fluorescent protein</i>
EOG	<i>Electro-olfactogram</i>
EPL	<i>External plexiform layer</i>
eTI	<i>External tufted interneurons</i>
G	
GABA	<i>Gamma-aminobutyric acid</i>
GFP	<i>Green fluorescent protein</i>
GL	<i>Glomeruli layer</i>
G _{olf}	<i>Olfactory G protein</i>
GrC	<i>Granule cell</i>
GrL	<i>Granule cell layer</i>

GrG	<i>Grüneberg ganglion</i>
H	
H ₂ O ₂	<i>Oxygen peroxide</i>
I	
IC	<i>Icilin</i>
IPL	<i>Internal plexiform layer</i>
IVC	<i>Isolated ventilated cage</i>
J	
JC	<i>Juxtaglomerular cell</i>
L	
LTMR	<i>Low threshold mecanoreceptor</i>
M	
MCL	<i>Mitral cell layer</i>
MDH	<i>Medullary dorsal horn</i>
MEN	<i>Menthol</i>
MiC	<i>Mitral cell</i>
MOB	<i>Main olfactory bulb</i>
MOE	<i>Main olfactory epithelium</i>
MVC	<i>Microvillar cell</i>
N	
Na ⁺	<i>Sodium ion</i>
Nav	<i>Sodium voltage-gated channel</i>
NGF	<i>Nerve growth factor</i>
NH ₃	<i>Ammonia</i>
NH ₄ HCO ₃	<i>Ammonium bicarbonate</i>
NO	<i>Nitric oxide</i>
O	
OB	<i>Olfactory bulb</i>
OCil	<i>Olfactory cilia</i>
OCT	<i>Optimum cutting temperature medium</i>
OEC	<i>Olfactory ensheating cell</i>
OFC	<i>Orbitofrontal cortex</i>
OMP	<i>Olfactory marker protein</i>
ONF	<i>Olfactory nerve fibroblast</i>
OR	<i>Olfactory receptor</i>
OSN	<i>Olfactory sensory neuron</i>
OT	<i>Olfactory Tubercle</i>
P	
PBS	<i>Phosphate buffer saline</i>
PCx	<i>Piriform cortex</i>
PEA	<i>Phenylethyl alcohol</i>
PG	<i>Periglomerular cells</i>
PKA	<i>Protein kinase A</i>

PKC	<i>Protein kinase C</i>
POC	<i>Primary olfactory cortex</i>
R	
RFP	<i>Red fluorescent protein</i>
ROS	<i>Reactive oxygen species</i>
S	
SA	<i>Short axon interneurons</i>
SC	<i>Schwann cell</i>
SCN	<i>Voltage-gated sodium channel gene</i>
SGC	<i>Satellite glial cell</i>
SNS	<i>Sensory neuron specific</i>
SO	<i>Septal organ</i>
SpV	<i>Spinal trigeminal nucleus</i>
SpVc	<i>Sub-nucleus caudalis of the spinal trigeminal nucleus</i>
SpVi	<i>Sub-nucleus interpolaris of the spinal trigeminal nucleus</i>
T	
TC	<i>Tufted cell</i>
TG	<i>Trigeminal ganglion</i>
TrkA	<i>Tropomyosin receptor kinase A</i>
TRP	<i>Transient receptor potential channel</i>
TRPA1	<i>Transient receptor potential channel ankyrin 1</i>
TRPM8	<i>Transient receptor potential channel melastatine 8</i>
TRPV1	<i>Transient receptor potential channel vanilloid 1</i>
TTX	<i>Tetrodotoxin</i>
TTX-R	<i>Tetrodotoxin -resistant</i>
TTX-S	<i>Tetrodotoxin-sensitive</i>
V	
V	<i>Trigeminal nerve (Fifth cranial nerve)</i>
V1	<i>Ophthalmic branch of V</i>
V2	<i>Maxillary branch of V</i>
V3	<i>Mandibular branch of V</i>
VGC	<i>Voltage-gated channel</i>
VGe	<i>Van Gehuchten cells</i>
VNO	<i>Vomeronasal organ</i>
V _p	<i>Vapour pressure</i>
VPMN	<i>Ventral postero-medial nucleus of the thalamus</i>

Acknowledgement

During my doctoral training, I realized that a Ph D thesis represents a challenge, both at the scientific and human level. I would not have been able to face this challenge and grow as a scientist and a person without the help of the many people surrounding me during these 4 years. First of all, I would like to express my gratitude to my supervisor, Dr. Richard Carr, for his continuous support throughout my Ph. D study, for his patience and for his guidance. Working with him and my colleagues from the Experimental Pain Research lab under the direction of Prof. Martin Schmelz was extremely motivating and inspiring. I also want to use this opportunity to express my sincere thanks to the Messlinger team who welcomed me in their lab in Erlangen and taught me different electrophysiological techniques with enthusiasm and kindness. Further, I would like to thank my second supervisor, Prof. Stephan Frings, for his availability and for transmitting his passion about the study of sensory systems. I am very grateful to Prof. Rüdiger Rudolf and Dr. Köhr for kindly agreeing to be my jury members. My gratitude extends to the SFB 1158 which financially supported the work comprised in this thesis and gave me the opportunity to present my work at several national and international conferences.

During my training, I had the chance to meet many fellow doctoral students and postdoc in the young CBTM and within the SFB 1158 group, Sara Laiouar, Dajana Tanasic, Felix Schmoehl, Veronica Bonalume, Daniela Rosenberger, Georg Sedlmeier, Vladimir Ryabov, Nitin Patil, Livia Filiz, Oscar Retana, Christopher Sliwinski. We have been there for one another and I am really grateful for all the good times spent together in the lab or during social events and the vivid discussions about science and life in general.

Besides the scientific environment, I would like to thank my roommate, Katia Rostetter, for the friendship she offered me since the day I arrived in Heidelberg. My appreciation also goes to my family for their moral support and for trying very hard to understand what I was studying. Finally, I am deeply grateful to my fellow scientist and partner Luca Guglielmi, for his encouragement and for his faith in me. His unwavering support helped me throughout the entire writing process.